LAPPEENRANTA UNIVERSITY OF TECHNOLOGY
LUT School of Energy Systems
Master's Programme in Energy Systems

Shelon Andriel Marini

DESIGN AND CFD ANALYSIS OF A FLAMELESS COMBUSTION CHAMBER FOR A 2-KW MICRO GAS TURBINE

Examiners: Professor Jari Backman
Ph.D. Ahti Jaatinen-Värri

ABSTRACT

Lappeenranta University of Technology
LUT School of Energy Systems
Master's Programme in Energy Systems

Shelon Andriel Marini

Design and CFD analysis of a flameless combustion chamber for a 2-kW micro gas turbine

Master's thesis

2018

105 pages, 42 figures, 9 tables and 1 appendix

Examiners: Professor Jari Backman
Ph.D. Ahti Jaatinen-Värri

Keywords: combustion chamber, micro gas turbine, flameless combustion, CFD

Motivated by the straightening regulations regarding pollutant emissions and the increasing demand for distributed generation, this thesis has the objective to develop a new combustion chamber design for 2-kW_{el} micro gas turbines, based on flameless combustion. This concept was chosen because of its potential for very low emissions, added to the uniform temperature distribution, low noise, low vibration and the capacity to handle low-quality fuels. These features were already proven in industrial furnace applications, however, the employment of flameless combustion in gas turbines is still a research topic that requires further investigation. Two fuels were considered in this study, natural gas and landfill gas, and the evaluation and enhancement of the design is done iteratively utilizing computational fluid dynamics (CFD).

The results demonstrated that the application of flameless combustion in gas turbines is very promising. The emissions of both CO and NO_x were found to be lower than 4 ppmv (in a dry basis and corrected for 15% O_2). Besides, if the turbine inlet temperature can reach levels as high as 1800 K, the dilution zone of the combustor can be completely eliminated, providing a very uniform temperature profile, characteristic of flameless combustion. Nevertheless, among many problems related to efficiency in a micro gas turbine of such scale, it was found that the pressure drop of the combustor can be minimized in these cases, what could represent an increment in the electrical efficiency of almost 2%.

ACKNOWLEDGEMENTS

I would like to express my gratitude to the teaching staff of LUT's School of Energy Systems for all the knowledge transmitted, that culminated in this thesis. Particularly, I want to thank people from Fluid Dynamics laboratory for the given support. This is the area which I developed a special interest and where I had the pleasure to work as intern for one summer. Besides, without the computational resources provided by them, the conclusions of this thesis could not have gone so far.

Special thanks to my supervisors, Professor Jari Backman and Ph.D. Ahti Jaatinen-Värri, for the suggestion to conduct this research about gas turbine combustors and for the valuable advises along the process.

I want also to thank my family, in particular my parents Gilberto and Aneli, for the support in all senses. They were fundamental for the successful conclusion of my studies in Finland. In addition, thanks to the friends and special people I met in Lappeenranta, who provided nice moments and motivation, also essential to keep me focused. In particular, thanks to Arja Ylä-Outinen, my "Finnish mom", who gave me very important guidance and help in difficult situations.

Shelon Andriel Marini
May 27, 2018
Lappeenranta, Finland

TABLE OF CONTENTS

1 INTRODUCTION 9
2 COMBUSTION CHEMISTRY 12
3 DIFFUSIVE COMBUSTORS 15
3.1 Main requirements and performance parameters 19
3.2 Combustor arrangements 22
3.3 Pollution control 24
4 DRY LOW NO_X/EMISSION COMBUSTORS 28
5 RICH-BURN, QUICK-MIX, LEAN-BURN COMBUSTOR (RQL) 30
6 FLAMELESS DISTRIBUTED COMBUSTION 32
7 PRE-DESIGN 42
7.1 Fuel analysis 42
7.2 Compounds and mixture properties 45
7.3 Thermodynamic cycle 47
8 DESIGN PROCEDURE 53
8.1 Numerical models 56
8.2 Geometry 59
8.3 Domains and mesh 62
8.4 Defining the cases and boundary conditions 64
9 RESULTS 68
9.1 Temperatures 68
9.2 Velocities 74
9.3 Pressures 76
9.4 Pollutants 78
9.5 Discretization uncertainty 80
10 CONCLUSIONS AND DISCUSSION 84
REFERENCES 87
APPENDIX I – VBA CODE FOR MIXTURE PROPERTIES 94

LIST OF SYMBOLS AND ABBREVIATIONS

Roman letters

a	coefficient in polynomial fit	[-]
AR	air to fuel ratio	[-]
b	coefficient in polynomial fit	[-]
c_p	specific heat capacity	[J/(kg K)]
C_p	molar heat capacity	[J/(mol K)]
Da	Damköhler number	[-]
F	fraction (mass or molar)	[-]
h	enthalpy	[J/kg]
H	molar enthalpy	[J/mol]
k	turbulence kinetic energy	[m^2/s^2]
K_{FG}	recirculation rate	[-]
L	stoichiometric air-fuel ratio	[-]
LHV	fuel low heating value	[J/kg]
$\dot{m}$	mass flow	[kg/s]
M	molar mass	[g/mol]
p	pressure	[Pa, bar]
Δp	pressure drop	[Pa, bar]
P	power	[W]
R	universal gas constant	8.314510 J/(mol K)
T	temperature	[K, °C]
u	velocity	[m/s]
X	generic specie concentration	[ppmv, -]

y	stoichiometric flue gas fraction	[-]

Greek letters

ε	turbulence eddy dissipation	[m^2/s^3]
ε_r	recuperator effectiveness	[-]
η	efficiency	[-]
π	pressure ratio	[-]
ρ	density	[kg/m^3]
τ	time scale	[s]
Φ	equivalence ratio	[-]

Subscripts

0	startup conditions
1	compressor inlet
2	compressor outlet, recuperator cold stream inlet
3	recuperator cold stream outlet, combustor inlet
4	combustor outlet, turbine inlet
5	turbine outlet, recuperator hot stream inlet
b	combustor
c	compressor
d	dilution air
ch	chemical
el	electrical
FG	flue gas
FL	full load

g	generator
i	index indicating multiple values
in	inlet
K	Kolmogorov
m	mass, mechanical
out	outlet
p	primary air
r	recuperator
ref	reference
SG	stoichiometric gas
ST	stoichiometric conditions
s	isentropic
sh	shaft
t	total, turbine
th	thermal
v	volumetric or molar

Abbreviations

CDC	colorless distributed combustion
CFD	computational fluid dynamics
CHP	combined heat and power
DLE	dry low emissions
DLN	dry low NO_x
EGR	exhaust gases recirculation
FC	flameless combustion

FLOX	flameless oxidation
HiTAC	high temperature air combustion
LHV	low heating value
MILD	moderate or intense low oxygen dilution
RQL	rich-burn quick-mix lean-burn
SRC	selective catalytic reduction
UHC	unburned hydrocarbon

1 INTRODUCTION

The stresses caused by humankind activity on our planet are considered one of the main issues of the present time. The elevation of temperatures, melting of polar ice caps, increased incidence of floods and storms, acidification of the oceans and accelerated species extinction rate are some symptoms of climate change. These phenomena are directly related and driven by the amount of greenhouse gases that are released to the atmosphere each single day, in a quantity larger than the sink capacity of the planet. (Panwar, et al., 2011)

Energy conversion is one of the major players contributing to excessive emissions, which includes electricity generation, heating, transportation or industrial processes. In fact, all these sectors tend to get continuously more interconnected, due to the electrification of transport and industries, as well as advances in waste heat recovery. Due to the critical environmental situation and the accelerated growth in electricity demand, significant investments and changes in energy policy have been done recently, especially by developed countries. They intend to promote renewable and sustainable generation alternatives. Solar and wind, complemented by biomass, geothermal and ocean energy, seem to be the technologies heading the transition that has the ultimate goal to phase out completely the utilization of coal and other fossil fuels. Although their great potential to mitigate emissions, a high penetration of renewables also brings challenges to the reliability and stability of the distribution grids, because of the characteristic intermittence of the resources. Thus, storage and other generation technologies are required to provide the necessary balance and maintain the reliability of the supply. (Bussar, et al., 2014)

Gas turbines have been an established technology for a long time, and they are utilized in both electricity generation and aircraft thrusters, among other applications. They have experienced substantial evolution during the past 25 years, related to advances in materials, coatings, cooling schemes and aerodynamics. These summed to increased compressor pressure ratios up to 45:1 led simple-cycle configurations to achieve thermal efficiencies up to 45%. Features of gas turbines such as low emissions compared to coal power plants, fuel flexibility, fast ramp up and high reliability make them a very attractive option to work in parallel with renewables. Even in a 100% renewable energy scenario, gas turbines could still play the essential balancing role, running on synthetic gas or gas derived from biomass. (Boyce, 2012)

The sum of the demand for cleaner energy with constrains about construction of new and long distribution lines, the advances in small-scale generation and especially the liberalization of electricity markets creates a new driving force, towards distributed generation. All these factors are contributing to make small generation units continuously more competitive with the previous concept of “economy of scale”, in which large centralized power plants were built in order to achieve lower electricity costs. Besides cutting the expenses with distribution networks, since the power and/or heat are generated close to the demand, distributed generation can offer more flexibility related to size, operation and expandability. In particular, small-scale gas turbines might be attractive not just to balance the oscillation of renewables, but in special where a source of waste biomass is available, as in farms, landfills and sewage treatment stations. In such places, biogas can be produced from organic residues through anaerobic digestion process and burned in a micro gas turbine to meet the local demand for power and heat. (Pepermans, et al., 2005)

In addition, many new applications are being developed, such as small autonomous vehicles, robots and military equipment that require high energy density. Batteries are still not feasible for many of these demands due to the low storage capacity per kilogram, summed to the charging time and problems in very low temperatures. Therefore, alternatives are required to meet the growing demand for portable power. An important drawback of micro gas turbines compared to reciprocating engines, their main competitor in small scale, is the low thermal efficiency. However, micro gas turbines have other key advantages, as the small size and weight, low emissions, low vibration, low maintenance costs, high reliability and fuel flexibility. (Xiao, et al., 2017; Hyung Do, et al., 2016)

The development of a thermal engine may involve several goals, among which some of the principal are increase efficiency, reduce emissions and reduce costs. The first two have direct impact on the environmental issues described previously. Indeed, increasing efficiency is one of the ways to reduce emissions, besides saving fuel. When scaling down a gas turbine up to micro scale – electrical output lower than 100 kW – the efficiency suffers due to gas leaks, heat losses, and limitations in materials and manufacturing processes. For example, it is usually impracticable to add cooling in turbine blades, also the blades cannot achieve as good aerodynamics as in larger scale and the clearances are relatively higher. These drawbacks might be somehow compensated by the employment of more complex thermodynamic cycles, involving recuperation, intercooling and reheating. Since these

techniques also add weight and costs, the feasibility of their use may depend on the application of the engine. (Tuttle, et al., 2017; Hyung Do, et al., 2016)

Another manner to mitigate emissions of a gas turbine is enhancing the combustion process itself. The combustion chamber, or simply combustor, is the component responsible for the heat input in gas turbines. In dated literature, combustors received less attention compared to compressors and turbines, probably because of the empiricism and lack of theoretical knowledge related to the development of this component. Still when CFD was not an available tool, combustion efficiencies close to 99% and pressure drops in the range of 2-10% of the compressor discharge pressure were achieved. In addition, the only pollutant concern in early designs was to avoid visible smoke, what was also solved back in 70s. This first generation of burners is usually referred as diffusive combustors. (Saravanamuttoo, et al., 2001)

The concerns with emissions started to increase during the following decades, leading to the necessity of combustors that have all the good features of diffusive designs, but with the additional capacity to limit pollutant formation, especially NO_x and CO. Techniques as water injection and selective catalytic reduction (SRC) were developed and successfully implemented to mitigate emissions, but accompanied by significant counterpoints. In parallel, new combustor concepts emerged in order to produce less emissions without external methods, as example of the dry low NO_x (DLN), the rich-burn, quick-mix, lean burn (RQL) and the flameless combustion (FC). The latter is an established technology in industrial furnaces that has already proven its potential for very low emissions, but more research is needed for its application in gas turbines. The achievement of flameless combustion with the higher pressures, energy densities and mass flows required for gas turbines have been studied recently and diverse combustor designs have been proposed. However, it is clear that the topic still requires more research and understanding of the phenomena under gas turbine conditions before this technology become commercially available. (Khidr, et al., 2017; Lefebvre & Ballal, 2010)

The present study provides a literature review of the main technologies currently established for gas turbine combustors and focus in the development of a new flameless combustion chamber design for a 2-kW_{el} micro gas turbine. Rather than pursue a refined design ready for commercialization, this thesis aims to investigate the applicability and proof some of the advantages of flameless concept in gas turbines. The other components of the engine have

not been designed yet, giving certain freedom about the layout and requiring cycle calculations in order to obtain input values for pressures, temperatures and mass flows. The electrical power of the engine was selected due to the increasing demand for distributed generation, added that it is one order lower than the smaller micro gas turbine commercially available at the moment. Therefore, the main objective of this study is to provide a functional flameless combustor design for a 2-kW_{el} gas turbine, based on the knowledge acquired from previous studies and with the support of CFD tools. In order to keep coherency with the purpose of fuel flexibility and the possibility to integrate micro gas turbines in fully renewable energy system, landfill gas is considered as one fuel option, in addition to natural gas, that is the main fuel used in gas turbines currently.

2 COMBUSTION CHEMISTRY

The simplest definition for combustion is the phenomenon that happens when material is burned. More specifically, it is a chemical process in which the material reacts with oxygen and releases heat and other new substances. In gas turbine context, combustion is a continuous process and the material burned is a hydrocarbon fuel. The most traditional fuel for gas turbines is natural gas, which is mostly composed by methane (CH_4). The combustion reaction of methane is given by Equation (1).

$$CH_4 + 4O \rightarrow CO_2 + 2H_2O + \text{Heat} \quad (1)$$

In a simplistic analysis, one part of methane requires four parts of oxygen for combustion, and results in one part of carbon dioxide and two parts of water, besides the heat. The oxygen required for combustion is taken from the atmosphere, and since the air is composed by 21% of oxygen and 79% of nitrogen, the corresponding amount of nitrogen has to be added to the equation. Noting that oxygen and nitrogen molecules are formed by two atoms, the real chemical equation of the combustion process is written as follows. (Saravanamuttoo, et al., 2001; Boyce, 2012)

$$CH_4 + 2(O_2 + 4N_2) \rightarrow CO_2 + 2H_2O + 8N_2 + \text{Heat} \quad (2)$$

The carbon dioxide appearing in previous equation is not the only pollutant present in the exhaust gases. Further reactions occur within the combustion chamber, as the formation of nitric oxides (NO_x), sulfur oxides (SO_x) and carbon monoxide (CO). There are three different pathways through which NO_x is originated inside the combustor, named thermal, prompt and nitrous oxide mechanisms. The thermal – or Zeldovich – mechanism requires large amounts of energy to be activated, therefore it is increasingly significant when the flame temperature becomes high. Previous studies showed that the production of thermal NO_x start to be considerably elevated when the combustion products are exposed to temperatures above 1600°C for some seconds or above 2000°C for some milliseconds. This suggests that even the presence of small high-temperature regions may lead to significant NO_x emissions. The Zeldovich mechanism is frequently the major pathway for NO_x formation in gas turbine combustors, especially in diffusive types. The reduction of the adiabatic flame temperature through exhaust gas recirculation and the minimization of residence time at high temperature zones are possible ways to mitigate the phenomenon. The governing reactions of this mechanism are defined as follows. (Wünning & Wünning, 1997; Hewson & Bollig, 1996)

$$O + N_2 \rightarrow NO + N \tag{3}$$

$$N + O_2 \rightarrow NO + O \tag{4}$$

$$N + OH \rightarrow NO + H \tag{5}$$

The prompt – or Fenimore – mechanism consists in fast reactions of molecular nitrogen with hydrocarbon radicals. The process does not require high temperature to occur, but it depends heavily on radical concentration. The prompt mechanism is the main responsible for NO_x production in flames under atmospheric conditions. In gas turbine combustors, on the other hand, it just becomes significative when the thermal NO_x is low, which means at lower temperatures or in cases of fuel-rich flame. The reactions of the Fenimore mechanism are given as follows. (Arghode & Gupta, 2010; Li & Williams, 1999; Hewson & Bollig, 1996)

$$N_2 + CH \rightarrow HCN + N \tag{6}$$

$$HCN + O \rightarrow NCO + H \tag{7}$$

The third mechanism of NO_x formation is through the reaction of nitrous oxide (N_2O) with oxygen. Although this usually represents less than the previous two procedures and it is negligible at atmospheric pressure, it is still relevant in gas turbine combustors. The reason is that the production of N_2O is favored at elevated pressures, and despite the NO_x formation does not increase proportionally, it is still not meaningless. The reactions of this mechanism are presented as follows. (Hewson & Bollig, 1996)

$$N_2 + O \rightarrow N_2O \tag{8}$$

$$N_2O + O \rightarrow 2NO \tag{9}$$

In addition, there is also the risk that the NO is further oxidized to NO_2 and then reacts with the water vapor resulting from methane combustion to form nitric acid (HNO_3). The reaction is presented in Equation (10). This process does not occur inside the combustion region, but mostly after the products are diluted and cooled down. (Boyce, 2012).

$$2NO + 3O + H_2O \rightarrow 2HNO_3 \tag{10}$$

Another common pollutant resulting from combustion process is sulfuric acid, which the reaction is given by Equation (11). Differently of the nitric oxide, the formation of sulfuric acid cannot be prevented by feasible means during the combustion process. Therefore, the best way to avoid it is removing sulfur from the fuel before it gets into the combustion chamber.

$$H_2S + 4O \rightarrow SO_2 + H_2O \rightarrow H_2SO_4 \tag{11}$$

Finally, carbon monoxide (CO) might also be present in the exhaust gases if the amount of oxygen for combustion is too low. In fact, the air discharged by the compressor is several times more than the required for a complete combustion, therefore the availability of oxygen is not a problem. However, the air has to be wisely distributed throughout the liner to provide also dilution and cooling. Boyce (2012) recommends a volumetric air-to-methane ratio of 10:1. If the mixture is richer than this, there will be carbon monoxide in the exhaust gas. The combustion reaction poor in oxygen is presented by Equation (12).

$$CH_4 + 1.5(O_2 + 4N_2) \rightarrow CO + 2H_2O + 6N_2 + \text{Heat} \quad (12)$$

3 DIFFUSIVE COMBUSTORS

According to Boyce (1982), the simplest combustor possible for a gas turbine would be a straight tube connecting the compressor outlet and the turbine inlet, where fuel is injected and burned without any barrier, as shown in Figure 1a. Such design is not feasible, firstly because the pressure loss in combustion processes is proportional to the fluid velocity squared. Considering that the flow velocity at the compressor discharge is possibly above 150 m/s, the pressure loss in the combustion chamber would represent up to a quarter of the pressure increment caused by the compressor. In addition, according to Wilson (1984) the maximum speed possible for turbulent flames is not much higher than 10 m/s, what means that the flow has to be drastically decelerated in order to keep the flame self-sustainable, without continuous ignition. The range of fuel-air mixtures that provide a stable combustion is a function of the velocity. As represented in Figure 2, the higher is the velocity, the more limited is the range of fuel-air ratio, narrowing in the direction of stoichiometric combustion until the peak velocity is achieved. After this point, no mixtures are able to produce a continuous combustion.

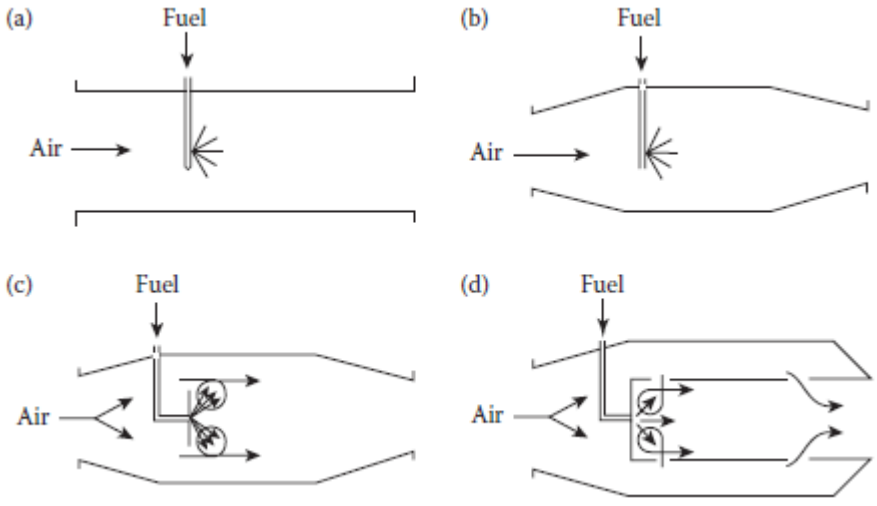

Figure 1. Development of the diffusive combustors (Lefebvre & Ballal, 2010).

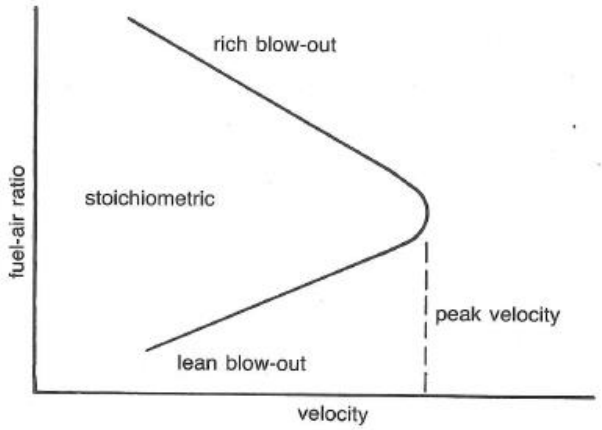

Figure 2. Range of burnable fuel-air ration in function of gas velocity (Boyce, 1982).

A diffuser at the compressor outlet is able reduce the flow velocity by about half (Figure 1b). However, even with a diffuser, the velocity is still excessively high to maintain a sustainable flame. Thus, the design of combustion chambers must include additional artifices to create a low velocity region where the flame is anchored. This is done with diverse shapes of baffles, resulting in a recirculating turbulent volume that enhances the mixing of fuel and air, competing the combustion reaction. The steady recirculating region provides the necessary conditions to keep the flame stable without continuous ignition. Nevertheless, the same characteristics that allow the flame stabilization are also responsible for high local pressure drop, and the design is then required to provide just enough turbulence as necessary for mixing and combustion, avoiding excessive losses. Figure 1c shows a possible solution with a simple plain baffle in the center, that creates the stabilization zone for the flame. (Lefebvre & Ballal, 2010; Boyce, 1982)

In fact, no real combustors are designed in this way due to poor airflow control. The amount of air necessary for stoichiometric combustion is much less than the total mass flow provided by the compressor, typically about 15%. Thereby, if the fuel-to-air ratio is excessively low, the mixture might be out of the flammability limits, characterizing a lean blow-out, as seen in Figure 2. Thus, as represented in Figure 1d, the air has to be injected in stages in order to provide just the necessary amount close to the fuel nozzle to achieve the desired fuel-air ratio. Figure 3 shows a more elaborated idea of the same principle, that is already much more similar to combustors found in commercial gas turbines. The region where the combustion takes place is called primary zone, and in diffusive combustors it needs to provide conditions close to stoichiometric for high-temperature and fast combustion. Next, in a secondary zone – or intermediate zone – additional air is injected in order to ensure complete combustion.

The last section downstream the combustor is the tertiary zone – or dilution zone – where the high-temperature combustion products are diluted with the remaining air. (Saravanamuttoo, et al., 2001)

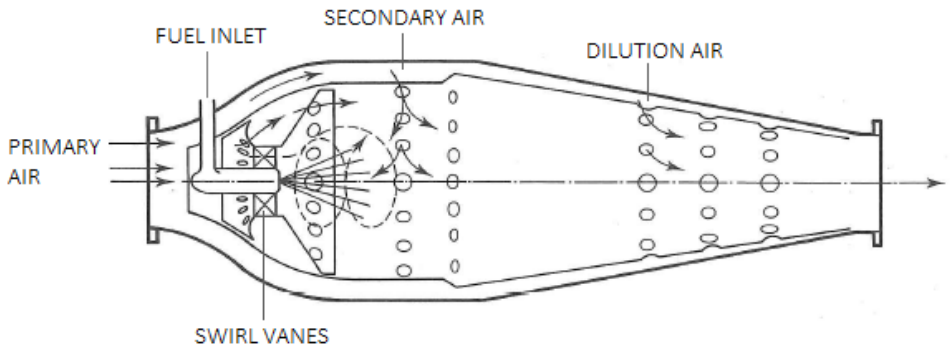

Figure 3. Design example of a conventional diffusive combustor (Saravanamuttoo, et al., 2001).

In order to produce a stable flame and enhance the combustion process, recirculation is a must in the primary zone. Some combustor designs, including the one in previous figure, admit the primary air partly into swirl vanes around the fuel injector and partly through a ring of streamwise holes close to the walls. The result is a vortex flow with low-pressure region along the axis that protects the walls of the flame tube – also called liner – from the high flame temperatures. The flame is kept within the central low-pressure region and radial jets feed the secondary air to the core of the vortex, inducing a phenomenon called toroidal recirculation that stabilizes the flame and helps to reduce soot formation. The introduction of secondary air must be done gradually and at the correct points to prevent chilling the flame that leads to incomplete combustion. The primary air represents about 15-20% of the total air mass flow, while the secondary air is about 30%. Some combustor designs do not utilize swirl vanes, as certain American models. In this case, the primary air is supplied by a ring of jets carefully positioned around the fuel nozzle to guarantee the proper recirculation. (Wilson, 1984; Saravanamuttoo, et al., 2001)

A remarkable advance regarding the aerodynamics of the primary zone was achieved by Lucas Combustion Group, combining both swirling vanes and radial jets to induce the recirculating flow. An illustration of the concept is given by Figure 4. As mentioned previously, each approach can generate the recirculation by itself. However, when they are combined with a wise positioning of the radial jets and proper angle, number and size of swirling vanes, the recirculating patterns created by each artifice are merged in a way that they complement and straighten each other. This results in increased stability, wider

operational range, enhanced ignition performance and reduced noise and pulsations. Influences from this concept can be found in the gas turbines of several British manufacturers. (Lefebvre & Ballal, 2010)

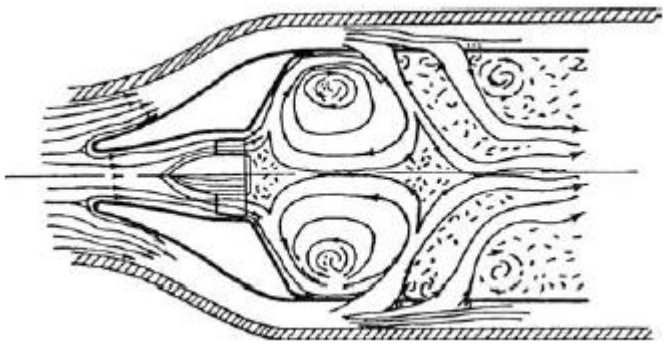

Figure 4. Primary zone concept by Lucas Combustion Group (Lefebvre & Ballal, 2010).

The flow velocity is a critical parameter in the primary zone. As mentioned before, it must be low enough to produce a moderate pressure drop and to allow a continuous flame. In addition, the mixture strength range for a stable flame is function of the velocity, as already seen in Figure 2. Different stabilization approaches, shapes and dimensions – including swirl vanes, baffles and jets – influence the limits of burnable mixtures for a fixed velocity. Usually in gas turbines the combustor is required to operate with a wide range of fuel-air ratios, therefore the design velocity is significantly lower than the maximum possible, that requires stoichiometric conditions. As an important parameter for the combustion chamber design, the gas velocity can be considered constant for all loads. This is a result of the constant speed of the compressor. Even when the mass flow changes due to load variation, the static pressure also changes, maintaining the volumetric flow approximately the same. Therefore, the velocity can be considered a constant parameter for flame stabilization. (Boyce, 2012)

In ideal conditions, the gases leave the secondary zone after complete combustion, and along the dilution zone the remaining air is injected. Thus, the hot gases are diluted, and the temperature reduced to an adequate level for the turbine inlet. The dilution zone usually has large holes in order to provide a jet that can penetrate up to the center of the stream, enhancing the turbulence and mixing to result in the most uniform temperature profile as possible. The presence of hot streaks in the flow could damage the blades of the turbine, besides increasing the formation of pollutants. In order to protect the walls of the liner from the high-temperature gases, additional small holes may be added to create the film cooling

effect, that consists in a layer of air at lower temperature close to the walls. The ideal position of the holes is a question solved by experience, experiments and CFD. (Wilson, 1984; Saravanamuttoo, et al., 2001)

3.1 Main requirements and performance parameters

According to Lefebvre & Ballal (2010), the main requirements for a combustor may vary depending on application, but in general there is a series of requisites that all combustors should satisfy. Some of them were already mentioned briefly in previous section and will be discussed more in detail. In a short summary they involve high combustion efficiency, smooth and reliable ignition, minimized pressure loss, wide flame stability limits, low emissions, no instability symptoms as pressure pulsation, shape and size in agreement with other components, reduced costs, easy to manufacture and to maintain, fuel flexibility and durability.

The combustion efficiency is a measure of the fuel burning completion. If the combustion is incomplete, the fuel does not release all its chemical energy as heat, what implies not only in increased consumption but also in more pollutants at the exhaust, as carbon monoxide (CO) and unburned hydrocarbons (UHC). In order to address current pollutant regulations, combustion efficiencies have to exceed 99%, and at no point of the operational range it should go below 90%. In order to avoid the formation of white smoke, at the least 96% is necessary (Lefebvre & Ballal, 2010). According to Boyce (2012) the combustion efficiency can be determined by Equation (12).

$$\eta_{\mathrm{b}} = \frac{\Delta h_{actual}}{\Delta h_{theoretical}} = \frac{(\dot{m}_{\mathrm{air}} + \dot{m}_{\mathrm{fuel}})h_4 - \dot{m}_{\mathrm{air}}h_3}{\dot{m}_{\mathrm{fuel}}LHV} \tag{13}$$

Where,
$h_3 =$ enthalpy of the air at combustor inlet [kJ/kg];
$h_4 =$ enthalpy of the flue gases at combustor outlet [kJ/kg];
$\dot{m}_{\mathrm{air}} =$ mass flow of the air [kg/s];
$\dot{m}_{\mathrm{fuel}} =$ mass flow of the fuel [kg/s];
$LHV =$ lower heating value of the fuel [kJ/kg].

The pressure loss occurring through the combustor cannot be eliminated, but it has to be reduced as much as possible since it impacts the fuel consumption and the power output, reducing the overall gas turbine efficiency. The total pressure loss across the combustor is a

sum of two different factors. The first regards the turbulence and skin friction caused by the flow through the internal geometry of the chamber, as it occurs in any other fluid application, and it is called cold loss. The second is related to the temperature increase caused by combustion, being called hot loss or fundamental loss. It occurs due to the density decrease related to temperature change, what ultimately increases the velocity and momentum of the flow. A force is required to allow this increase in momentum, that entails in the fundamental pressure loss. Therefore, the total pressure loss in the combustor can be defined as follows. (Saravanamuttoo, et al., 2001; Boyce, 2012)

$$\Delta p_{\mathrm{b}} = \Delta p_{\mathrm{cold}} + \Delta p_{\mathrm{hot}} \tag{14}$$

The cold losses are normally much larger than the fundamental losses, and a factor of 20 between them is common. The determination of Δp_{cold} is a classic fluid dynamics problem that depends on the geometry of the combustor. Experimentally, it can be measured as the difference between inlet and outlet pressures of the combustor when no combustion takes place. Cold losses are representative because the combustor requires certain amounts of turbulence for flame stabilization and mixing, obtained by swirl vanes, baffles and air jets along the liner. Indeed, the better is the mixing, the higher is the pressure loss, so a compromise must be found between them for an optimum design. (Saravanamuttoo, et al., 2001)

In turn, according to Lefebvre & Ballal (2010), if the flow is considered incompressible due to the low velocity and the cross-sectional area of the chamber is assumed constant, the fundamental loss can be expressed by Equation (22).

$$\Delta p_{\mathrm{hot}} = \frac{1}{2}\rho_3 u_3^2 \left(\frac{T_4}{T_3} - 1\right) \tag{15}$$

Where,
$\rho_3 =$ density of the air at the combustor inlet [kg/m³];
$u_3 =$ velocity of the air at the combustor inlet [m/s];
$T_3 =$ temperature of the air at the combustor inlet [K];
$T_4 =$ temperature of the flue gas at the combustor outlet [K].

Although the simplifications adopted are not completely true for a combustor, the result gives a fair approximation of the Δp_{hot} order of magnitude. As can be observed in Equation

(22), and as already introduced previously, the fundamental loss is proportional to the velocity squared, reaffirming the need to maintain the velocity in moderate levels. In modern literature about gas turbine design it is found that the typical range for total pressure loss through the combustor is 2-5% of the compressor discharge pressure. (Lefebvre & Ballal, 2010; Boyce, 2012)

Regarding the flame stability limits, they are a particular characteristic of each combustor design and the typical loop was shown in Figure 2. Although these limits are usually taken at the blow out point of the flame, instability is commonly observed before they are reached. This means poor combustion, with oscillations and vibration that may reduce the useful life of not only the combustion chamber, but also the turbine blades. The stable range between weak and rich limits are restrained as the mass flow increases, until a certain point which no mixture can be burned. Naturally, the combustor must be able to meet all the air-fuel ratios and mass flow ranges required by the gas turbine, which may vary substantially during acceleration and deceleration. When ramping up, for example, the fuel mass flow increases rapidly, while the air mass flow delays to reach the equilibrium point since it increases at the same peace as the engine speed. Thus, during these moments the combustor is required to work with very rich mixtures. Usually the control system of the gas turbine limits the change rate of fuel mass flow in order to prevent blow out and steep temperature transients at the turbine inlet. Nevertheless, the stability limits are affected by the pressure. Higher pressures influence the chemical reactions procedure in a way that the limits are widen. Therefore, engines that work with elevated pressure ratios present less design challenges compared to the ones with low pressure ratio. (Saravanamuttoo, et al., 2001)

The last requirement that will be emphasized in this section is the uniform temperature profile at the combustor outlet. This is important not just to avoid temperature peaks on turbine guide vanes, but also because it influences the useful level of the turbine inlet temperature. Large gradients induce lower average temperature, which leads to increased fuel consumption and reduced power output, ultimately reducing the thermal efficiency of the engine. (Boyce, 2012)

3.2 Combustor arrangements

The simplest arrangement that a combustion chamber may have is called single-can or tubular. It consists of just one liner, and the illustration shown in Figure 3 would represent the whole combustor. Alternatively, the tubular configuration may have multiple cans, arranged in a circular array, as schematically shown in Figure 5a. Another common configuration is the can-annular or tuboannular, in which each tube has its own fuel injector, but the inlet air is supplied by a common chamber, as observed in Figure 5b. A third usual combustor arrangement is the annular, shown in Figure 5c. In this case, the fuel injectors are disposed in an annulus without any physical separation between them. (Boyce, 1982)

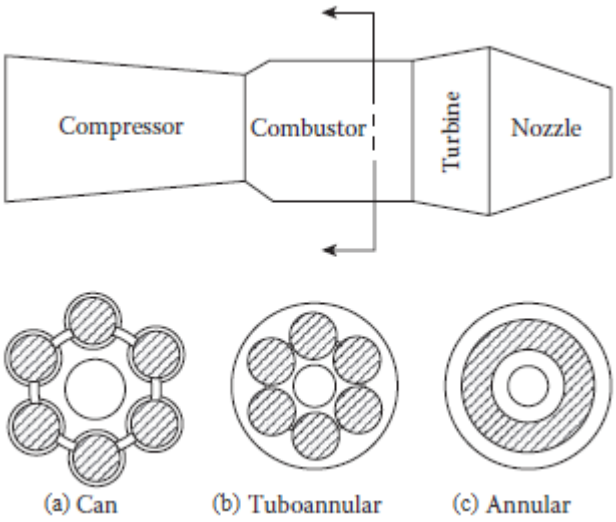

Figure 5. Multiple can (a), can-annular (b) and annular (c) combustors (Lefebvre & Ballal, 2010).

The tubular was the design employed in early gas turbines, and it has the advantages of simplicity and long lifetime due to low heat release rates. Though, these combustors can be very large depending on the turbine capacity and in such cases, the liner is composed by special tiles that are easily replaced in case of damage. In addition, they usually have multiple fuel injectors to improve the distribution of the large central flame, however, the temperature profile is still not as even as in can-annular configuration. Tubular combustors can have both straight-through and reverse-flow designs, although the second is more common. In straight-trough configuration the compressed air reaches first the primary zone, as in Figure 3, while in reverse-flow design the same air arrives first in the secondary zone, as exemplified by Figure 6. Straight-through combustors are thinner and longer than the reverse-flow option. (Boyce, 1982)

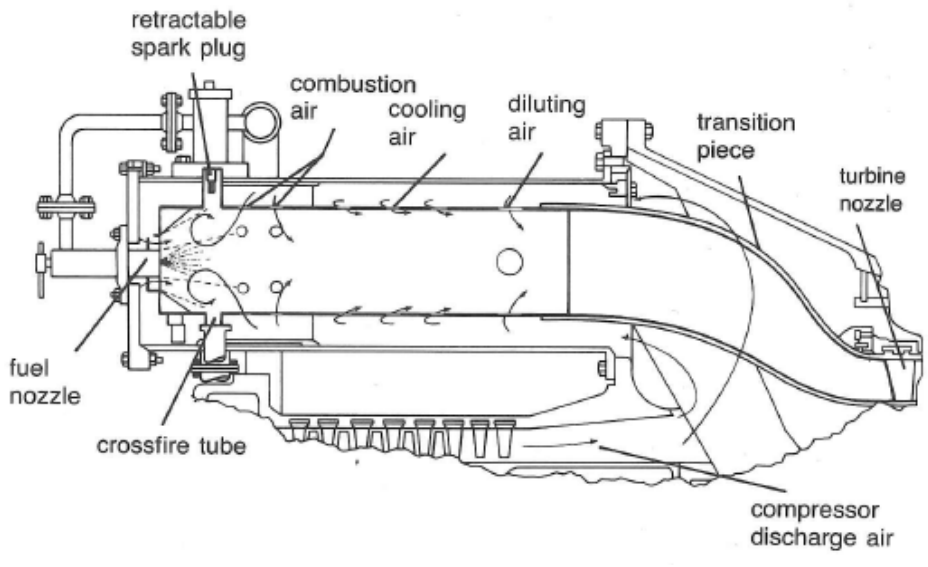

Figure 6. Reverse-flow can-annular combustor manufactured by GE (Boyce, 1982).

The can-annular is the most employed design in American gas turbines. They are easy to maintain since it is possible to remove and work on each can separately. The cans are usually connected by cross-over tubes, which have the function to equilibrate the pressure in all cans, also allowing the flame to travel from the ignition cans to all others during start-up. This increases the reliability. Can-annular combustors have better temperature distribution compared to single-can and are easier to experiment compared to annular, since just one can is required instead of the whole combustor. In addition, can-annular design is feasible for both straight-through and reverse-flow designs. The straight-through option is preferred for aircraft applications due to the smaller frontal area, while reverse-flow is more common in industrial engines. As a counterpoint, can-annular combustors require more cooling air than single-can and annular arrangements due to the larger surface area. When the fuel used has high LHV this may not be a great problem. In turn, the air required for combustion of low-LHV fuels may be up to 35% of the total air flow, reducing the amount available for cooling. (Boyce, 1982; Boyce, 2012)

Annular combustors are typically straight-trough flow and the most attractive choice regarding compactness. It makes the best use of the space available for a certain diameter, what also favors a reduced pressure loss. However, they initially presented some disadvantages against can-annular design, as the difficulty to obtain a uniform outlet temperature distribution and the unavoidable weaker structure that leads to buckling of the tube walls. They are also more difficult to maintain, and it is usually necessary to build a complete combustor with related test equipment in order to realize experimental work.

Nevertheless, these problems were greatly attacked along the years and currently the annular configuration is popular especially for aircraft applications. In addition, annular arrangement become more interesting with high temperatures or low-LHV fuels, since the amount of air required for cooling is much less compared to can-annular option. (Saravanamuttoo, et al., 2001; Boyce, 2012)

A fourth type of combustion chamber is called silo, consisting in a large cylindrical chamber externally assembled in vertical position, as presented in Figure 7. This configuration is possible in industrial gas turbines, where the space occupied is not very critical. The large size results in reduced flow velocities, consequently reducing the pressure loss. Moreover, fuels of lower quality can be burned in this design. Silo combustors are in essence similar to single-can, therefore they have similar advantages as simplicity, easy maintenance and long lifetime due to low heat release rates. (Saravanamuttoo, et al., 2001; Boyce, 2012)

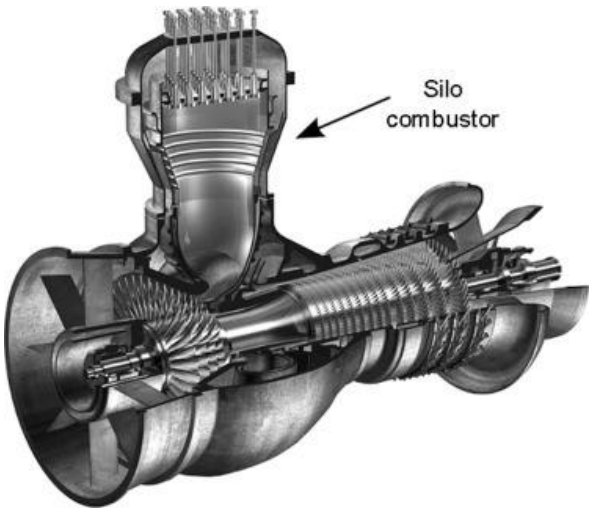

Figure 7. Silo type combustor (Andreades, et al., 2014).

3.3 Pollution control

In early gas turbine designs, the only concern about pollution was to avoid visible smoke in the exhaust gas. It has been found that soot is formed in local regions of the combustor where the mixture is rich in fuel, usually close to the fuel nozzle. They are formed when burned products are carried upstream, due to the recirculation within the primary zone, involving some amount of fuel in a high-temperature low-oxygen region. In fact, this is a common phenomenon in combustors and great part of the soot is consumed downstream in regions richer in oxygen. Therefore, the visible smoke in exhaust gases is the difference between

large amounts of soot produced and consumed within the combustor. It was found that pressure, fuel composition and the equivalence ratio influence the smoke level. In general, for pressures lower than 6 bars and equivalence ratios below 1.3, no soot is formed. An additional solution is to provide extra air to the punctual excessive rich regions. The equivalence ratio is defined by the following equation. (Lefebvre & Ballal, 2010)

$$\Phi = \frac{\dot{m}_{O_2}/\dot{m}_{\text{fuel}} \; at\ stoichiometric\ condition}{\dot{m}_{O_2}/\dot{m}_{\text{fuel}} \; at\ actual\ condition} \tag{16}$$

Where,
$\dot{m}_{O_2}$ = mass flow of oxygen [kg/s];
$\dot{m}_{\text{fuel}}$ = mass flow of fuel [kg/s].

Along the years, the concerns with other pollutants also became a major issue in combustion chamber design. It is important to clarify that the components in the exhaust gas can be divided in two categories. The major species are found in proportionally large amounts and include carbon dioxide (CO_2), nitrogen (N_2), water vapor (H_2O) and oxygen (O_2). Their concentrations are referred as percentage. The minor species, also called pollutants, involve nitrogen oxides (NO_x), carbon monoxide (CO), unburned hydrocarbons (UHC), sulfur oxides (SO_x) and other particulates measured in parts per million by volume (ppmv). In fact, this unit by itself is still vague, and it should be clarified that unless otherwise mentioned, all the values presented in this report with this unit are in dry basis and corrected for 15% oxygen (Pavri & Moore, 2001). Later, during the design process, only the molar or mass fractions of these species can be obtained from CFD solutions, therefore adequate conversions must be done. ANSYS Inc (2017) provide the following formula to convert molar fraction to ppmv, recalling that for ideal gases molar and volume fractions are the same.

$$X_{\text{ppmv}} = \frac{X_{\text{molar}} \cdot 10^6}{1 - H_2O_{\text{molar}}} \tag{17}$$

Where,
X_{ppmv} = concentration of specie X by volume in dry basis [ppmv];
X_{molar} = molar fraction of specie X [-];
H_2O_{molar} = molar fraction of H_2O [-].

Then, in order to correct the concentration obtained from Equation (16) for a reference oxygen concentration, the U.S. Code of Federal Regulations (2010) provide the following formula.

$$X_{\text{ppmv,ref}} = X_{\text{ppmv}} \frac{20.9 - O_{2,\text{molar,ref}}}{20.9 - O_{2,\text{molar}}} \tag{18}$$

Where,
$X_{\text{ppmv,ref}}$ = concentration of specie X corrected for a reference O_2 [ppmv];
$O_{2,\text{molar,ref}}$ = reference molar fraction of O_2 [-];
$O_{2,\text{molar}}$ = actual molar fraction of O_2 [-].

Although the minor species consist in a very small portion of the exhaust gases, the large mass flows involved end up releasing a significant amount of these elements. Nitrogen oxides (NO_x) and sulfur oxides (SO_x) are a concern because they are the main causes of acid rain. In addition, NO_x can react with volatile organic compounds under sunlight and form a visible pollution, called photochemical smog. Nevertheless, they are harmful to the ozone layer – a natural protection against ultraviolet rays – what can lead to increased cases of skin cancer. The carbon monoxide (CO) can lead to death if inhaled in sufficient amount and UHC is also a potential reagent for photochemical pollution. (Najjar, 2011)

The formation of NO_x has an exponential relation with the flame temperature, which the maximum is theoretically achieved at stoichiometric conditions. Moving the operational point towards either lean or rich conditions indeed reduce the NO_x, but on the other hand it increases CO and UHC formation, as shown in Figure 8. There is just a reasonably tight low-emissions window, in which NO_x and CO levels can remain below 15 and 25 ppmv, respectively, at the same time. Conventional combustors operate with a large temperature range, that can vary from 1000 K to 2500 K, however, the low-emissions span shown in Figure 8 is limited between 1670 K and 1900 K. Therefore, the intention of many approaches for emissions control is to maintain the temperature of the combustion gases in a reduced span for the whole operational range of the gas turbine. In addition, the residence time – the time that the gases recirculate inside the combustor – also has influence in emissions, although not as strong as the temperature. Reducing the residence time decreases the NO_x formation, but again in counterpart, extending it is favorable to reduce CO and UHC. Therefore, a compromise has to be found to balance these influences to the optimum point. (Saravanamuttoo, et al., 2001; Lefebvre & Ballal, 2010)

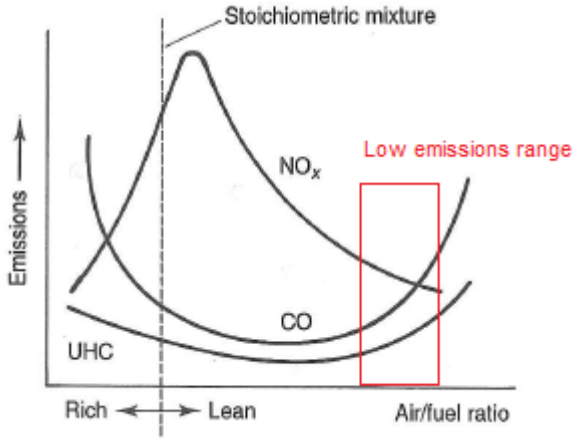

Figure 8. Emissions in function of air-fuel ratio (Saravanamuttoo, et al., 2001).

The first successful measure adopted to reduce emissions of gas turbines happened during 1970s, when it was found that injecting water or steam into the combustor could reduce up to 40% the formation of NO_x (< 75 ppmv), due to the decrease in flame temperature. In order to achieve this level, the necessary amount of water was 40% of the fuel amount, consisting in a substantial consumption. This method implies in a certain efficiency decrease, since extra fuel is required to heat up the water to the chamber temperature, but on the other hand, more power is produced by the turbine due to the additional mass flow. In addition, the water utilized has to be free of minerals, at the level of boiler feedwater, what brings a considerable extra expense. This is necessary to avoid corrosion and deposit problems at the downstream components. Further findings indicated that increasing more the water injection still reduces the NO_x, however, CO and UHC start to increase rapidly, due to the temperature relation presented previously. Despite all these concerns, water/steam injection was a successful method to control emissions while more sophisticated techniques were developed. (Pavri & Moore, 2001; Lefebvre & Ballal, 2010)

Another solution, that can be even complementary in cases which the emissions limit is extremely low (NO_x < 10 ppmv), is the Selective Catalytic Reduction (SCR). In this approach, the NO_x is not prevented but rather treated in the exhaust by the injection of a catalyst and ammonia (NH_3), leading to a reaction that transforms NO_x into N_2 and water. The chemical equations of the process are as follows. (Forzatti, 2001)

$$4NH_3 + 4NO + O_2 \rightarrow 4N_2 + 6H_2O \quad (19)$$

$$2NH_3 + NO + NO_2 \rightarrow 2N_2 + 3H_2O \quad (20)$$

$$8NH_3 + 6NO_2 \rightarrow 7N_2 + 12H_2O \quad (21)$$

The term “selective” is used because of the capacity of ammonia to react selectively with NO_x instead of oxygen, what would result in additional NO, N_2O and N_2 in case it occurs. The same ability is not observed in other potential reagents, as CO and UHC. However, these catalytic reactions occur fast enough only in the temperature range of 250-400°C, limiting the application of the method to systems featured with waste heat recovery. Moreover, the use of SRC brings additional issues, as increased costs, difficulty to operate in partial load and manipulation of dangerous fluids. (Saravanamuttoo, et al., 2001; Forzatti, 2001)

Technological advances in combustion chambers currently allow to prevent the formation of NO_x and other pollutants at the source, without the use of water or steam. This certainly eliminates many of the problems mentioned previously and although water injection is still used, dry controls are gradually replacing them. They consist in new generations of combustor design, that normally operate with lower temperatures compared to diffusive combustors. Some of them achieve this with lean combustion, as the dry low NO_x (DLN) and the RQL concepts, while others rely also on exhaust gas recirculation, as in flameless combustion (FC). These concepts are further discussed in the next sections.

4 DRY LOW NO_X/EMISSION COMBUSTORS

Dry low NO_X (DLN), or dry low emission (DLE) combustors emerged as a smart solution to mitigate pollutants formation without creating as much side effects as in water injection and catalytic reduction. With this method, it is possible to achieve NO_x emissions below 25 ppmv at the design point. The main characteristic of DLE approach is the division of fuel burning in stages, as exemplified in Figure 9. About 83-97% of the fuel is injected through the primary nozzles into a premixing region with large amounts of air to compose a lean mixture before burning. The remaining fuel is introduced pure by the central pilot nozzle, in order to ensure a reliable and continuous combustion. This strategy moves the full-load operating point from the stoichiometric condition towards the lean condition in Figure 8, corresponding to lower flame temperatures and reduced NO_x. Nevertheless, accurate control is necessary to avoid excessively lean mixtures that could result in the risk of flame blowout and increased levels of CO and UHC. (Saravanamuttoo, et al., 2001; Boyce, 2012)

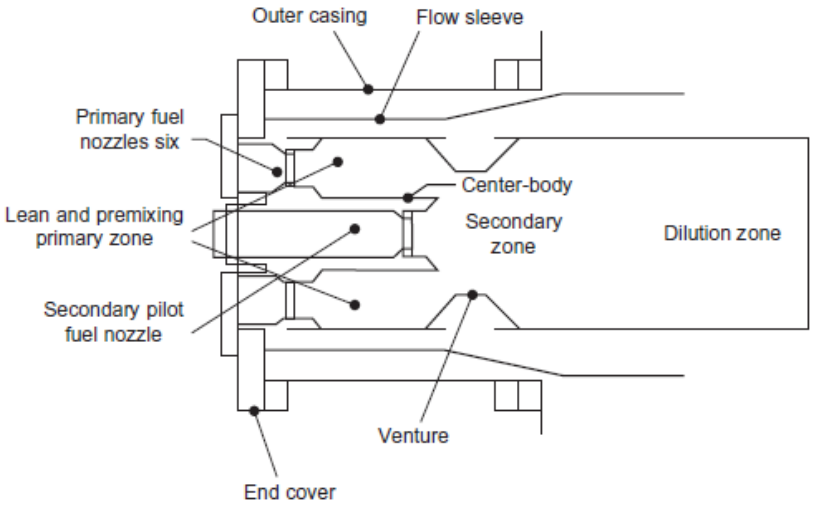

Figure 9. Dry low emission (DLE) combustor design (Boyce, 2012).

Figure 9 is the schematic of a design utilized by General Electric, in which the converging-diverging section was added to accelerate the flow and prevent the transition from the secondary zone back to the primary zone. In addition, it creates a recirculating region downstream that enhance the flame stability. Indeed, the flame in DLE combustors is not stable for a range of air-fuel mixtures as wide as in conventional diffusion combustors. However, this is the price to be paid for lower NO_x emissions. The fact is that the air-fuel mixture has to be more precisely controlled for all loads in order to keep the DLE combustion stable. Issues as oscillations in fuel composition, heating value (LHV), environmental conditions, grid frequency and transient load irregularities may influence the flame stability. In case of flame extinction, the combustion cannot be reestablished safely without shutting the engine down and restarting the ramp up procedure. (Saravanamuttoo, et al., 2001; Boyce, 2012)

Dry low emission combustors are especially sensitive to sudden load changes. In order to overcome this problem, fuel-staged or air-staged designs are employed, as schematically presented in Figure 10. The fuel-staged with two zones is the most used configuration, in which the fraction of air supplied to each zone is constant, while the fuel is dosed differently for each operating condition. In turn, the air-staged combustor controls the airflow, deviating part of the air directly to the dilution zone when operating in low load. Nevertheless, the two techniques can be combined. (Boyce, 2012)

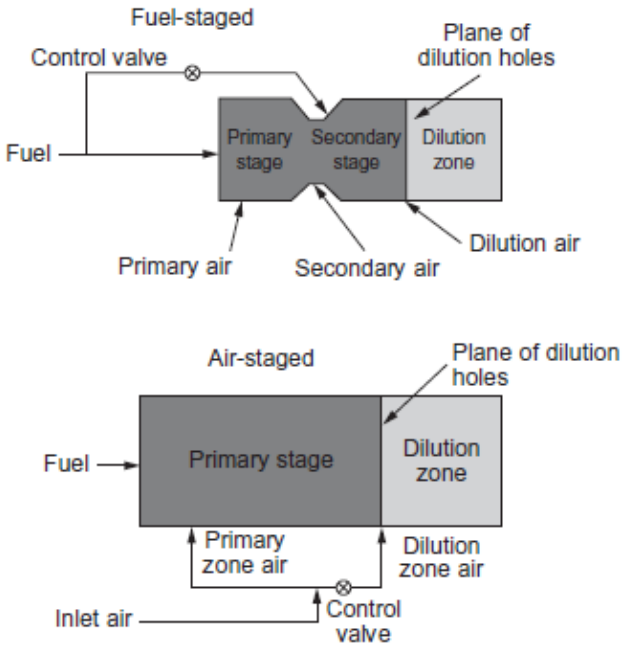

Figure 10. Fuel-staged and air-stage schematic concepts (Boyce, 2012).

A fuel-staged combustor with design similar to the one presented in Figure 9 would have four different operating modes. In the first, from ignition to 20% load, all the fuel is supplied to the primary nozzles and the flame stays in the primary zone only. Next, in the range of 20-50% load, about 30% of the fuel is injected in the pilot nozzle and lean combustion is induced in both primary and secondary zones. The third operation mode is only used during the transient to loads above 50%, in which all the fuel is supplied to the pilot nozzle and combustion takes place only in the secondary zone. This mode is utilized to extinguish the flame in the primary zone, since it has to be utilized as premixing chamber in the last operating mode. Finally, from 50% to 100% load, fuel is injected in all nozzles, with at the least 83% going to the primary nozzles and the remaining to the central pilot nozzle. The primary zone is then used for premixing and the combustion happens just in the secondary zone. The premixing mode produce the lowest levels of emissions. (Saravanamuttoo, et al., 2001; Boyce, 2012)

5 RICH-BURN, QUICK-MIX, LEAN-BURN COMBUSTOR (RQL)

The RQL combustor, as the name suggests, relies on a sequence of three processes to achieve low-emission combustion. It takes advantages of both rich and lean burn characteristics. In order to provide high reliability and flame stability, a rich mixture is burned at the primary zone, with equivalence ratio between 1.2 and 1.8. This results in low NO_x production due to

the relatively low temperature and low oxygen concentration, but with the penalty of increased CO and UHC (see Figure 8). Therefore, additional air is necessary to further oxidize CO and unburned hydrocarbons. If this air is gradually injected, the process will follow the high NO_x route show in Figure 11, due to the relatively large time close to stoichiometric conditions, that are associated with high temperatures. (Samuelsen, 2006)

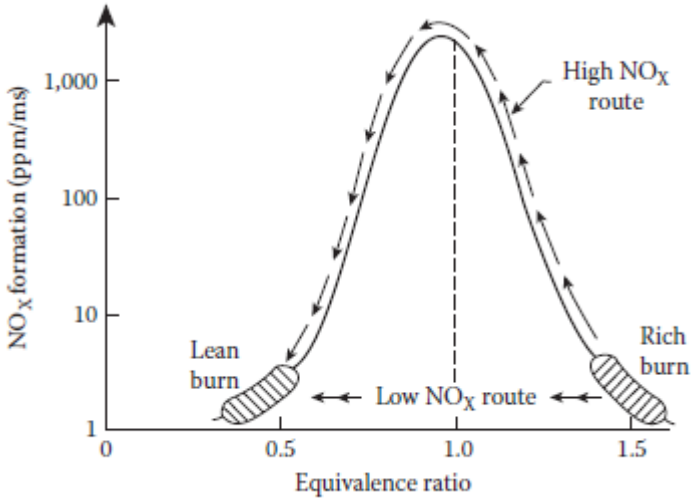

Figure 11. Principle of RQL combustion (Lefebvre & Ballal, 2010).

However, if the amount of air necessary to complete the combustion and to create lean conditions is injected in a very short time, stoichiometric conditions are nearly prevented and small amounts of NO_x are formed in the transition, following the low NO_x route of Figure 11. This is the "quick mix" step, and it is the main concept behind RQL combustors. At the secondary zone, where lean conditions are imposed, the temperature has to be low enough to control the NO_x formation, but it needs a certain lever to consume the remaining unburned hydrocarbons, carbon monoxide and soot. The equivalence ratio for lean burn is typically between 0.5 and 0.7. Figure 12 shows a schematic section of a RQL combustor. (Lefebvre & Ballal, 2010)

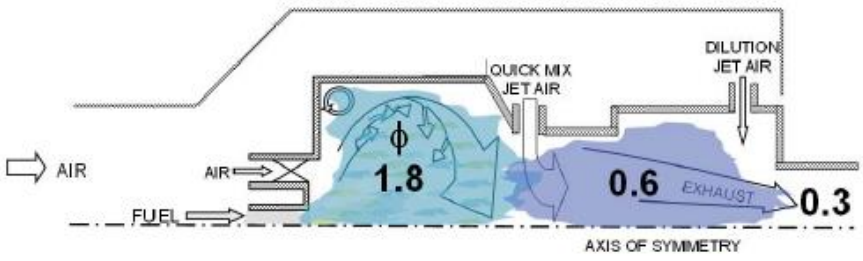

Figure 12. Schematic design of a RQL combustor (Samuelsen, 2006).

One of the challenges in RQL design is the overheating of the liner at the primary zone. The use of conventional film cooling is not possible in this region in order to avoid near-stoichiometric mixtures close to the walls, that are associated with high NO_x production. Therefore, the materials have to be carefully selected for this application. Another technique to mitigate the problem is making the air flow outside the liner before it enters the primary zone, providing a backside cooling. An additional and perhaps more complex challenge is the quick-mix region design. The effectiveness of the RQL combustor in preventing emissions is directly connected to the performance in mixing the air and primary zone outlet gases. It is during this process that the mixture passes through the stoichiometric point, and it must be fast enough to produce insignificant amounts of NO_x. Therefore, most of the researches regarding these combustors have historically been focused in the development of the quick-mix section. (Samuelsen, 2006; Lefebvre & Ballal, 2010)

The RQL concept is applied in commercial aircraft engines by Pratt & Whitney, due to its higher reliability and performance throughout the whole operational range compared to lean premixed combustors. In industrial applications, DLN combustors are the typical choice, since the reliability is less critical to safety, the operational range is reduced, and the NO_x emissions are considerably lower compared to RQL. However, there is a growing interest in RQL combustors for stationary applications since they can effectively operate with fuels of complex and varying composition, what is more problematic for DLN design. This is relevant because of the global movement towards renewable fuels, what includes biomass derivatives, such as landfill gas and digester gas, that may not have the same quality as natural gas. (Samuelsen, 2006)

6 FLAMELESS DISTRIBUTED COMBUSTION

One of the methods that is receiving substantial attention from combustion researchers currently is the flameless distributed combustion. This topic had origin in 70s, when it was observed that recirculating exhaust gases in a high temperature furnace produce no flame or UV-signal, although the fuel still burns smoothly and stably with very low NO_x emissions. Different research lines gave origin to diverse combustion methods based on this phenomenon, as Flameless Combustion (FC), Colorless Distributed Combustion (CDC), Moderate or Intense Low Oxygen Dilution (MILD), High Temperature Air Combustion (HiTAC) or Flameless Oxidation (FLOX). Even though these methods have some

differences, all of them rely on the same essential principles: provide exhaust gas recirculation and operate above the self-ignition temperature. The terms “colorless” and “flameless” are adopted because the combustion process is not visible, or at the least require special conditions to be visible. In turn, the “distributed” means that the combustion takes place uniformly in a large volume of the combustor, instead of being concentrated in a delimited stable flame. (Khidr, et al., 2017; Xing, et al., 2017)

Flameless combustion is a stablished technology in furnace applications at atmospheric pressure, especially through the methods HiTAC and FLOX, and it has already proven its potential for very low emissions (NO_x < 10 ppmv). Currently, the challenge is to improve the understanding of this phenomenon in order to allow its application in gas turbines. As already shown by previous studies, the method has great versatility, being able to burn virtually any kind of fuel – solid, gaseous or liquid – including biomass derivatives and low calorific value fuels. This is an important factor due to the different employments of gas turbines in both industrial and aircraft fields. (Khalil & Gupta, 2017; Khidr, et al., 2017; Kruse, et al., 2015)

As firstly introduced by Wünning & Wünning (1997), in order to achieve the flameless combustion regime, a high recirculation rate of exhaust gases is necessary, as shown in Figure 13. In fact, recirculation can also effectively reduce the NO_x formation in flame combustors, due to the addition of inert gases to the flow and reduction of peak flame temperature. However, in order to keep a safe margin from the unstable region, the recirculation rate must be low in these cases. The recirculation rate is defined by Equation (22).

$$K_{\mathrm{FG}} = \frac{\dot{m}_{\mathrm{FG}}}{\dot{m}_{\mathrm{fuel}} + \dot{m}_{\mathrm{air}}} \tag{22}$$

Where,
$\dot{m}_{\mathrm{FG}}$ = mass flow rate of recirculated exhaust gases [kg/s].

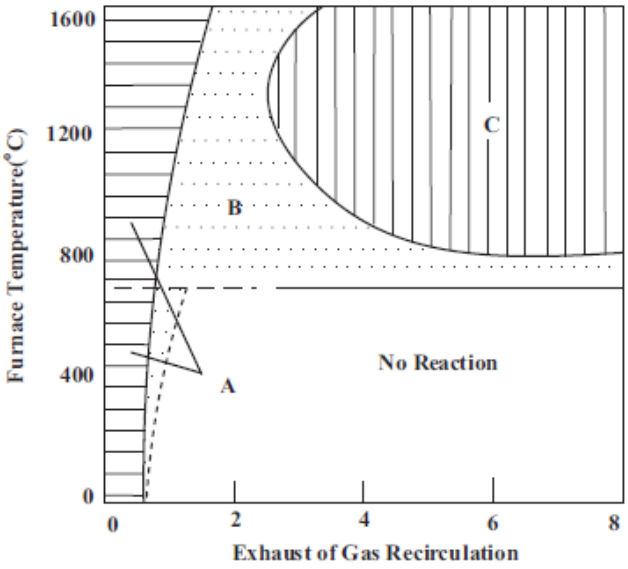

Figure 13. Diagram of combustion stability. A – stable flame, B – unstable flame, C – flameless combustion (Xing, et al., 2017).

It is important to clarify that just the exhaust gases recirculating into the air and fuel before the beginning of the reaction are considered recirculated exhaust gases. Thus, the recirculation inside the combustion zone is not taken into account here. As observed in Figure 13, stable flame combustion is possible in the whole range of temperatures with low recirculation rates (zone "A"). However, if the recirculation rate is higher than 0.3 during the startup – limit that rises slightly in high temperatures – the combustion become unstable. The flame starts to be carried downstream until it blows out (zone "B"). Nevertheless, under certain conditions of high recirculation rate and high furnace temperature, the fuel is burned in a very stable form, without any visible or audible signs, that characterizes the flameless combustion (zone "C"). From the previous diagram, it is noticed that FC is not possible in a cold chamber. In fact, the combustor temperature has to be above the self-ignition temperature of the fuel in order to reach this special regime, thus it is necessary to preheat the combustor with flames before switching to flameless operation. (Wünning & Wünning, 1997; Levy, et al., 2004)

The exhaust gas recirculation (EGR) can be realized in two different ways, externally or internally. External recirculation in a gas turbine consists in take part of the exhaust gases from the turbine or recuperator outlet and drive it back to the compressor inlet. Such procedure is necessary because of the pressure difference between the combustion chamber and the turbine discharge. Figure 14 illustrates the externally recirculated cycle proposed by

Cameretti, et al (2013). Here, a recuperator by-pass is added to give flexibility between electrical and thermal outputs, since it was designed for CHP.

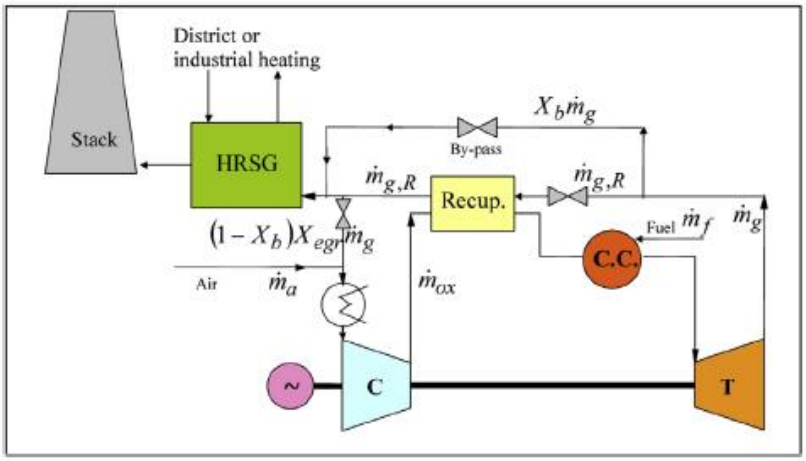

Figure 14. Gas turbine schematic cycle with external EGR (Cameretti, et al., 2013).

Although the NO_x emissions were greatly reduced in this case, the higher temperatures at the compressor inlet results in a severe penalty to the cycle efficiency, being that a 0.3 recirculation rate caused 2% decrease in thermal efficiency (Cameretti, et al., 2013). Considering that to approach flameless combustion regime a recirculation rate of 3 or more might be necessary, the external EGR is not practical for this purpose.

In turn, internal exhaust gas recirculation is achieved with an aerodynamically favorable combustor design. In this way, the exhaust gases are recirculated before they leave the combustion chamber, avoiding the drastic efficiency loss of the previous method. The high recirculation rate of hot products helps to maintain the chamber temperature above the self-ignition temperature of the fuel, ensuring a continuous combustion. This also characterizes the combustor as adiabatic, since the gases are recirculated before any heat is extracted from them, which is a difference between gas turbine and industrial furnace applications. An additional difference is the higher pressure levels in gas turbines. (Wünning & Wünning, 1997; Levy, et al., 2004)

Flameless combustion is characterized by a very homogeneous thermal field, differently from a stable flame, that has very high temperature and concentration gradients. Due to the internal and adiabatic EGR at high rates, the temperature rise in the reaction is relatively small, in the range of few hundreds Kelvin, while the reacting volume is large. The lower temperature favors a decreased NO_x formation and reduce or even eliminate the necessity to cool the liner and to dilute the hot gases before the turbine inlet. In addition, the thermal

uniformity prevents hot streaks, providing a balanced radial temperature profile near the combustor outlet. This avoids excessive thermal stresses in the turbine blades, extending the lifetime of the components and reducing maintenance costs. (Levy, et al., 2004; Khidr, et al., 2017; Khalil & Gupta, 2017)

In addition to the high EGR rate and temperatures above the fuel self-ignition, strong turbulence is required especially close to the inlets, in order to achieve a very homogeneous mixture of exhaust gases, air and fuel before the combustion reaction. Uniformity is important to avoid localized peaks of temperature that lead to increased NO_x formation. After all, there is no point in reducing the average temperature of the flame if hot spots are still present. Ideally, for flameless combustion, the fuel should be injected just after a complete mixing of combustion air and recirculating exhaust gases. In this way, premature ignition in the unstable flame region is avoided. (Wünning & Wünning, 1997; Levy, et al., 2004; Kruse, et al., 2015; Khidr, et al., 2017)

Several combustor designs have been proposed in order to optimize the conditions for FC operation. Arghode, et al (2012) grouped in a list more than 30 combustor models based in flameless oxidation, with the respective main parameters. About a third was specifically designed for gas turbine purposes, what means higher thermal density (>15 MW/m^3). The configurations included straight-through and reverse flow, with fuel being supplied at the same side, opposite side or in cross flow with the air inlets. The inlet air velocity in most of the cases dedicated to gas turbines is above 140 m/s, while the fuel inlet velocity is in average slightly below 100 m/s. These magnitudes are remarkably higher than the required to maintain a stable flame. Regarding the emissions, most of them achieved very NO_x, with levels below 10 ppmv, while the CO did not show any pattern, varying from below 10 ppmv up to 220 ppmv. An important design parameter is the equivalence ratio, that for all these designs was set in the range of 0.4 to 0.7.

Plessing, et al (1998) realized laser-optical measurements in an experimental flameless combustor developed by the German company WS Wärmeprozesstechnik (Figure 15), in order to improve the understanding of the phenomena. The design is reverse-flow with fuel inlet, air inlet and exhaust gases outlet located all at the same side and it can operate both in stable flame and in flameless modes. Initially, the air from “3” and fuel from “1” are mixed in the volume “2” and ignited to produce a stable flame that heats up the chamber.

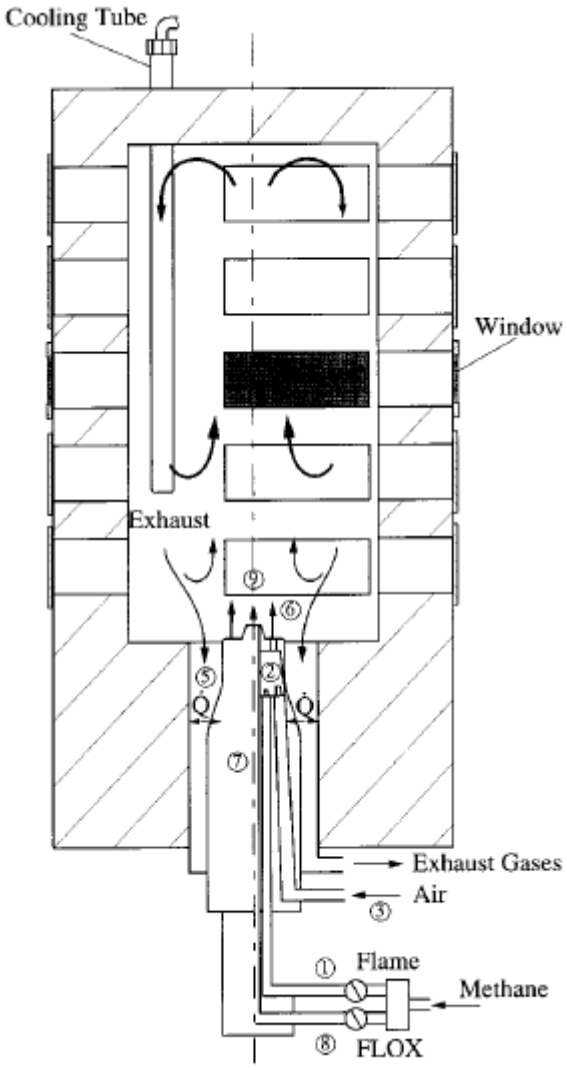

Figure 15. Experimental reverse-flow flameless combustor (Plessing, et al., 1998).

When the temperature suitable for flameless regime is achieved (in this case 800°C), the fuel supply is switched from "1" to the main central tube "8". At this moment the flames extinguish, and the incoming air is mixed with a substantial amounts of exhaust gases before it reaches the central fuel jet. The mixture of air, fuel and exhaust gases are continuously heated up by the recirculating gases while moving downstream, until the fuel is self-ignited and the flameless oxidation takes place. A sudden drop in NO_x levels is observed in the exhaust gases when the transition occurs, as shown in Figure 16. The portion of exhaust gases that are not recirculated leaves the chamber through the annular channel "5" and proceed to the thermal process where it is required.

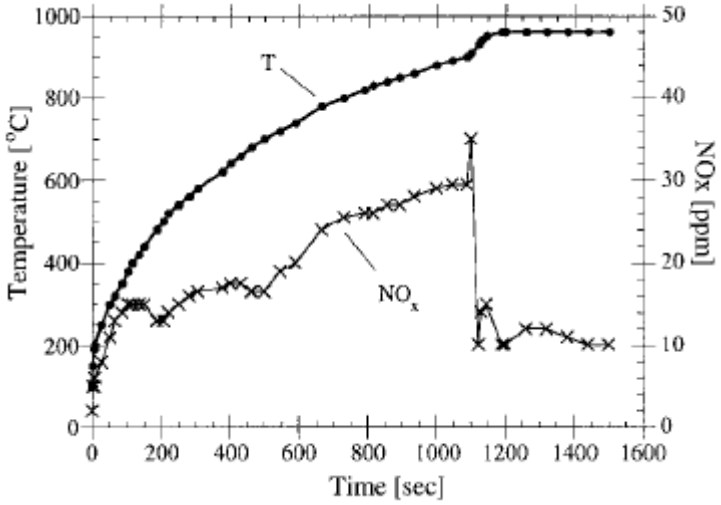

Figure 16. Temperature and NO_x formation along the time (Plessing, et al., 1998).

Kruse, et al (2015) refined the previous design for gas turbine application, proposing a new nozzle that partially premix the air and fuel even in flameless operation. The design is shown in Figure 17. Another difference is that the initial heating is provided by an auxiliary small chamber located at the opposite side.

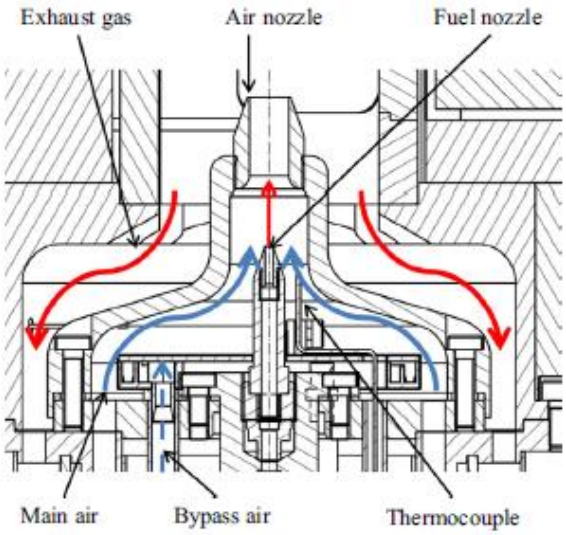

Figure 17. Air and fuel nozzle (Kruse, et al., 2015).

The authors conducted both CFD simulations and experiments, firstly at atmospheric pressure, and after at 2.5 and 5 bars, aiming to determine the pressure influence to achieve flameless combustion. The results indicated that at atmospheric pressure and with inlet air temperature of 873 K, the optimal equivalence ratio for very low NO_x and CO formation (< 10 ppmv) is in the range of 0.3 to 0.5. In addition, the reduction of the air nozzle diameter – resulting in increased velocity – demonstrated to enhance the exhaust gas recirculation and reduce NO_x. Though, when the pressure was increased while keeping the same nozzle

diameter and mass flow, the emission became higher. According to the authors, the effect is related to consequent modifications on NO_x formation chemistry and longer residence time, since the inlet velocity is reduced. The range of optimum equivalence ratios for coupled low NO_x and CO became lower and tighter for increased pressures, being $\Phi = 0.25$-0.40 for 2.5 bars, and $\Phi = 0.25$-0.30 for 5 bars. It might be highlighted that the lower theoretical flammability limit is $\Phi = 0.20$. Nevertheless, when the nozzle diameter was changed in order to equalize the inlet velocity for all pressures, the emissions demonstrated to be even lower at higher pressures compared to atmospheric level. This emphasizes the importance of the velocity and recirculation in order to achieve the conditions for flameless combustion. The authors also reported a flame close to the nozzle under higher pressures, what may indicate a design problem due to the premixing of air and fuel before any contact with the exhaust gases. (Kruse, et al., 2015)

Veríssimo, et al (2013) conducted a study with a 10 kW straight-through combustor fueled by methane in order to determine the influence of the inlet air velocity and the equivalence ratio on the establishment of flameless combustion. The variation in velocity was achieved by changing the diameter of the air nozzle, therefore, keeping the mass flow constant. The air inlet is positioned at the axis of the combustor, while the fuel is injected by 16 orifices distributed in a circle around the air nozzle, as seen in Figure 18. The inlet fuel velocity was fixed in 6.2 m/s, the equivalence ration in 0.77 and the air inlet velocity was varied in the range of 113 to 311 m/s. The results shown that flameless combustion was possible in all cases, with a trend to decrease the maximum temperatures with higher air inlet velocities, due to the better recirculation and entrainment rate with exhaust gases and fuel. The CO emissions increased gradually with higher velocities, while NO_x reduced. Overall, the lowest emissions were achieved with the lowest velocity, but in all cases the levels stayed below 21 ppmv for CO and 7 ppmv for NO_x, demonstrating the effectiveness of the method. It was also found that, for this combustor configuration, there is a critical minimum momentum for the air inlet jet, below which it is not possible to establish flameless combustion due to lack of recirculation. This minimum momentum increases if the equivalence ratio is reduced until 0.58. Below this level, flameless combustion is not possible anymore independent of the inlet air momentum, what may represent limitation of this design for gas turbine applications.

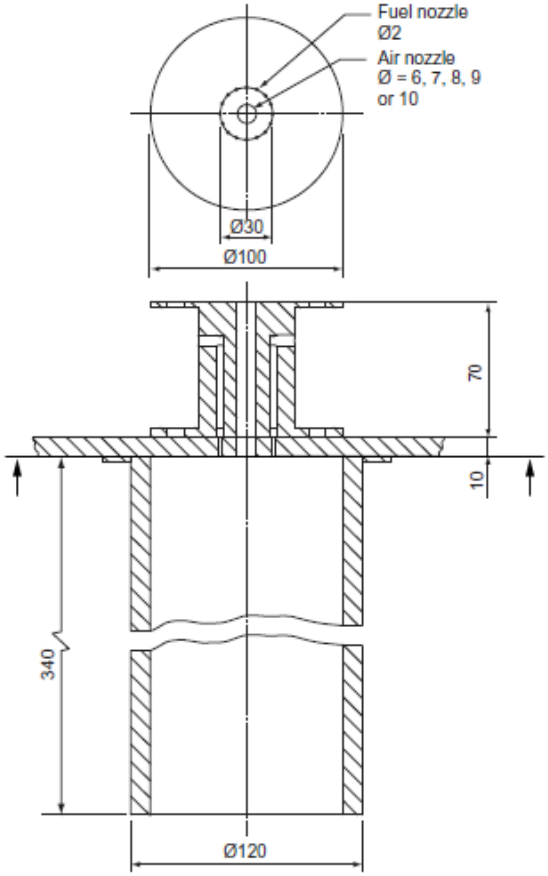

Figure 18. Straight-through flameless combustor (Veríssimo, et al., 2013).

Several other configurations have been proposed to enable flameless combustion in gas turbines. Lammel, et al (2010) presented the straight-through model shown in Figure 19a, in which the fuel and air are injected partially premixed by twelve high-momentum jets, organized in annular form (left side of the figure). The high velocity of the jets creates a vortex at the center for the first third of the chamber, where the exhaust gases are recirculated. The model was simulated numerically with pressures up to 7 bars, being able to achieve NO_x levels below 10 ppmv. Galletti, et al (2007) studied experimentally and numerically the burner shown in Figure 19b, that consists in a reverse-flow design. Fuel and air are injected axially in the inner tube, where the reaction takes place. At the end of this tube, the gases are driven back through the outer annular chamber and leaves the combustor at the same plane of the inlet. Windows positioned at the beginning of the inner tube provide the recirculation required for flameless combustion. This burner could achieve NO_x emissions as low as 30 ppmv.

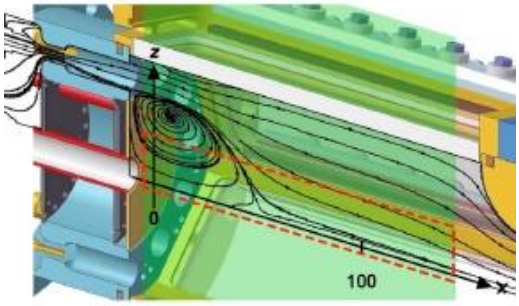

(a)

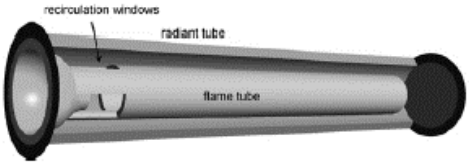

(b)

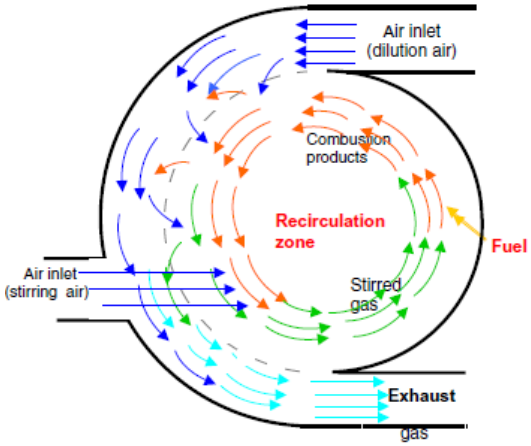

(c)

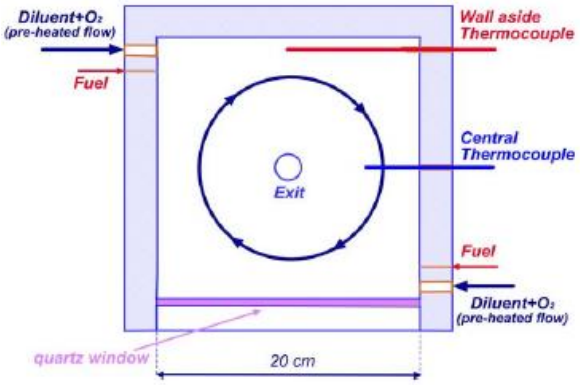

(d)

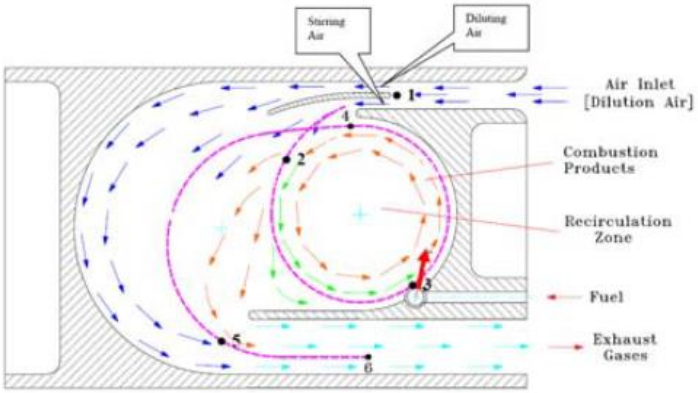

(e)

Figure 19. Flameless combustor designs proposed by (a) Lammel, et al (2010), (b) Galletti, et al (2007), (c) Levy, et al (2004), (d) Sorrentino, et al (2015), (e) Rao & Yeshayahou (2010).

The combustors of Figure 19c and Figure 19e were presented by Levy, et al (2004) and Rao & Yeshayahou (2010), respectively. Although the designs are slightly different, especially regarding the position of the stirring air inlet, the concepts are very similar. Both rely on a radial flow configuration, in which the geometry favors the establishment of a round recirculating zone and the mixing of the streams occur due to centrifugal forces. Numerical

or experimental performance data were not available for these models. Finally, the design of Figure 19d was introduced by Sorrentino, et al (2015). It consists in a cuboid geometry with the air and fuel nozzles located adjacently to two opposite faces, creating a cyclonic flow pattern, while the exhaust gases leave the combustor through an axial passage. This configuration provides great mixing of reactants and extended residence time. Experiments and numerical simulations were done with this combustor utilizing diluted propane (C_3H_8) as fuel, air inlet velocity of 39 m/s and fuel inlet velocity of 50 m/s. The stable and distributed flameless regime was achieved when the air inlet temperature surpassed 800°C. No information about emissions were provided.

7 PRE-DESIGN

The first step in a gas turbine combustor design procedure is the definition of the concept to be adopted. Taking into account its potential to achieve very low emission levels, the capacity to operate with different fuels and the necessity for further research in the area, the flameless combustion concept was chosen.

Before any design choice or definition can be done, it is necessary to know the requirements of the component. The combustion chamber designed in the present study is intended for a 2-kW_{el} micro gas turbine, able to run on natural gas and landfill gas. Since the other components were not designed yet, a cycle calculation is necessary to obtain input values for pressures, temperatures and mass flows.

7.1 Fuel analysis

The fuel composition has high influence on the internal chemistry and thermodynamics of the combustor, especially about the mass flows required for a given thermal power. Therefore, this section analyses the two fuel options considered for the combustion chamber design: natural gas and landfill gas. Methane (CH_4) is the main component of natural gas, usually representing 87-97% of the total moles, while nitrogen (N_2) and carbon dioxide (CO_2) account for 0.2-5.5% and 0.05-1.0%, respectively. Other hydrocarbons are also present in natural gas, as ethane (C_2H_6), propane (C_3H_8), butane (C_4H_{10}) and pentane (C_5H_{12}), that together might represent 1.5-12% of the total moles. The landfill gas – here considered without upgrading – has lower quality than the natural gas, with methane varying

between 45-60%, carbon dioxide in the range of 40-60% and nitrogen 2-5% of the total. Residual amounts of oxygen, hydrogen, sulfide and other components are also present in both fuels, but they are disregarded for the purpose of this study. (Union Gas Ltd., 2017; MDEP, 2016)

Table 1 presents the molar composition assumed for these two fuels. In the case of natural gas, all hydrocarbons are considered as methane since no significative differences were found in overall heating value and oxygen requirements for combustion with this simplification.

Table 1. Composition and oxygen required for stoichiometric combustion.

Compound	Composition [% mole]	Molar mass [g/mol]	Composition [% mass]	Mols / kg Fuel	Mols O_2 required
Natural gas					
Methane (CH_4)	98.00	16.0425	96.087	59.895	119.790
Nitrogen (N_2)	1.50	28.0134	2.568	0.917	-
Carbon dioxide (CO_2)	0.50	44.0095	1.345	0.306	-
Landfill gas					
Methane (CH_4)	50.00	16.0425	27.002	16.832	33.663
Nitrogen (N_2)	2.00	28.0134	1.886	0.673	-
Carbon dioxide (CO_2)	48.00	44.0095	71.112	16.158	-

Table 1 also shows the conversion of the composition from molar percentage to mass percentage, realized with Equation (23). Then, the number of moles of each specie in one kilogram of fuel is calculated dividing the mass fraction by the molar mass. Finally, the number of oxygen moles necessary for stoichiometric combustion can be found. As seen previously in Section 2, each mole of CH_4 requires two moles of O_2 for complete combustion.

$$F_{\mathrm{m},i} = \frac{F_{\mathrm{v},i} M_i}{\sum F_{\mathrm{v},i} M_i} \tag{23}$$

Where,
$F_{\mathrm{m}} =$ mass fraction of the compound [-];
$F_{\mathrm{v}} =$ molar fraction of the compound [-];
$M =$ molar mass of the compound [g/mol];
$i =$ index of each compound in the fuel [CH_4, N_2, CO_2].

According to Bauer & Forest (2001), the lower heating value (LHV) of pure methane is 50.020 MJ/kg. Therefore, utilizing the mass fractions calculated above it is possible to find the LHV of the natural gas and the landfill gas, as shown in Table 2. In the same table, all the steps taken to calculate the mass of air necessary for stoichiometric combustion per kilogram of fuel are presented. In gas turbines, the oxygen is taken from atmospheric air, that is composed by approximately 79% of nitrogen and 21% of oxygen, neglecting residual elements (Mackenzie & Mackenzie, 1995). Therefore, the amount of N_2 corresponding to the amount of O_2 required to complete the combustion is necessarily added together into the chamber. It is observed that the landfill gas demands about one fourth of the air needed by the natural gas for stoichiometric combustion, due to the lower amount of methane in composition.

Table 2. Fuels low heating value (LHV) and calculation of stoichiometric air.

Parameter	**Natural gas**	**Landfill gas**	**Unit**
Fuel LHV	48.06	13.50	MJ/kg
Moles of O_2 required	119.79	33.66	mols / kg Fuel
Fraction of O_2 in the air	21%	21%	-
Corresponding moles of N_2	450.64	126.64	mols / kg Fuel
Molar mass of O_2	31.9988	31.9988	g/mol
Molar mass of N_2	28.0134	28.0134	g/mol
Mass of O_2 required	3.833	1.077	kg O_2 / kg Fuel
Corresponding mass of N_2	12.624	3.548	kg N_2 / kg Fuel
Mass of air required	16.457	4.625	kg Air / kg Fuel

The last step in the fuel analysis consists in evaluate the stoichiometric gas resulting from combustion of each fuel. Here, the stoichiometric gas is defined as the products of the reaction between the fuel and the stoichiometric amount of air. The flue gas that arrives at the turbine inlet is the sum of the stoichiometric gas with the amount of air not used for reaction. A mass balance in the combustor provides the following equation, in accordance to Backman et al (2002).

$$\dot{m}_{\text{air,in}} + \dot{m}_{\text{fuel}} = \dot{m}_{\text{air,out}} + \dot{m}_{\text{SG}} \tag{24}$$

Where,
$\dot{m}_{\text{air,in}}$ = inlet air mass flow [kg/s];

$\dot{m}_{\text{fuel}}$ = fuel mass flow [kg/s];
$\dot{m}_{\text{air,out}}$ = non-reacting air mass flow [kg/s];
$\dot{m}_{\text{SG}}$ = stoichiometric gas mass flow [kg/s].

The natural gas combustion can be derived from Equation (2), that regards the pure methane. If the additional compounds are added in the molar proportions described in Table 1, the reaction become as shown in Equation (25), and after simplifications the final form is presented by Equation (26).

$$98[CH_4 + 2(O_2 + 4N_2)] + \frac{3}{2}N_2 + \frac{1}{2}CO_2 \Longrightarrow 98(CO_2 + 2H_2O + 8N_2) + \frac{3}{2}N_2 + \frac{1}{2}CO_2 + \text{Heat} \quad (25)$$

$$CH_4 + 2O_2 + \frac{1571}{196}N_2 + \frac{1}{196}CO_2 \Longrightarrow \frac{197}{196}CO_2 + 2H_2O + \frac{1571}{196}N_2 + \text{Heat} \quad (26)$$

The same is done for landfill gas, in which the carbon dioxide represents a much more significative parcel. The reactions are presented by Equations (27) and (28).

$$50[CH_4 + 2(O_2 + 4N_2)] + 48CO_2 + 2N_2 \Longrightarrow 50(CO_2 + 2H_2O + 8N_2) + 48CO_2 + 2N_2 + \text{Heat} \quad (27)$$

$$CH_4 + 2O_2 + \frac{201}{25}N_2 + \frac{24}{25}CO_2 \Longrightarrow \frac{49}{25}CO_2 + 2H_2O + \frac{201}{25}N_2 + \text{Heat} \quad (28)$$

At this point the molar composition of air, fuels and stoichiometric gases are known, allowing the calculation of their properties. The methods utilized for this purpose are described in the next section.

7.2 Compounds and mixture properties

In order to calculate the cycle thermodynamics, which will provide requirements for the combustor design, some properties of the gases need to be known, as the gas constants, specific heat capacities and specific enthalpies. Since the molar composition of the relevant gases for this project were defined previously, the next step consists in establish functions to calculate the properties of each of these compounds. Based on data provided by McBride, et

al (1993), empirical polynomial correlations are defined for molar heat capacity and molar enthalpy as follows:

$$\frac{C_p(T)}{R} = a_1 + a_2 T + a_3 T^2 + a_4 T^3 + a_5 T^4 \tag{29}$$

$$\frac{H(T)}{RT} = a_1 + a_2 \frac{T}{2} + a_3 \frac{T^2}{3} + a_4 \frac{T^3}{4} + a_5 \frac{T^4}{5} + \frac{b_1}{T} \tag{30}$$

Where,
C_p = molar heat capacity [J/(mol K)];
H = molar enthalpy [J/mol];
R = universal gas constant, 8.314510 J/(mol K);
T = temperature [K].

The coefficients a_i and b_1 are singular for each compound and given by McBride, et al (1993). The specific heat capacities and the specific enthalpies are then found dividing the previous values by the molar mass of the specie, as follows.

$$c_p(T) = \frac{C_p(T)}{M} \tag{31}$$

$$h(T) = \frac{H(T)}{M} \tag{32}$$

Where,
c_p = specific heat capacity [J/(kg K)];
h = specific enthalpy [J/kg];
M = molar mass [kg/mol].

These functions were implemented for oxygen, nitrogen, carbon dioxide, water vapor and methane. Once the properties of each compound are accessible, the specific heat capacities, specific enthalpies and gas constants of the mixtures are calculated as follows.

$$c_{p,mix}(T) = \sum F_{\mathrm{m},i} c_{p,i} \tag{33}$$

$$h_{\mathrm{mix}}(T) = \sum F_{\mathrm{m},i} [h_i(T) - h_i(273.15\ \mathrm{K})] \tag{34}$$

$$R_{\mathrm{mix}} = \sum \frac{R}{M_i} F_{\mathrm{m},i} \tag{35}$$

In Equation (34), the absolute value of specific enthalpy at the temperature T is reduced by the enthalpy at 273.15 K because of discrepancies in the reference temperature of each compound, what could lead to errors in calculations. All functions implemented, including the values of each coefficient are presented in Appendix I.

7.3 Thermodynamic cycle

In large-scale gas turbines, many times it is advantageous to work with the basic Brayton cycle, because the increment in efficiency that could be provided by heat recuperation, intercooling and reheating may not compensate for the increased costs. However, when scaling down turbomachinery beyond certain limits, the efficiency starts to drop drastically. The main reasons behind this problem are related to low Reynolds number, relatively high surface roughness and tip clearance, limited feature size and the non-adiabatic effect. Some of them are restrictions due to the manufacturing processes, that do not allow a reduction in surface roughness and tolerances proportionally to the scaling factor. In addition, the geometry itself cannot be unrestrictedly scaled down with accuracy. The walls must have a minimum thickness, similar blade geometries may not be practicable in very small scale and the trailing edges may not be as sharp as in large rotors. The non-adiabatic effect is caused by the increase in the surface to volume ratio of the impellers, leading to situations which the process starts to deviate considerably from the adiabatic assumption. (Schiffmann & Favrat, 2010; Tiainen, et al., 2017)

Therefore, more elaborated thermodynamic cycles are frequently considered for micro gas turbines, in order to somehow compensate for all these losses. The typical choice is the recuperated Brayton cycle shown in Figure 20, because it keeps the complexity (i.e., costs) and weight in moderated levels, while the thermal efficiency can be raised by a factor higher than two. The same advantage is not observed in large gas turbines, and the reason is the fact that micro gas turbines usually work with a single-stage radial compressor, due its simplicity and low cost, what consequently limits the pressure ratio. Therefore, the low pressure ratio leads to a large difference between the temperature of the air at the compressor outlet and the flue gases at the turbine outlet, making recuperation more interesting. (Xiao, et al., 2017)

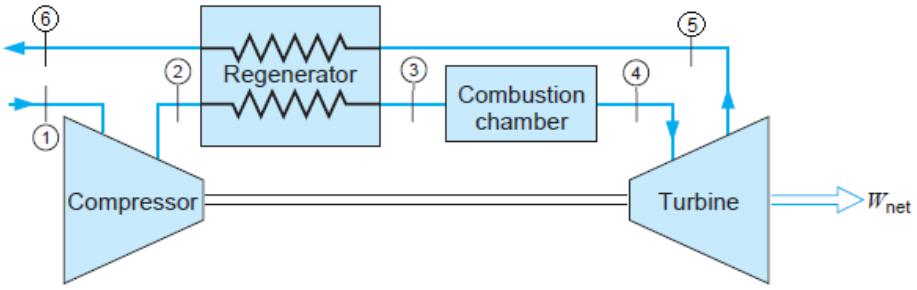

Figure 20. Regenerative Brayton cycle (Borgnakke & Sonntag, 2009).

Taking the previous considerations into account, the recuperated – or regenerative – Brayton cycle is chosen for this study. In order to proceed with the calculations, some assumptions must be done, as the isentropic efficiencies of the compressor and turbine, compressor pressure ratio, turbine inlet temperature (TIT), recuperator effectiveness and the pressure drops at the combustor and recuperator.

The isentropic efficiencies of the compressor and turbine are expected to be lower than the standard for large-scale turbomachinery, due to reasons already mentioned. In order to define values for them, previous studies regarding small compressors and turbines are considered. Han, et al (2010) developed a 500-W_{el} ultra-micro gas turbine, which is expected to have lower efficiencies than the gas turbine of the present study, since it is even smaller scale. They defined the pressure ratio as $\pi = 3$, the turbine inlet temperature as 1200 K, the rotational speed as 400,000 rpm and the obtained isentropic efficiencies are 68% and 70% for the compressor and turbine, respectively. Clay & Tansley (2011) explored a simple design micro gas turbine of 1 kW_{el} for domestic CHP purposes. The engine has pressure ratio $\pi = 2.5$, TIT = 1200 K and the isentropic efficiencies are 73% for the compressor and 75% for the turbine. Benini & Giacometti (2007) designed and manufactured a small turbo-jet engine, with pressure ratio $\pi = 2.66$, TIT = 950 K and rotational speed of 60,000 rpm. The compressor had isentropic efficiency of 78% and the turbine 80%. Finally, Nagasaki, et al (2003) developed a concept of recuperator for a 3-kW_{el} micro gas turbine. In the same study, the main parameters of the other components were defined as pressure ratio $\pi = 3$, turbine inlet temperature of 1223 K and isentropic efficiencies of the compressor and turbine 75% and 80%, respectively. Considering these data, it is estimated that the compressor and turbine for the intended 2-kW_{el} micro gas turbine will have isentropic efficiencies of 74% and 77%, respectively.

Regarding the recuperator, it is a key component of the regenerative Brayton cycle, and the determination of its main parameters – effectiveness and pressure drop at cold and hot sides – are necessary to advance in calculations. Once again, since this component is not designed yet, the values utilized are based on the literature. High effectiveness is required to recover the heat from exhaust gases as much as possible, enhancing the cycle thermal efficiency. This quantity is increased by adding heat transfer surface area to the heat exchanger, however, the same measure also increases the pressure drop, which in turn depletes the overall efficiency. Finding a compromise between these two influences is therefore the main challenge in recuperator design. Nevertheless, this issue becomes even more critical in small-size recuperators, since the pressure drop is increased by the narrower channels and the performance is generally penalized by streamwise heat transfer through the walls. (Rogiers, et al., 2006)

Xiao, et al (2017) states that an effectiveness above 90% and a relative pressure drop below 3% are desired for micro gas turbines. According to the same author, these parameters are expressed by Equations (36) and (37), respectively.

$$\varepsilon_{\mathrm{r}} = \frac{T_3 - T_2}{T_5 - T_2} \tag{36}$$

$$\Delta p_{\mathrm{r}} = \Delta p_{\mathrm{r,cold}} + \Delta p_{\mathrm{r,hot}} = \frac{\Delta p_{2\text{-}3}}{p_2} + \frac{\Delta p_{5\text{-}6}}{p_5} \tag{37}$$

The first and second terms at the right-hand side of Equation (37) are also referred as the relative pressure drops at the cold and hot side, respectively. After further investigations in literature, the reference values given by Xiao, et al (2017) for effectiveness and pressure loss seem coherent for micro gas turbines with power above 100 kW_{el}, however they are probably too optimistic for the 2-kW_{el} engine considered here. For example, Lagerström & Xie (2002) developed a high-performance recuperator for VOLVO and Avesta Sheffield, intended for a 100-kW_{el} micro gas turbine, achieving ε_{r} = 89% and Δp_{r} = 4.5%. In a scale closer to the required in the present study, Nagasaki, et al (2003) designed a recuperator for a 3-kW_{el} micro gas turbine, reaching ε_{r} = 80% and Δp_{r} = 6.3%. Traverso & Massardo (2005) presented an approach to optimize micro gas turbine recuperators from both technical and economical points of view. One of their study cases regarded a 50-kW_{el} engine, which the optimization procedure resulted in ε_{r} = 87% and Δp_{r} = 5%. Finally, Stevens & Baelmans

(2008) investigated the optimal pressure drop ratio for small-size gas turbines, establishing a new optimization procedure. The application of the method in a 1.5-kW_{el} micro gas turbine resulted in a recuperator with ε_r = 89.9% and Δp_r = 6%. However, the authors stated that in order to achieve such values, a very large number of channels are required, making the recuperator expensive and difficult to manufacture. In addition, they concluded that the pressure losses should be preferably located at the cold side of the heat exchanger and that the optimal ratio $\Delta p_{r,cold}/\Delta p_{r,hot}$ is a function of the compressor pressure ratio. The value of 1.79 was found for the 1.5-kW_{el} previously mentioned, that has a pressure ratio π = 3.3. Considering all these studies, it was found prudent to define the effectiveness of the recuperator as 82% and the total relative pressure loss as 6%. Following the findings of Stevens & Baelmans (2008) for a similar engine, the ratio $\Delta p_{r,cold}/\Delta p_{r,hot}$ is defined as 1.7.

The mechanical and generator losses were also estimated with an analogy with similar engines. Vick, et al (2016) presented a design concept of an 11-kW_{el} gas turbine which the generator has efficiency of 92%. Clay & Tansley (2011) explored a simple and compact-design micro gas turbine for domestic CHP application with capacity of 1 kW_{el}. The mechanical efficiency obtained was 90% and the generator efficiency was not reported. Lastly, Bakalis & Stamatis (2012) analyzed full and part load exergy of a coupled micro gas turbine and fuel cell system. The gas turbine is 30-kW_{el} and its mechanical and generator efficiencies are 97% and 96%, respectively. Based on these values and considering the scale differences, it is assumed a mechanical efficiency of 93% and electrical efficiency of 92% for the current case.

Regarding the turbine inlet temperature (TIT), it is beneficial for the overall efficiency of the engine to increase it as much as possible, however the upper limit is typically imposed by the material thermal resistance. In order to achieve reasonable efficiency while allowing the turbine to be manufactured with metallic alloys, such as the type 625 and HR120 instead of ceramic materials, the TIT is defined as 1100 K. (Micheli, et al., 2007)

The pressure ratio is then iterated using all the previous input values until the optimum is found, leading to the highest thermal efficiency. In addition, some parameters of the combustion chamber also have to be assumed for cycle calculations and they can be verified after design and CFD procedures. At this point, respecting the performance requirements for modern combustors presented in Section 3.1, the combustion efficiency is set to 99.5% and the total pressure drop as 5% of the pressure at the compressor discharge.

The steps for gas turbine cycle calculations follow the principles and recommendations of Backman et al. (2002) and are not described in detail here. One point that should be clarified is the assumption that an external compressor is raising the pressure of the fuel to the combustion chamber level right before it enters in the process. Therefore, the temperature of the fuel is higher than the ambient temperature, and it was calculated utilizing the same isentropic efficiency of the main compressor of the gas turbine. However, if the fuel is provided by other means, for instance a compressed natural gas bottle, the difference in fuel temperature does not affect the cycle very significantly, since the fuel mass flow is very small compared to the air mass flow. Table 3 summarizes the results of cycle calculations utilizing both natural gas and landfill gas. The values with yellow background represent inputs and assumptions, while the green ones are the calculated outputs. All specific heats, gas constants and enthalpies are calculated with the equations presented in Section 7.2.

Table 3. Cycle calculations utilizing natural gas and landfill gas. Values in yellow are inputs or assumptions, and values in green are calculated outputs.

Parameter	**Symbol**	**Natural gas**	**Landfill gas**	**Unit**
Selected GT power	P_{GT}	2.00	2.00	kW
Mechanical efficiency	η_{m}	0.93	0.93	-
Generator efficiency	η_{g}	0.92	0.92	-
Shaft power	P_{sh}	2.34	2.34	kW
Air constant	R_{air}	287.0	287.0	J/(kg K)
Fuel constant	R_{fuel}	508.2	279.9	J/(kg K)
Stoichiometric gas constant	R_{SG}	300.6	286.9	J/(kg K)
Fuel heating value	LHV	48.1	13.5	MJ/kg
Compressor				
Pressure ratio	π	3.5	3.5	-
Pressure at the inlet	p_{t1}	101	101	kPa
Temperature at the inlet	T_{t1}	15	15	K
Total pressure at the outlet	p_{t2}	353.5	353.5	kPa
Isentropic mean c_p at the compressor	$c_{p,\mathrm{c,s}}$	1009	1009	J/(kg K)
Isentropic total temperature at outlet	T_{t2s}	411.6	411.6	K
Isentropic efficiency	$\eta_{\mathrm{s,c}}$	0.74	0.74	-
Total temperature at outlet	T_{t2}	454.9	454.9	K
Mean c_p at the compressor	$c_{p,\mathrm{c}}$	1011	1011	J/(kg K)
Stoichiometric air-fuel ratio	L	16.46	4.62	-

Stoichiometric flue gas fraction	y	0.1248	0.1463	-
Air mass flow	$\dot{m}_{\mathrm{air}}$	30.7	29.4	g/s
Compressor power	P_{c}	5.18	4.95	kW
Recuperator				
Effectiveness	ε_{r}	0.82	0.82	-
Temperature of outlet air	T_{t3}	812.3	813.5	K
Pressure drop at the cold side	$\Delta p_{\mathrm{r,cold}}$	3.8%	3.8%	-
Pressure drop at the hot side	$\Delta p_{\mathrm{r,hot}}$	2.2%	2.2%	-
Combustion chamber				
Pressure drop	Δp_{b}	5.00%	5.00%	-
Combustion efficiency	η_{b}	99.50%	99.50%	
Enthalpy of the inlet air	$h_{\mathrm{air,3}}$	562.4	563.7	kJ/kg
Enthalpy of the outlet air (in FG)	$h_{\mathrm{air,4}}$	888.0	888.0	kJ/kg
Enthalpy of stoichiometric gas (in FG)	$h_{\mathrm{SG,4}}$	1005.1	992.7	kJ/kg
Mean c_p of inlet fuel	$c_{p,\mathrm{fuel}}$	2268	1270	J/(kg K)
Isentropic temperature of inlet fuel	$T_{\mathrm{t,fuel,s}}$	381.5	379.7	K
Temperature of inlet fuel	$T_{\mathrm{t,fuel}}$	414.4	411.9	K
Enthalpy of the inlet fuel	h_{fuel}	325.0	178.2	kJ/kg
Enthalpy parameter	ΔHu	2932.4	1477.0	kJ/kg
Fuel mass flow	$\dot{m}_{\mathrm{fuel}}$	0.22	0.78	g/s
Fuel power	P_{b}	10.65	10.68	kW
Turbine				
Temperature at the inlet	T_{t4}	1100	1100	K
Mass flow	$\dot{m}_{\mathrm{FG}}$	31.0	30.1	g/s
Pressure at the inlet	p_{t4}	322.4	322.4	kPa
Pressure at the outlet	p_{t5}	103.6	103.6	kPa
Isentropic mean c_p at the turbine	$c_{p,\mathrm{t,s}}$	1155	1158	J/(kg K)
Flue gas constant	R_{FG}	288.7	286.9	J/(kg K)
Isentropic temperature at outlet	T_{t5s}	828.3	830.1	K
Isentropic efficiency	$\eta_{\mathrm{s,t}}$	0.77	0.77	-
Temperature at the outlet	T_{t5}	890.8	892.2	K
Mean c_p at the turbine	$c_{p,\mathrm{t}}$	1161	1163	J/(kg K)
Power	P_{t}	7.52	7.29	kW
Gas turbine				
Net shaft power	P_{sh}	2.34	2.34	kW
Thermal efficiency	η_{th}	0.219	0.219	-
Electrical efficiency	η_{el}	0.188	0.187	-

From these results it is clearly observed that the performance can be very similar burning either natural gas or landfill gas, as long as the mass flow of landfill gas is larger enough to compensate its lower LHV. The estimated electrical efficiency of about 18.8% is low if compared with large gas turbines, but for the scale aimed here, considering all shortcomings of the downsizing already discussed, it is taken as reasonable. Table 3 also shows that the pressure ratio chosen is 3.5. This value was found to be the optimum through successive iterations, which the results are shown in Figure 21.

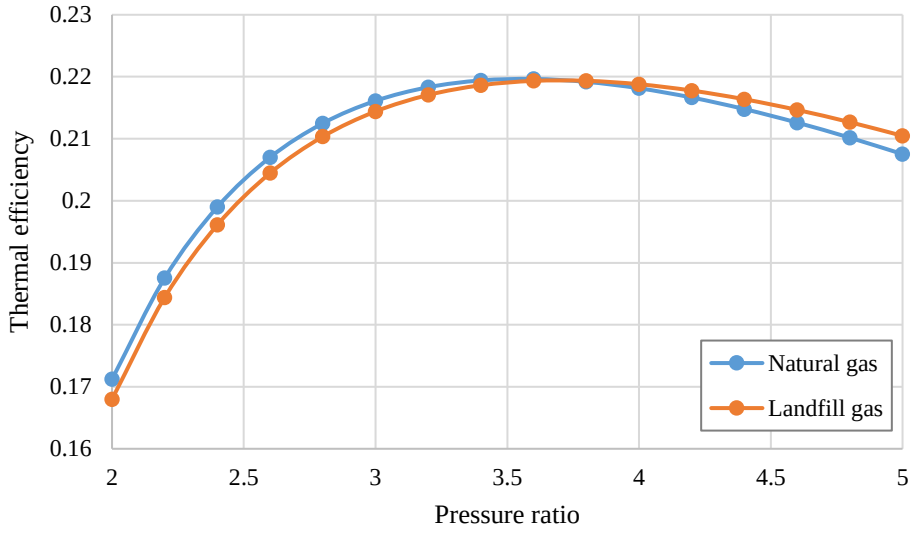

Figure 21. Thermal efficiency in function of the pressure ratio.

It is also interesting to observe how the difference between the fuels behave in function of the pressure ratio. With pressure ratios higher than 3.6, the use of landfill gas start to be more efficient than natural gas.

8 DESIGN PROCEDURE

Utilizing the cycle information calculated previously, the design procedure of the combustion chamber can take place. Firstly, it is important to highlight and remember the main objectives and requirements for this component. The flameless concept is chosen because of its potential for very low emissions, added to the uniform temperature distribution, low noise, low vibration and the capacity to handle low-quality fuels. Therefore, a successful design need to be able to achieve the flameless regime, what requires high flue gas recirculation rates. As seen previously, external recirculation induces significant thermal efficiency loss, therefore the recirculation has to be done internally through aerodynamic

means, characterizing an adiabatic combustor. In addition, the same geometry need to able to operate in stable flame mode in order to warm up the chamber until a suitable temperature that allow switching to flameless mode. Considering that the self-ignition temperature of methane is about 580°C, the combustor medium should be well above this level before the stable flame is extinguished. Developing a geometry able to handle both flame and flameless combustion is essentially a great design challenge since both regimes cannot be established under similar conditions. This task is apparently impracticable without additional air and/or fuel controls. Another important point is that, as seen before, the flameless combustion happens with very homogeneous temperature and this temperature is a key design parameter. According to the literature reviewed, the span of combined low emissions of CO and NO_x happens between 1670 K and 1900 K, therefore it is one of the main goals of the design to keep the operational temperature in this range. The temperature is controlled by the equivalence ratio at the primary zone.

Additional goals consist in drive the dilution air along the external surface of the liner and provide good mixing before the outlet. The former is important because of the difficulty to implement a cooling system in this scale, therefore the dilution air helps to attenuate the problem of high temperatures close to the walls, a characteristic of flameless combustors. The latter is a general combustor requirement. Since a dilution zone is unavoidable in this case, the mixing should be well done to provide the most uniform temperature profile as possible at the outlet in order to avoid damages on the turbine blades.

Having all these considerations been done, the design procedure follow the diagram presented in Figure 22. It is a substantially long process that requires several iterations before the final design is obtained.

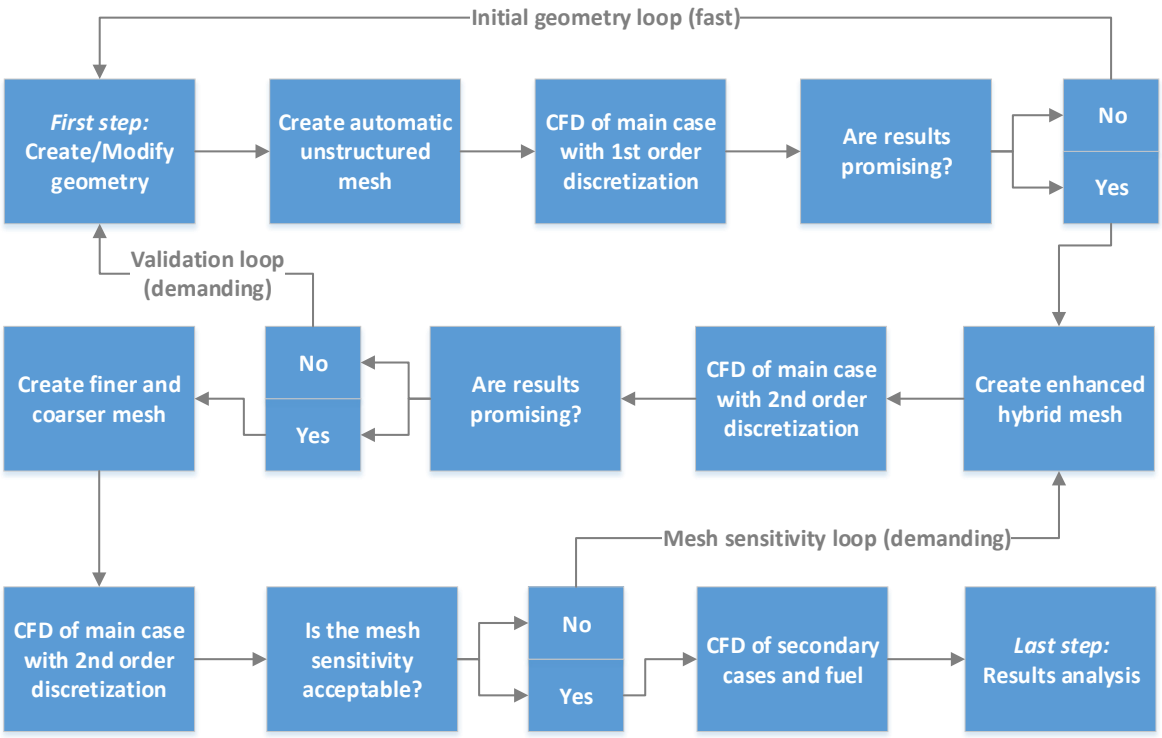

Figure 22. Diagram of the design process.

The geometry is initially drawn in 3D utilizing the CAD software SolidWorks. Then, for fast design iteration, a fully unstructured mesh is created with Ansys Mesh and a CFD simulation is run in Ansys Fluent with first order upwind spatial discretization. At this point, both flameless and stable flame operational modes are simulated with just one fuel, which was chosen to be natural gas. The first iterations are also used to test and define the most suitable models for the problem, which involves turbulence, turbulence-chemistry iteration, chemical reactions, species transport and radiation. After a reasonable geometry is found, an enhanced mesh is created manually using the software Pointwise. In this step, efforts are done to keep the mesh primarily structured, just relying on unstructured blocks in very complex regions, characterizing a hybrid mesh. Then, once again the main cases are simulated in Ansys Fluent, but at this time utilizing second order upwind discretization. If the results are still acceptable, two other versions of the mesh are created and just the flameless case is ran in order to provide sensitivity analysis. In case the solutions demonstrate to be fairly independent of the mesh, the geometry and mesh are accepted as final and the remaining and secondary cases employing alternative fuel are ran. The last step consists in the analysis of the results and confirmation that the main objectives were achieved.

8.1 Numerical models

Computational fluid dynamics of a combustion chamber involve reasonably complex phenomena, requiring certain additions to the modelling that are not necessary for other components of a gas turbine. The flameless regime is especially challenging due to the strong relation between chemical kinetics and turbulent mixing. In stable high-temperature and non-premixed flames, turbulence gradually mix oxidizer and fuel into reaction zones, where they are quickly burned. Under these conditions, it is a fair approximation to assume that the mixing is the limiting factor for combustion and the complex chemical kinetic rates are negligible. In other words, this means considering that the compounds are instantaneously burned when mixed. The Damköhler number establish the relation between flow time scale and chemical reaction time scale, as $Da = \tau_{\mathrm{K}}/\tau_{\mathrm{ch}}$. Therefore, under the stable flame conditions mentioned previously, $Da \gg 1$. However, when dealing with flameless combustion, the chemical kinetics have an essential role and the chemistry rate cannot be considered infinite anymore. In this case, the influence of the chemistry and the turbulence are comparable, in a way that $Da \approx 1$. This implies in the necessity to utilize different turbulence-chemistry iteration models for each operational mode. (Miniati, et al., 2015; Bao, 2017; ANSYS Inc., 2017)

Ansys Fluent v18.2 provides four options for turbulence-chemistry interaction for reactive flows under the species transport model. The Eddy-Dissipation model has the assumption of instantaneous combustion after mixing, which makes it suitable for stable flame simulations. On the other hand, the same model is not valid for flameless regime, where a finite-rate chemistry must be considered. Two models are able to handle this condition, the Finite-Rate/Eddy-Dissipation (FR/ED) and the Eddy-Dissipation Concept (EDC). The first is a combination of the two models that compose its name, computing the effective reaction rate as the minimum of the Finite-Chemistry rate and the Eddy-Dissipation rate (ANSYS Inc., 2017). In turn, the second is an extension of the Eddy-Dissipation model that allows inclusion of detailed chemical mechanisms in turbulent flows (ANSYS Inc., 2017). In the literature, it was found that the EDC model is more applied in flameless combustion researches than the FR/ED, as example of Miniati et al. (2015), Stazi et al. (2011), Kim et al. (2008) and Fortunato, et al. (2015). In a study that analyzed the effect of the kinetic mechanism and combustion model effect on flameless combustion, Parente et al. (2008) stated that if detailed chemistry is used (i.e., pollutants post-processing) the FR/ED model

will lead to incorrect results due to the way the model controls the production and destruction of species. During the initial simulations of the present work, both models were tested and both were able to predict the flameless regime, without the addition of detailed chemistry. The results were pretty similar, with the exception of one particular simulation which the FR/ED model resulted in a behavior that seems physically incorrect. Taking all these facts into account, the EDC model is chosen to model the turbulence-chemistry interactions. Nevertheless, it should be mentioned that the FR/ED model demonstrated to require much less computational power than the EDC model.

As in the largest part of engineering applications of CFD, the Reynolds-Averaged Navier-Stokes (RANS) equations are utilized to solve the flow field. The most popular turbulence model applied to solve the Reynolds stress and provide closure to RANS in the literature related to flameless combustors is the k-ε and its derivatives. Very rare cases in this area were found using k-ω based models, as example of Stazi et al. (2011). Possible reasons are the lack of interest in solving the physics inside the boundary layers and the virtual absence of separation from the walls, areas were the k-ω model historically performs better. From the perspective of the flow field, combustion chambers are mainly a problem of round and radial jets. According to Wilcox (2006), the k-ε model of Launder & Spalding (1972), also known as the standard k-ε model, predicts a spreading rate for round jets 25% above the measured values and 2% below the experimental data for radial jets. Attempting to overcome the deficiency of the model predicting round jets, some authors as Fortunato et al. (2015) and Galletti et al. (2007) adopt a modified version of the k-ε model, in which the constant $C_{1\varepsilon}$ is modified from 1.44 to 1.6. This modification was tried in the present work, however the result was a stretching of the round jet physically suspicious. Another option is the version of k-ε model presented by Shih et al. (1995), known as the realizable k-ε model. According to ANSYS Inc. (2017), this model differs from standard k-ε by containing an "alternative formulation for the turbulent viscosity" and by having a "modified transport equation for the dissipation rate ε, that was derived from an exact equation for the transport of the mean-square vorticity fluctuation". Shih et al. (1995) documented the better performance of the realizable k-ε model predicting the spreading rate of an axisymmetric jet. In addition, diverse studies already applied this model successfully in flameless CFD, for instance Vascellari & Cau (2012), Danon et al. (2011) and Noor et al. (2013). Having all these been considered, the realizable k-ε model with scalable wall functions is selected to provide the closure to RANS in this work.

The heat transfer by radiation represents an important mechanism in combustion chambers due to the high temperature of the gases, therefore it has also to be modelled. The Discrete Ordinates (DO) model seem to be almost a unanimity for this task in flameless combustion research. Examples are the studies of Galletti et al. (2007), Noor et al. (2013), Parente et al. (2008), Fortunato et al. (2015) and Kim et al. (2008). This model solves the equation of radiative transfer for a finite number of discrete solid angles, which have to be given in the model settings. The higher the number of directions solved, the higher is the accuracy, however, the calculation time can be severely affected. Following the recommendations of ANSYS Inc. (2017) for problems involving periodic boundaries, the total number of directions solved in the three-dimensional domain is 72. The experience running simulations for this case showed that solving the radiation each 3 iterations of the energy equation provides a good compromise between convergence speed and computational requirements. In addition, when a radiation model is enabled, the absorption and scattering coefficients of the materials have to be set in their proprieties. Since CO_2 and H_2O are present in the medium as combustion products, the absorption may be considered. ANSYS Fluent accepts a variable absorption coefficient through the domain as function of the local mass fractions of CO_2 and H_2O, utilizing the Weighted-Sum-of-Gray-Gases model (WSGGM). This feature is utilized to calculate the absorption coefficient of the fluid domains in simulations of the present work, while the scattering is neglected setting its coefficient to zero. The solid domain that include the walls of the combustor is excluded from radiation calculations since the walls are opaque.

Finally, after the main solution is obtained, the Decoupled Detailed Chemistry model is enabled in order to calculate the pollutants. This requires the importing of a gas kinetics mechanism in CHEMKIN format related to the specific combustion process, which contains thermochemical data of all the species involved and the respective reactions. As example of other studies on flameless combustion as Galletti et al. (2007), Kruse et al. (2015) and Tabacco et al. (2002), the GRI-3.0 mechanism was adopted. ANSYS Fluent v18.2 includes a GRI-3.0 mechanism for methane combustion that contains 50 species and all related reactions. However, since we are interested just on pollutants formation, only the equations for CO, NO and NO_2 are solved.

8.2 Geometry

The first concept visualized for the combustion chamber being designed was a reverse flow configuration, inspired on the work of Plessing et al. (1998) and Kruse et al. (2015), as already presented in Figure 15 and Figure 17, respectively. The reverse flow design seemed the best option to provide high recirculation of exhaust gases and mixing with the incoming air and fuel. Taking some principles from these previous studies, enhancing the aerodynamics and size for micro gas turbine application, and implementing a burner similar to the one suggested by Wünning & Wünning (1997) resulted in the design shown in Figure 23.

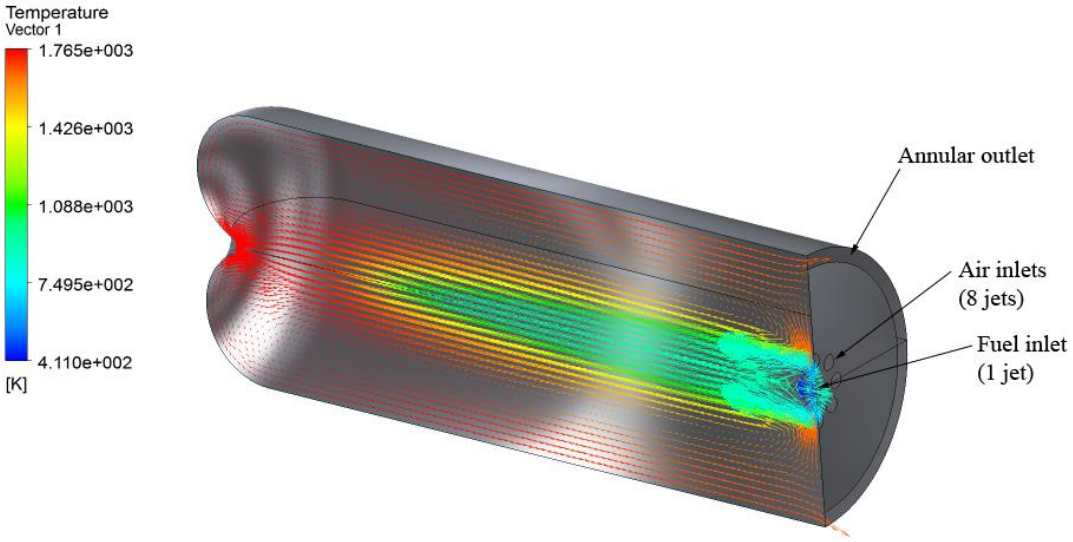

Figure 23. First design studied.

It has a central fuel inlet surrounded by eight air jets that, depending on the velocities, create the conditions for flameless combustion. At the end of the chamber, the geometry drives the high velocity flue gases at the central region to the peripheries, where they flow back to the right side. Part of these gases then leave the combustor through the outlet and part are recirculated with the incoming air and fuel. The outlet is an annulus located at the same side of the inlets, characterizing the reverse flow design. It should be clarified that the dilution zone was not modelled here and would have to be added downstream the outlet. Although successful in achieving the flameless regime, this concept demonstrated to be problematic in creating conditions for a stable flame. In addition, since all inlets and outlet are located at the same side, the cooling of the walls become an issue, that is summed to layout difficulties that the design brings for the layout of the gas turbine due to the position of the hot gases outlet and incoming air and fuel. Because of these reasons, this design was discontinued.

Nevertheless, if a solution to warm up the chamber up to the temperature required for flameless combustion is found, for example, with an auxiliary chamber, and the cooling problem could be solved with external liquid cooling, this design might still be useful for some case.

Following the difficulties to establish the flame mode and to cool the walls with a reverse flow configuration, a new straight through design was created. Taking some inspiration from the design of Lammel et al. (2010), shown in Figure 19a, and replacing the annular jets by a central burner similar to the one presented by Noor et al. (2013) resulted in the design presented in Figure 24.

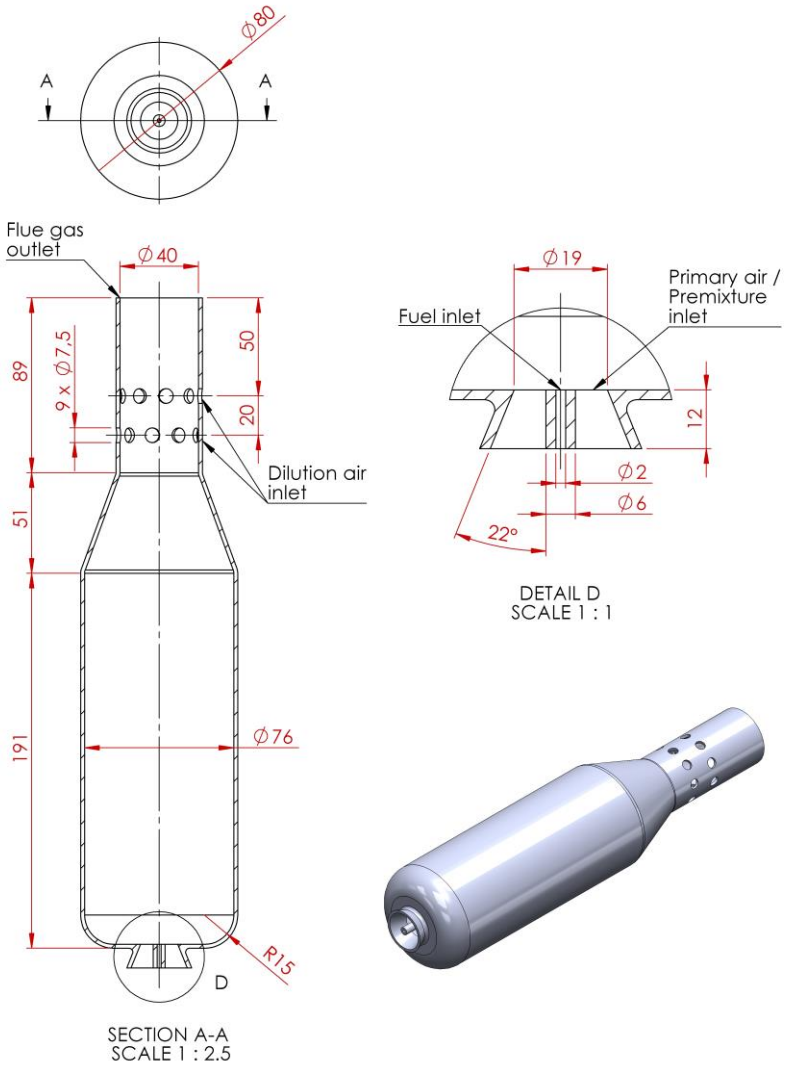

Figure 24. Final combustion chamber technical drawing (dimensions in mm).

In this design, the stable flame mode is achieved by injecting the primary air – the air necessary for combustion according to the desired equivalence ratio – through an annulus

that has converging upstream geometry in order to drive the flow in the axis direction, enhancing the mixing with fuel. In turn, the fuel is injected through an axial small jet with a velocity at the least four times higher than the primary air. Naturally, an ignition system is required to start the flame and although it is not shown in Figure 24, it could be positioned on the wall adjacent to the inlet jets. The amount of air that is not utilized for combustion is driven along the outside wall of the combustor, providing some helpful cooling. This air enters the combustor at the dilution zone, where the combustion is theoretically complete, through two circular patterns of nine holes of 7.5 mm. The odd number of holes in the pattern is strategically chosen in order to avoid jets in exactly opposite directions. In addition, the second pattern of holes is in staggered position in relation to the first one with the purpose to enhance the mixing. The diameter of the dilution holes also play an important role in this matter. Smaller holes produce higher velocity radial jets, which penetrate deeper into the core of the main flow at the cost of higher pressure drop. On the other hand, larger holes provide lower temperatures close to the walls downstream. Considering the total number of holes chosen, the diameter of 7.5 mm was found to be a good compromise, reducing most of the hot spots at the core and at the vicinity of the walls.

When the stable flame had raised the temperature of the chamber enough, the operational mode is changed to flameless. The flame is extinguished by switching the fuel flow from the central jet to secondary jets not shown in Figure 24, but that should be located upstream the burner, inside the primary air channel. In this way, the annular jet will provide premixed air and fuel to the chamber. The key feature that makes this design work for both regimes is that the equivalence ratio in flameless mode is lower than in flame mode. Therefore, more air is injected into the primary zone for flameless regime, what means higher velocities and higher turbulence that favors the recirculation and do not allow the establishment of a flame. The larger diameter at the primary zone is also essential to enable the recirculation. In turn, the opposite is valid for flame mode. With less air being injected into the primary zone, the velocities are lower allowing a flame to be stabilized. Therefore, it is evident that both air and fuel controls are necessary for successful operation. In fact, there is the possibility that the flameless regime can be achieved just by increasing the air mass flow into the primary zone, without the necessity to switch the fuel inlet and premixing. However, such a case was not simulated in the present study.

8.3 Domains and mesh

Before creating the mesh necessary for CFD simulations, suitable domains have to be defined considering the geometry presented and the phenomena involved. Since the dilution air flows along the outside wall of the combustor, it is important to define a fluid domain also around the chamber. A channel of 10 mm was added for this purpose, shown in green in Figure 25. This allows the modelling of the heat transfer through the solid domain shown in grey, that represent the walls of the combustor. Therefore, the cooling effect of the outside flow is included and the temperatures at the chamber walls are better predicted, what is an important parameter to check the suitability of the chosen material.

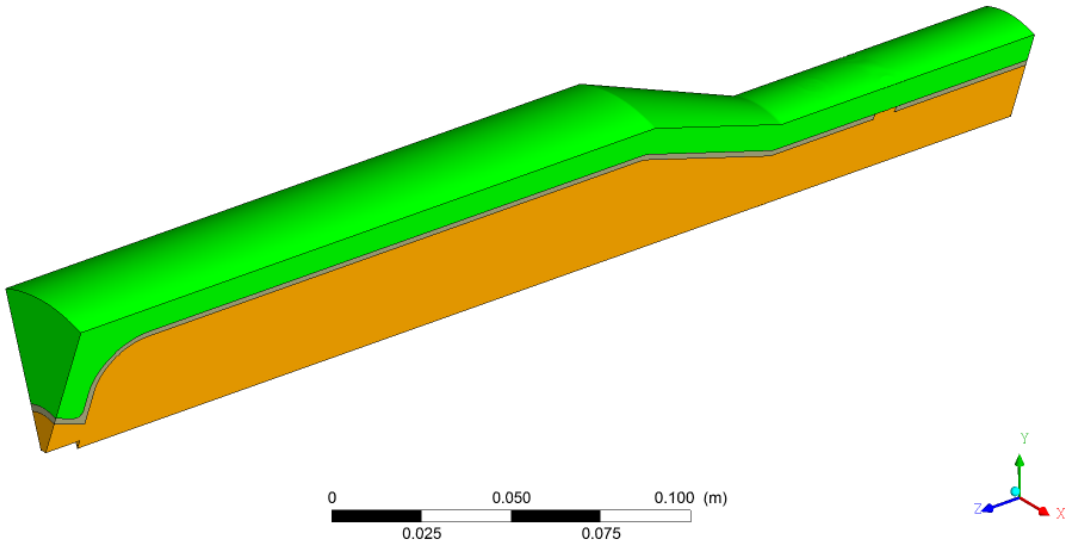

Figure 25. Domains defined for meshing.

The geometry presented in Figure 24 is axisymmetric, except by the dilution holes. The domains in this kind of problem can be simplified with rotational periodicity. This means that just a slice of the combustion chamber is in fact modeled, as seen in Figure 25, since the results at the other regions are expected to be exactly the same. Because of the dilution holes, the angle cannot be freely chosen, having to be necessarily equal to the angle between the holes. Thus, the domains consist in 1/9 of the whole combustor, equivalent to 40°.

Next, a mesh is created utilizing the software Pointwise to discretize the domains. Following the good practices for finite volume method, a structured mesh was built in every possible region. The only exception is the portion of the inner fluid domain below the dilution holes. In that region, great difficulties were found to keep the mesh structured due to the necessary

extension of the holes to the converging central part, characteristic of periodic geometries. Figure 26 and Figure 27 present detail views of the hybrid mesh close to the inlet and outlet, respectively.

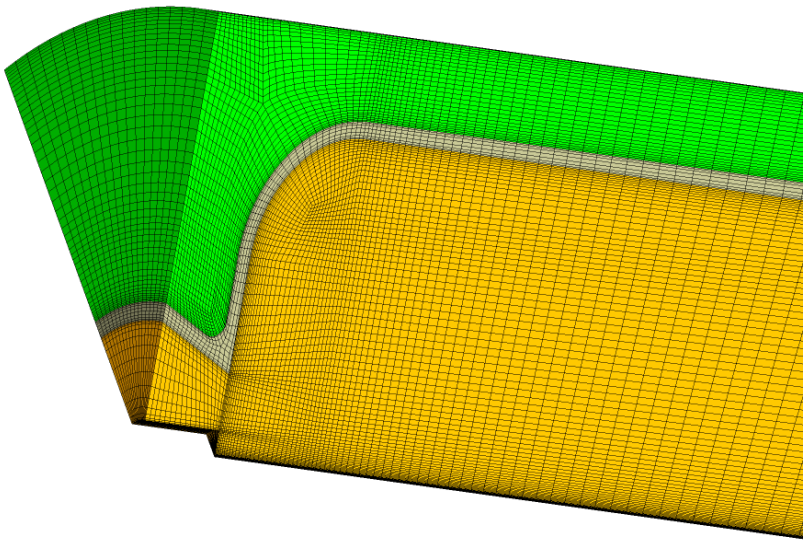

Figure 26. Perspective view of the mesh at the inlets.

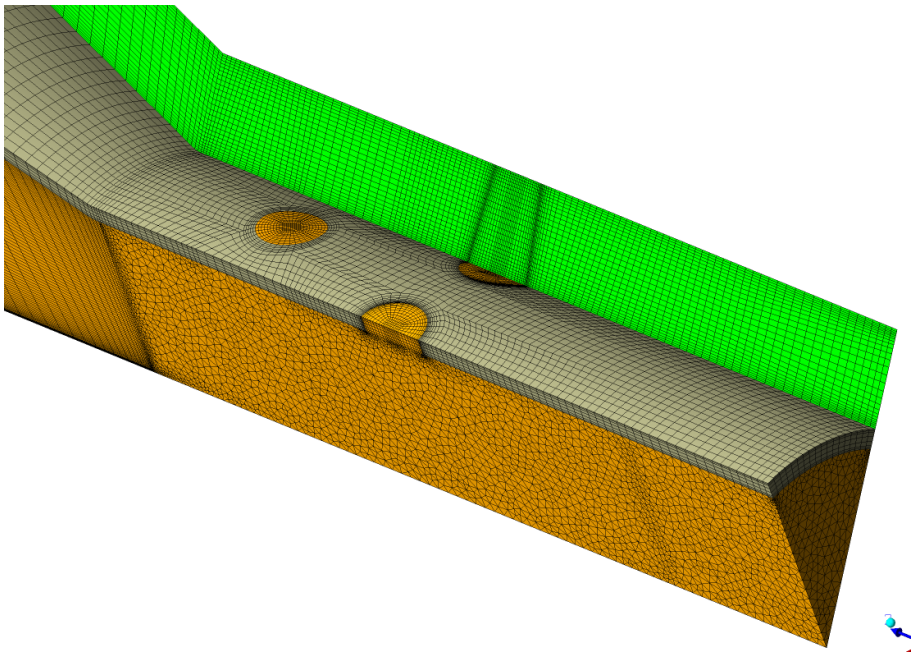

Figure 27. Perspective view of the mesh at the dilution zone and outlet.

The quality of the mesh is considered fair. The maximum equiangular skewness in hexahedral elements is 0.68, while at the tetrahedral and pyramidal regions very few elements had skewness up to 0.91. They were difficult to avoid due to the transition from

structured to unstructured mesh. The average equiangular skewness of the whole mesh is 0.21. In turn, the maximum aspect ratio was found to be 89.1, located at the stretched hexahedral elements around the axis of the combustor. This value is considered very good, since ANSYS Inc. (2017) recommend to maintain it below 1000 when utilizing double precision solver. The average aspect ratio is 6.0.

The mesh presented has a total of approximately 581,000 cells, being 421,000 hexahedrons, 156,000 tetrahedrons and 4,000 pyramids. In order to evaluate the influence of the mesh on solutions, a mesh sensitivity analysis is done and it is presented in Section 9.5.

8.4 Defining the cases and boundary conditions

In order to define the cases and boundary conditions to be simulated, a recall in the gas turbine startup procedure is useful. From shutdown conditions, a gas turbine is started by an electric motor, or the generator may have the feature to play also the motor role for startup. Only when the compressor is already discharging a certain amount of air the combustion chamber is fired. The present combustor should then ignite a flame that will warm up the chamber and cause the gas turbine to accelerate. It is not clear at this point if the combustor will reach a temperature high enough to enable the flameless mode before the gas turbine achieve full load operation or not. Therefore, it is assumed that the stable flame is maintained until the full load point and then the operation is switched to flameless. In this way, it is necessary to guarantee that the flame can be maintained through the whole operational range of the gas turbine. Thus, two simulations are ran for flame mode, one with startup boundary conditions and another in full load. In this work, the flameless mode is simulated just in full load conditions.

With the goal to determine the boundary conditions at the startup, it is assumed that the combustor is fired when the pressure increase caused by the compressor achieve 15% of the pressure increase in full load operation. This means $(\pi_0 - 1)/(\pi_{\mathrm{FL}} - 1) = 0.15$, where π_0 is the pressure ratio in which the combustor is fired and π_{FL} is the full load pressure ratio. The air mass flow corresponding to this pressure ratio would have to be found through the compressor operating map, that is not available. Therefore, an estimation is done using a generic compressor performance map provided by Boyce (2012), as shown in Figure 28.

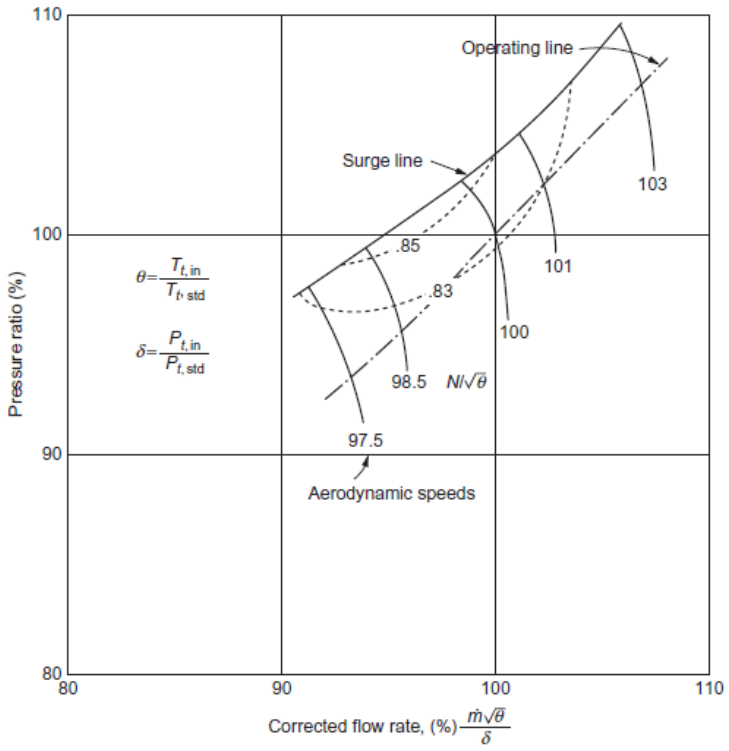

Figure 28. Typical performance map of a centrifugal compressor (Boyce, 2012).

Observing the operating line, it is concluded that for a rough estimation, the ratio of mass flows can be considered equal to the ratio of pressure increase. Similar behavior can be found for the low-pressure compressor of the small gas turbine designed by Jaatinen-Värri et al. (2016). Therefore, $\dot{m}_{\text{air},0}/\dot{m}_{\text{air,FL}} = 0.15$, where $\dot{m}_{\text{air},0}$ and $\dot{m}_{\text{air,FL}}$ are the total air mass flows at the startup and in full load, respectively.

Although the total mass flows of fuel and air are already defined, the parcel of the air to be injected into the primary zone for combustion and the parcel that is added just at the dilution zone depends on the desired equivalence ratio. This is a very important point because the equivalence ratio affects the velocities, thus, the whole functioning of the combustor. In addition, the equivalence ratio is the parameter used to control the maximum temperature in flameless mode, what is one of the main goals of this project. In order to keep the flameless temperatures in the low-emissions range previously presented, the ideal equivalence ratio was found to be 0.55. This result was obtained by iterative CFD method. In turn, when a flame needs to be established, the velocities inside the chamber must be lower, what is achieved decreasing the primary air and increasing the equivalence ratio. A suitable value for the latter in flame mode was found to be 0.80. Having these defined, the primary air mass flow is obtained with Equation (38).

$$\dot{m}_{\text{air,p}} = \frac{AR_{\text{ST}}}{\Phi}\dot{m}_{\text{fuel}} \tag{38}$$

Where,
$\dot{m}_{\text{air,p}}$ = mass flow of primary air [kg/s];
AR_{ST} = stoichiometric air to fuel ratio [-].

The stoichiometric air to fuel ratio AR_{ST} was calculated in Table 2, while the mass flow of fuel $\dot{m}_{\text{fuel}}$ comes from cycle calculations. Next, the dilution air mass flow is obtained by subtracting the primary air mass flow from the total air mass flow, that is $\dot{m}_{\text{air,d}} = \dot{m}_{\text{air}} - \dot{m}_{\text{air,p}}$. In the case of flameless combustion, which the primary air and fuel are injected premixed, the mass flow is simply the sum of $\dot{m}_{\text{air,p}}$ and $\dot{m}_{\text{fuel}}$, while the temperature is calculated as a weighted average.

The mass fractions of species also have to be assigned for all inlets, and in methane-air combustion they consist in CH_4, O_2, CO_2 and H_2O. If the sum of the mass fractions is lower than 100%, the remaining parcel is automatically assumed to be N_2. In the case of the premixture, the species are defined proportionally to the amount of air and fuel. For example, if the mixture has 3.23% of natural gas and the pure natural gas has 96.09% of methane, the parcel of methane in the mixture is obviously $3.23\% \cdot 96.09\% = 3.10\%$. A summary of all inlet boundary conditions for natural gas and landfill gas are presented in Table 4 and

Table **5**, respectively. To all of them, it is assigned a turbulence intensity of 5%, considered a medium level.

Table 4. Inlet boundary conditions for natural gas.

Natural gas	**Momentum (mass flow)**	**Thermal (temperature)**	**Species (mass fraction)**
Full load, flameless			
Premix inlet	6.932 g/s	801 K	3.11% CH_4 22.54% O_2 0.04% CO_2
Dilution air inlet	24.442 g/s	814 K	23.29% O_2
Full load, stable flame			
Primary air inlet	4.612 g/s	814 K	23.29% O_2
Fuel inlet	0.224 g/s	411 K	96.09% CH_4 1.34% CO_2

Dilution air inlet	26.539 g/s	814 K	23.29% O_2
Startup, stable flame			
Primary air inlet	0.692 g/s	330 K	23.29% O_2
Fuel inlet	0.034 g/s	321 K	96.09% CH_4 1.34% CO_2
Dilution air inlet	3.981 g/s	330 K	23.29% O_2

Table 5. Inlet boundary conditions for landfill gas.

Landfill gas	**Momentum (mass flow)**	**Thermal (temperature)**	**Species (mass fraction)**
Full load, flameless			
Premix inlet	7.538 g/s	770 K	2.87% CH_4 7.56% O_2 20.82% CO_2
Dilution air inlet	23.241 g/s	815 K	23.29% O_2
Full load, stable flame			
Primary air inlet	4.631 g/s	815 K	23.29% O_2
Fuel inlet	0.801 g/s	388 K	27.00% CH_4 71.11% CO_2
Dilution air inlet	25.346 g/s	815 K	23.29% O_2
Startup, stable flame			
Primary air inlet	0.695 g/s	330 K	23.29% O_2
Fuel inlet	0.120 g/s	321 K	27.00% CH_4 71.11% CO_2
Dilution air inlet	3.802 g/s	330 K	23.29% O_2

The outlet boundary conditions are the same for all cases, consisting in zero gauge pressure. In case of reverse flow at the outlet, the temperature is set to 1100 K, that is the TIT previously defined, and the species mass fractions are set according to de flue gas composition, depending on the fuel. The operating pressure of the combustor is obtained by taking the pressure at the compressor discharge and discounting the pressure loss at the cold side of the recuperator. This results in 340.1 kPa in full load and 138.9 kPa for the startup case.

All the walls of the combustor are treated as no slip wall, and the temperature is solved by the heat transfer between the inside and outside flows. The thermal conductivity is defined

considering that the material is the ferritic alloy 4736, that according to the supplier Outokumpu (2018), can resist to temperatures up to 1420 K. The emissivity of the walls and the diffuse fraction of radiation, that depend on the surface color and roughness, are both arbitrarily set to 0.8. Lastly, the walls that involve the outside fluid domain are set as adiabatic.

9 RESULTS

The convergence criteria utilized to finish the simulations included the mass, total energy, oxygen mass fraction and methane mass fraction of the internal fluid domain. When all these quantities become relatively stable, the solution was considered converged. In some cases, the RMS residuals could not be reduced further than 10^4.

9.1 Temperatures

The combustor proposed demonstrated to be operational in all cases simulated, that consist in flameless full load, stable flame full load and stable flame startup, for both natural gas and landfill gas. One of the most revealing postprocessing tools for these cases is the temperature contours at the longitudinal section of the combustor. Figure 29 present these contours for the startup case, utilizing both fuels.

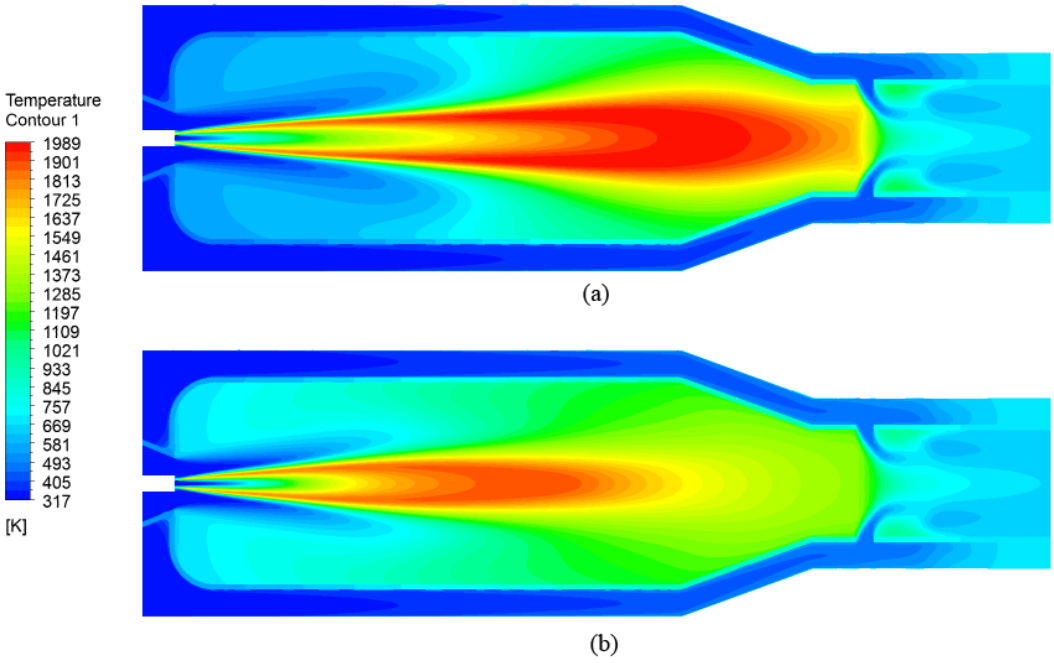

Figure 29. Temperature contours of startup stable-flame mode with natural gas (a) and landfill gas (b).

It is clearly seen in these images that the natural gas produces a larger and higher-temperature flame than the landfill gas for the same air mass flow, with a difference very close to 100 K. In addition, the higher velocity of the landfill fuel jet apparently increases the recirculation, and the chamber is heated more evenly at the surroundings of the flame. Following this stage, the mass flows of air and fuel are increased up to the full load conditions, and the temperature contours at this point are shown in Figure 30.

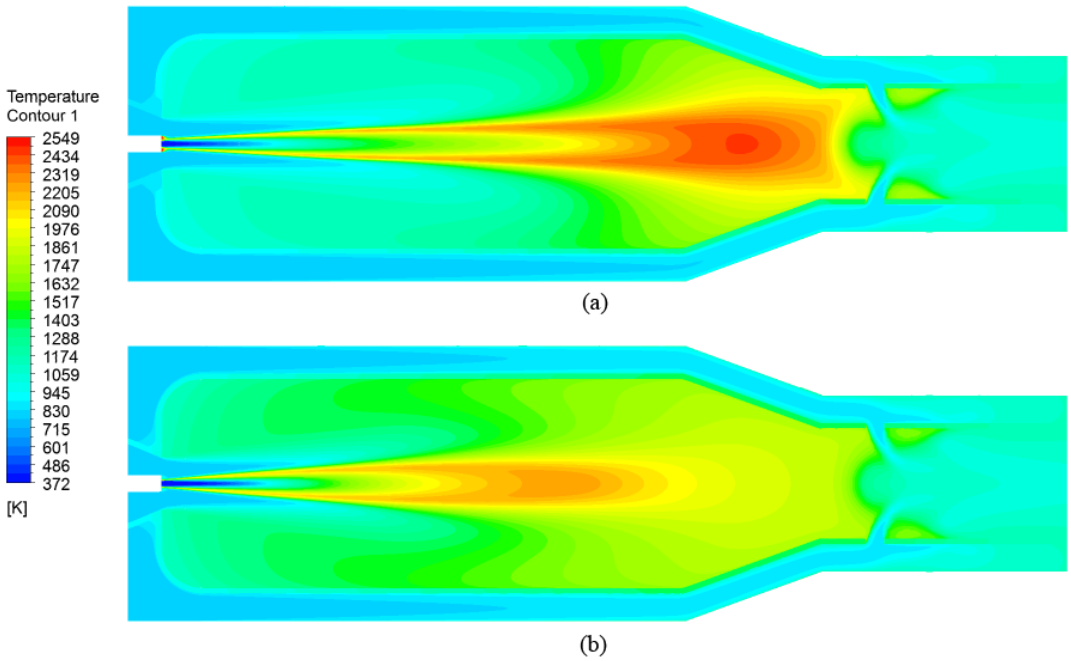

Figure 30. Temperature contours of full-load stable-flame mode with natural gas (a) and landfill gas (b).

Here it is seen that the larger mass flows and consequent velocities cause the natural gas flame to stretch, and it is probably close to the blowout point. The same effect is not evident for the landfill gas, that indeed shows a better performance in these simulations, since the flame seems more stable and the chamber is preheated more evenly. The regions close to the inlets achieved temperatures above 1300 K with landfill gas, while with natural gas they were about 150 K lower. This means that the higher velocity of the fuel jet when using landfill gas is closer to the ideal for the proposed combustor. The velocities are discussed in more detail further.

It is also remarkable the highest temperature achieved in these cases, corresponding to 2550 K for natural gas and 2245 K for landfill gas. At these levels, large amounts of thermal NO_x are produced, as it happens in conventional diffusive combustors, however, the present combustor is supposed to operate in flame mode just for a short span of time. After this point, the operation is switched to flameless and both fuels were successful in preheating the

chamber enough for this purpose, since the self-ignition temperature of methane is about 850 K. The temperature contours of this last stage are presented in Figure 31.

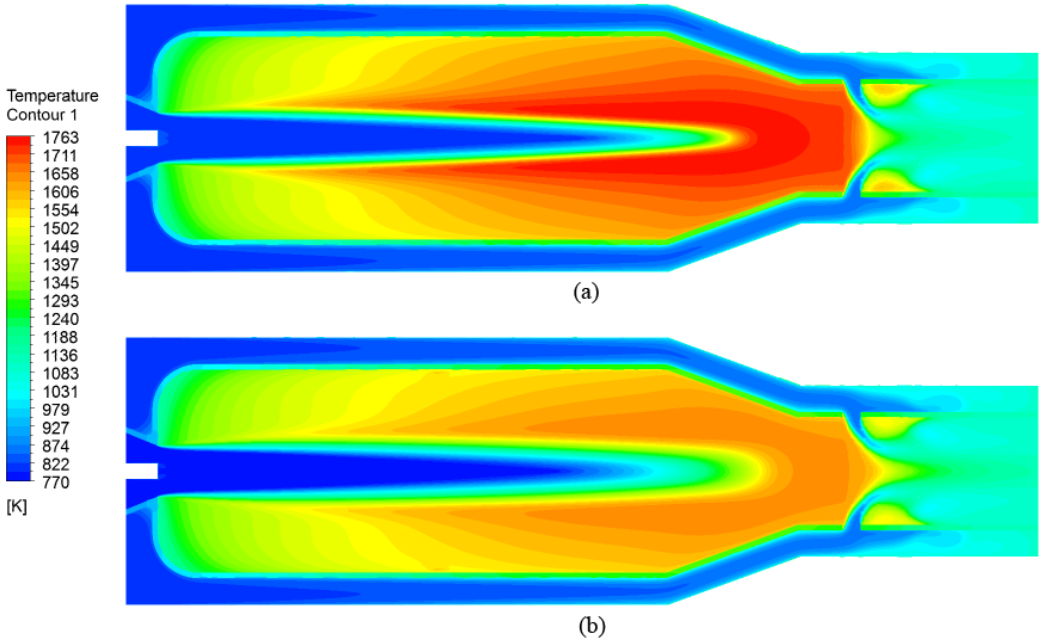

Figure 31. Temperature contours of flameless mode with natural gas (a) and landfill gas (b).

The highest temperatures in these contours, much lower than in full-load flame mode, confirm the accomplishment of one of the main goals of the present project. The maximum temperature was calibrated for natural gas by controlling the equivalence ratio, and it is equal to 1763 K. This is considered an ideal level and fall inside the range for combined low emissions of CO and NO_x given by Lefebvre & Ballal (2010), that is from 1670 K to 1900 K. When utilizing landfill gas, the same equivalence ratio of 0.55 was applied, leading to a maximum temperature of 1654 K. Although it is a slightly below, this is still quite close to the lower limit of the range previously mentioned.

The temperature profiles are more similar between the two fuels in flameless mode, although the central jet with landfill gas is more diffused, while the natural gas present higher gradients. This behavior might be explained by the higher concentration of methane in natural gas, causing faster reactions. In addition, the temperature is not completely evenly distributed through the primary zone, as mentioned in Section 6. This is because the heat transfer through the combustor walls is being modelled, and the flow of dilution air was intentionally positioned along the outside walls to provide cooling. Therefore, it was expected that the internal temperature could not be completely even since heat is being

transferred to outside. However, this heat is not lost, but rather reintroduced to the main flow later with the dilution air at the dilution zone.

In order to provide a sequential visualization of the process, Figure 32 presents the contours of the three stages utilizing natural gas with the same temperature scale. These contours make the relative differences clearer. It is observed that the chamber is cold at the startup; the temperature of the flame at the startup is not as high as in full load; in flame full load mode the chamber has temperature high enough to switch to flameless; in flameless mode the temperature distribution is much more even than in stable flame cases and the maximum temperature is lower.

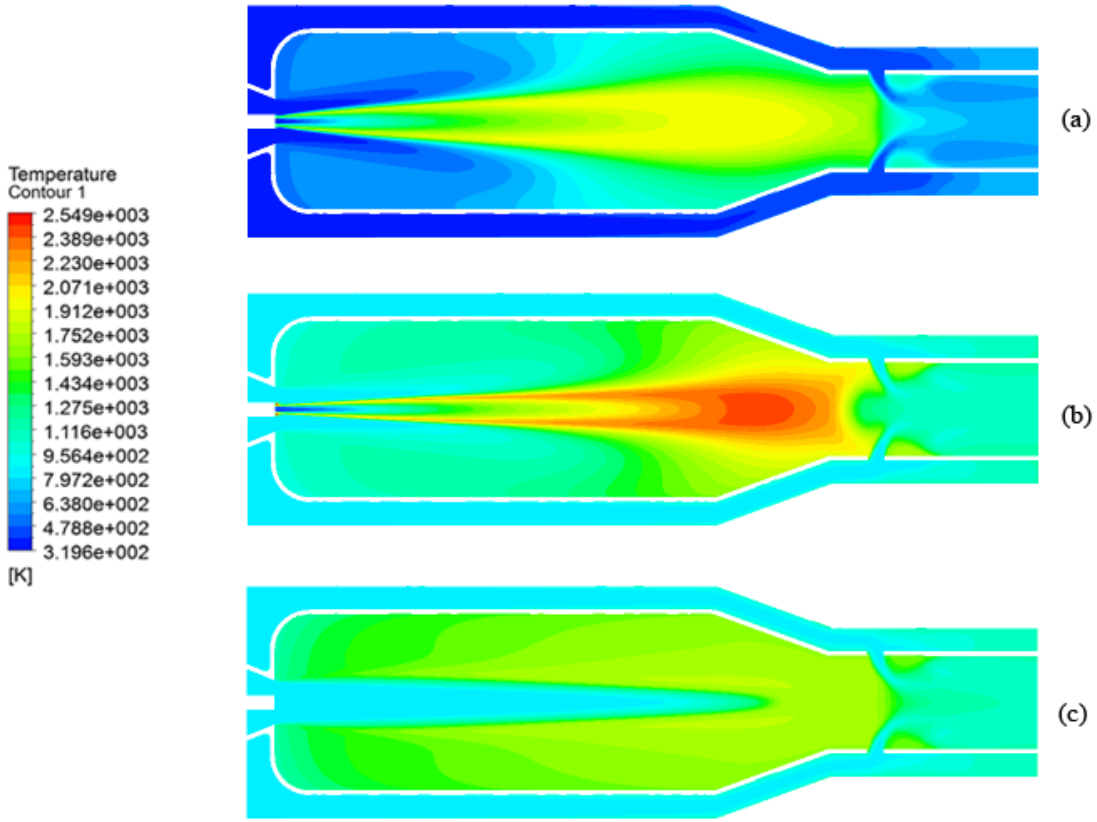

Figure 32. Temperature contours with natural gas in flame startup mode (a), flame full load mode (b) and flameless full load mode (c).

Having the longitudinal contours of temperature been analyzed, what gives better understanding about the functioning of the combustor, it is very important to verify if the outlet temperature matched the design value of the TIT. In addition, another primary characteristic of combustion chambers for gas turbines is the outlet temperature profile, that should be as even as possible to avoid temperature peaks and consequent damages on the

turbine blades. Table 6 summarizes the maximum temperature and the mass-weighted average of the temperature at the outlet of the combustor.

Table 6. Maximum and mass-weighted average of temperature at the outlet.

Case	Maximum temperature at the outlet [K]	Mass-weighted average of outlet temperature [K]
Natural gas		
Startup flame	670	645
Full load flame	1180	1095
Full load flameless	1150	1100
Landfill gas		
Startup flame	665	650
Full load flame	1160	1090
Full load flameless	1135	1100

It is observed that the peak temperatures are higher in full-load stable-flame mode. This was expected, firstly because the temperature profile before the dilution zone is much more uniform in flameless mode and, secondly, because the dilution zone was optimized for flameless operation. The average outlet temperatures under flameless regime with both fuels are very close to the value of 1100 K defined in Section 7.3. On the other hand, the temperatures in full-load flame mode are a bit lower, raising the possibility that a small portion of the fuel is not being burned. This is not considered problematic since it is just a transition stage and the temperatures are considered close enough to the design TIT. In order to provide an illustrative comparison between the outlet temperature profiles, Figure 33 presents the contours of temperature of all full-load cases in the same scale. The startup cases were excluded from this comparison since the temperatures are much lower.

It is clearly seen that the temperature gradients are more pronounced in stable flame modes, and the hot spots located at the peripheries are created in between the nine jets of the dilution holes. The iterative design procedure showed that up to certain limit, the smaller are the dilution holes, the better is the mixing at the center and the worse it is at the periphery, due to the increased velocity. The differences between maximum and minimum temperatures in the profiles of Figure 33a, b, c and d consist in 65 K, 126 K, 45 K and 108 K, respectively. The flameless cases are close to the targeted temperature difference for gas turbine combustors according to Boyce (2012), that is about 56 K. On the other hand, the differences

are higher in stable-flame cases, but due to the short period of operation in these modes, it is not considered a problem.

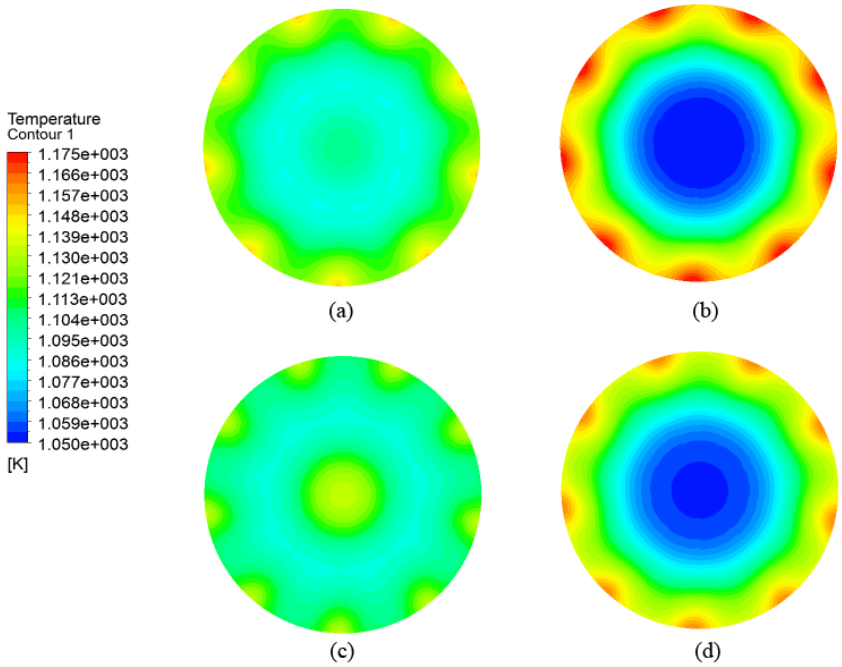

Figure 33. Contours of temperature at the outlet for natural gas flameless (a), natural gas full load flame (b), landfill gas flameless (c) and landfill gas full load flame (d) modes.

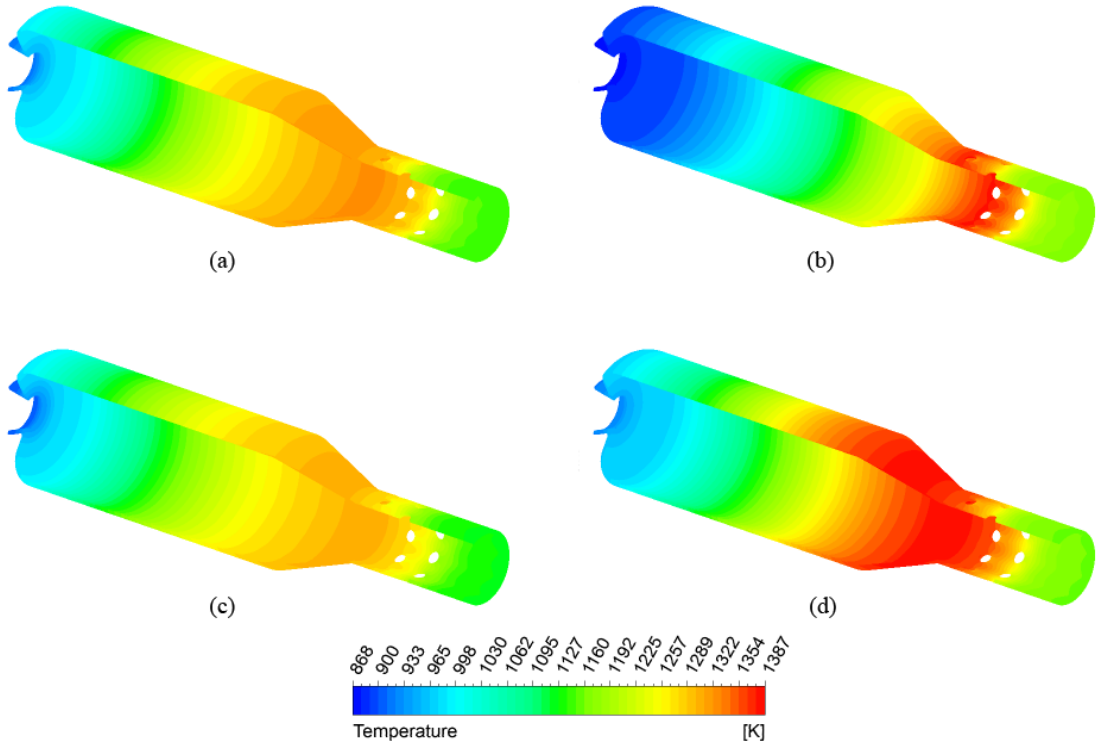

Figure 34. Temperature contours on the combustor walls for natural gas flameless (a), natural gas full load flame (b), landfill gas flameless (c) and landfill gas full load flame (d) modes.

The last consideration about temperatures regards the walls of the combustor, what influences the material choice. Figure 34 shows the temperature contours on the combustor walls for all full-load cases in a common scale. From these images, the effect of the cooling provided by the dilution air flowing outside the combustor is very clear. It causes the temperature gradient observed in longitudinal direction, especially in flameless cases that otherwise would have a much more uniform temperature. The highest temperature is achieved burning landfill gas in stable-flame mode, reaching 1387 K, closely followed by the case burning natural gas with a stable flame, that achieve 1383 K. In flameless cases, the maximum temperatures on the walls are 1323 K for natural gas and 1308 K for landfill gas. These results suggest that the ferritic alloy 4736 can be applied, although it is close to the limit of 1423 K given by the supplier Outokumpu (2018).

9.2 Velocities

The velocity field of a combustor is one of the most fundamental parameters that dictates whether it is functional or not. In flameless operation, high levels of turbulence and recirculation are necessary, while lower velocities are required for a stable flame.

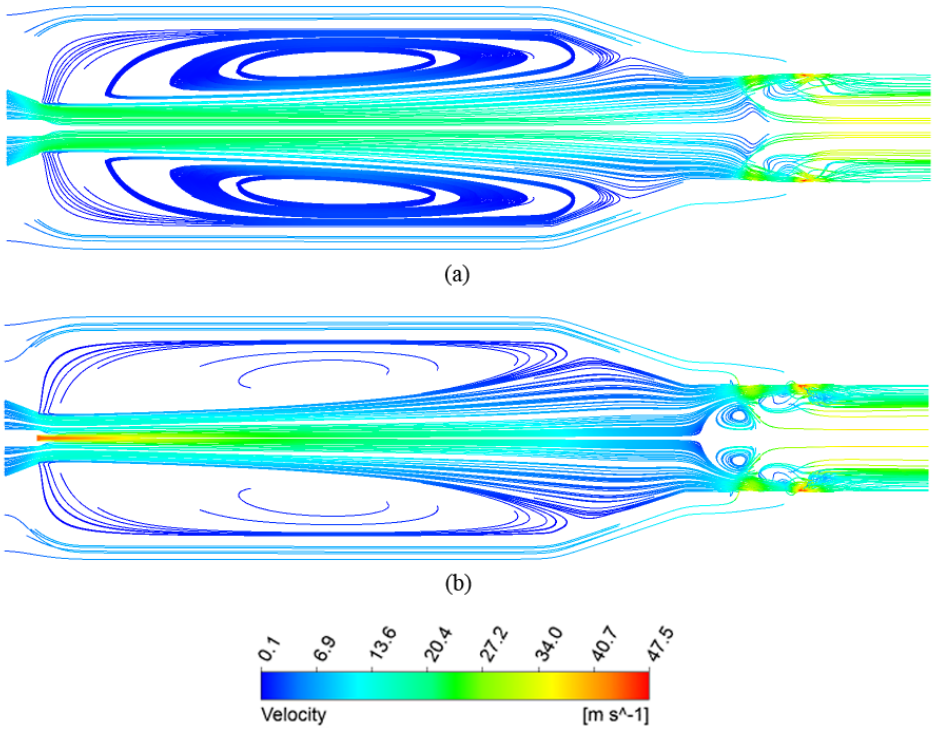

Figure 35. Vector fields and stream lines of velocity for natural gas in flameless (a) and full-load flame (b) modes.

Figure 35 presents the stream lines of the combustor burning natural gas in both flameless and full-load flame modes. It is clearly seen that the central jets produce a recirculating effect at the surroundings, and this phenomenon is maximized in flameless case due to the higher momentum of the axial jet. This is of primary importance for the correct functioning of the combustor, since the flameless regime requires high exhaust gases recirculation rate. However, it should be noted that even in flameless mode, the velocity of the flow in upstream direction is substantially low, implying in a moderate recirculation rate. This is a consequence of utilizing a common central jet for both flameless and stable-flame operation. While maintaining the design simple, the single axial jet provides relatively low recirculation, what may lead to conditions out of the ideal for flameless combustion. This could be improved with the implementation of dedicated inlets for flameless mode, positioned around the axis. Nevertheless, at least in CDF simulations, the common axial inlet did not prevent a successful operation.

Further important observations are associated to the velocity fields. In stable-flame mode, the inlet air has lower velocity compared to flameless, around 12 m/s, while the fuel is injected at 44 m/s. This velocity difference between air and fuel demonstrated to be essential for flame operation, because it provides the friction necessary for fast mixing and reaction. It should be recalled that the maximum speed of a turbulent flame of natural gas is about 15 m/s, and the flow velocity at the central part of the chamber achieve this level just at the second half of the liner. This explains the stretching of the natural gas flame observed in Figure 30a. Furthermore, as already mentioned, the different air inlet velocities are possible due to the different equivalence ratio between the two cases. A consequence of this is since less air enters the primary zone in flame mode, more air has to be added at the dilution zone, increasing the momentum of the dilution jets. The effect is clearly observed in Figure 35b, where a recirculation region is formed upstream the dilution zone due to the shock between the jets.

Figure 36 presents analog results for landfill gas. The main difference regards the velocity of the fuel jet, that is almost the double compared to the natural gas. This is required because of the lower LHV of the landfill gas, therefore more fuel is necessary to elevate the temperature of the air to the same level. Although the intuition may lead to the thinking that higher velocity might be prejudicial to the stable flame since it has a limited speed to be established, the results provided different conclusions, as already presented in Figure 30. The apparent better performance of the landfill gas flame with a higher velocity jet is

possibly related to the higher friction with the air, enhancing the mixing and the reaction speed, or because of its different composition, that may affect the chemical kinetics.

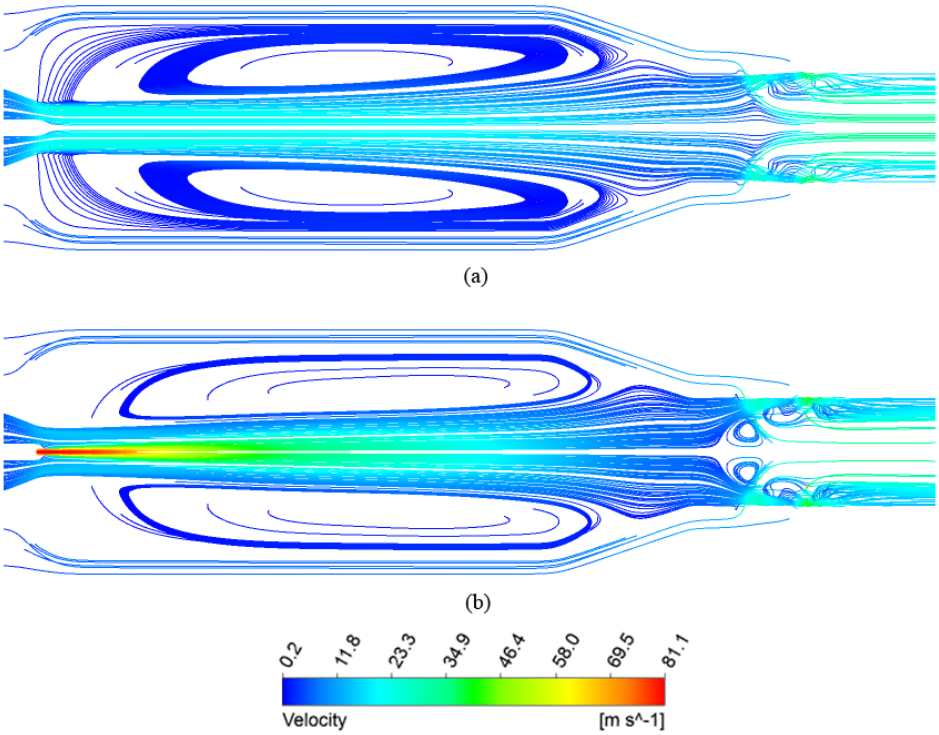

Figure 36. Vector fields of velocity for landfill gas in flameless (a) and full-load flame (b) modes.

9.3 Pressures

As stated in Section 3.1, the pressure drop is one of the main performance parameters of a combustor, having a direct impact on the thermal efficiency of the gas turbine. As much as possible, the pressure drop should be minimized to avoid significative losses. Figure 37 shows the static pressure contours for all full-load cases. The static values are being presented instead of the total ones because there are relatively high local dynamic pressures at the fuel jets of flame cases, that bring the total pressure scale high enough to make all contours look similar. However, it should be clear the total values are utilized to calculate the pressure drop.

It is observed in Figure 37 that the pressure is always higher at the outside fluid volume. In fact, since the inlet boundary conditions are given as mass flows, these contours are saying that in order to allow such a flow, the pressure has to be higher at the dilution inlet. In practice, this is achieved by adding a control valve at the primary fuel inlet, that creates the required pressure difference between the two air inlets. Assuming that the pressure

immediately upstream the valve is equal to the pressure at the dilution air inlet, the pressure drop of the combustor is then $\Delta p_{\mathrm{b}} = p_{\mathrm{air,d}} - p_{\mathrm{out}}$.

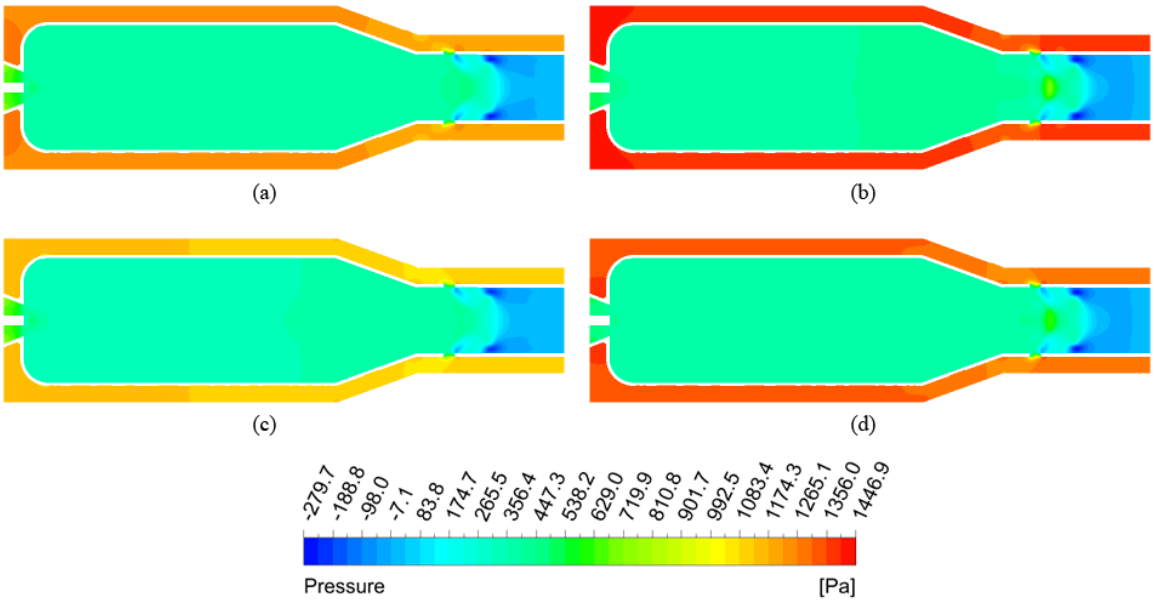

Figure 37. Static pressure contours for natural gas flameless (a), natural gas full load flame (b), landfill gas flameless (c) and landfill gas full load flame modes.

Table 7 summarizes the pressure drop required from the primary air stream valve and the absolute and relative combustor pressure drops for all full-load cases. The relative losses are calculated in relation to the inlet total pressure, that for full-load cases is equal to 340,067 Pa.

Table 7. Absolute and relative pressure drops for all full-load cases.

Case	Valve pressure drop [Pa]	Combustor pressure drop [Pa]	Combustor relative pressure drop [-]
Natural gas			
Full load flame	873	1055	0.31%
Full load flameless	535	922	0.27%
Landfill gas			
Full load flame	831	994	0.29%
Full load flameless	404	831	0.24%

These relative pressure drops are remarkably low for a gas turbine combustor. The main reasons are the low velocities, that minimize both hot and cold losses, and the simple straight-through geometry, that also induce very small cold losses. Indeed, among many disadvantages of scaling a gas turbine down to an electric power of 2 kW, this appears to be

an advantage. In large gas turbines, the volume of the combustion chamber is a limiting factor, therefore the flow velocities probably cannot be reduced to the levels utilized in the present combustor. In micro gas turbines, on the other hand, if the application does not impose special requirements, it is much easier to adopt a relatively large combustor. The impact of these low pressure drops are easily quantified by going back to the cycle calculations of Section 7.3. Replacing the guessed losses of 5% by the 0.27% obtained in flameless mode burning natural gas, the electrical efficiency rises from 18.8% to 20.7%, what is a considerable improvement.

9.4 Pollutants

One of the most attractive characteristics of flameless combustion is the potential to produce much lower emissions compared to diffusive combustors, even lower than DLN/DLE designs. Therefore, the pollutants formation is an important part of the analysis and it was evaluated with the Decoupled Detailed Chemistry of ANSYS Fluent, solving the concentrations of CO, NO and NO_2. Due to the computational expenses, only the cases of flameless and full-load stable-flame for natural gas were solved with detailed chemistry. The results are presented in Figure 38.

The contours of pollutant mole fraction show very interesting results. The first is that the flame cases present small regions with very high concentration of CO and NO, while in flameless there is more distribution and lower concentrations. In turn, for NO_2 both cases present distributed concentrations, with levels again higher for flame mode. It is also noted that the NO_2 has lower representativeness than NO, especially in the flame case.

In order to make final conclusions about pollutants, it is important to analyze the concentrations at the outlet in the same unit utilized by most of other similar studies. It consists in parts per million by dry volume (i.e., ppmv). The conversion from molar fraction to ppmv is done with Equation (17) and corrected to 15% of oxygen utilizing Equation (18).

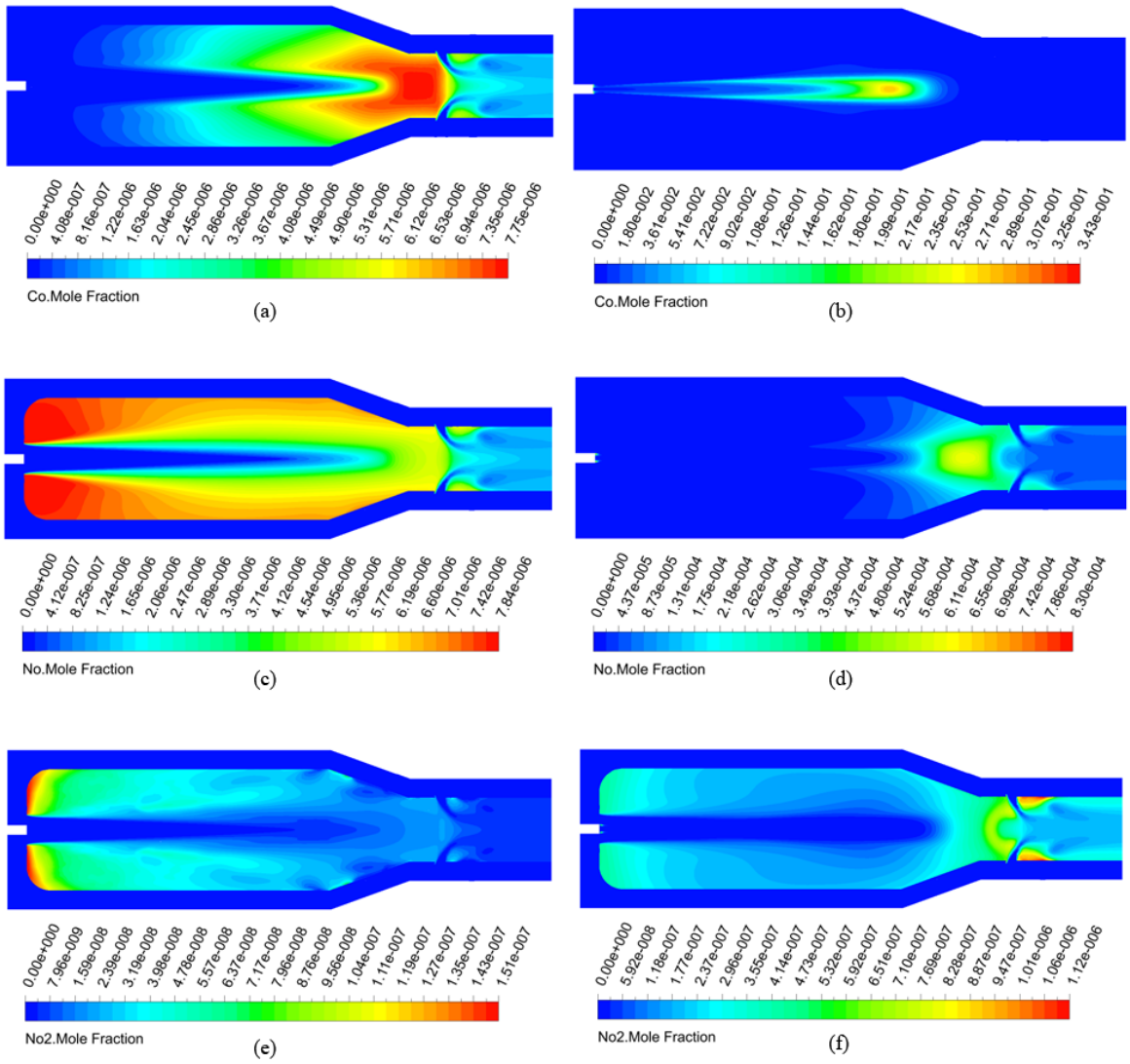

Figure 38. Contours of pollutants mole fraction for flameless case at the left and full-load stable-flame at the right, both burning natural gas.

After the conversion, the values are comparable to all others mentioned previously in this report. The results are presented in Table 8.

Table 8. Pollutants concentration at the outlet corrected to 15% O_2, using natural gas as fuel.

Pollutant	**Flameless mode [ppmv]**	**Stable-flame mode [ppmv]**
Carbon monoxide (CO)	3.20	98.83
Nitric oxide (NO)	3.04	145.79
Nitrogen dioxide (NO_2)	0.01	0.59

According to all literature reviewed, these values are apparently in a realistic range and if the numbers for flameless mode can be in fact reproduced experimentally, the results are

considered exceptional. It should be recalled that when steam injection was firstly introduced, it allowed the reduction of NO_x emissions to levels below 75 ppmv. In very demanding applications, SCR is used to provide NO_x < 10 ppmv, while DLN/DLE combustors usually have as target NO_x < 25 ppmv. Therefore, the obtained marks of about 3 ppmv for both CO and NO_x are considered very low. A comparison with the results in stable-flame mode makes clear the difference between the conventional combustion technique and the flameless combustion. The emissions of CO and NO_2 are one order lower and the NO is two orders lower in flameless mode.

Based on the literature previously reviewed, the values of NOx obtained for stable-flame operation are considered realistic for a conventional combustion without any emissions reduction technique. In turn, the CO seems to be somehow high, since there is no reason for its increased production under high temperature. A possible reason might be that a small amount of the fuel is not being burned in full-load stable-flame mode, since the presence of CO in the exhaust gases is usually accompanied by UHC. This conclusion also agrees with the fact that the average outlet temperature in this mode is slightly lower than what it should be. However, since the flame mode is just a transient stage, this is not considered problematic.

9.5 Discretization uncertainty

Computational fluid dynamics simulations are always subject to numerical error and/or uncertainties due to the spatial discretization. Therefore, establishing a standard procedure to estimate the error is essential to understand how trustworthy the results are. In the present study, the method presented by ASME (2008) for estimation and reporting of uncertainties related to CFD applications is employed.

The procedure requires initially the simulation of the cases with three different meshes, that should have a recommended relative difference in the number of cells. With this purpose, the mesh presented in Section 8.3 was utilized as basis to create a coarser and a finer mesh, according to the given criteria. The result was one mesh with 227,000 cells and another with 1,637,000 cells, being that the main mesh has 581,000 cells.

The case chosen for uncertainty analysis was the flameless burning natural gas. After the calculations are done with the three meshes, some important quantities for the study have to

be selected for comparison. Here, the maximum temperature in the fluid volume, the mass-weighted temperature at the outlet and the mass-weighted total pressure at the dilution air inlet are chosen. It would be also interesting to add the pollutants at the outlet in the analysis, however they were not calculated with the secondary grids due to the computational power required, especially for the fine grid. Next, following the procedure described by ASME (2008), the apparent order of discretization, the approximated relative error, the extrapolated relative error and the fine-grid convergence index are calculated. The latter is then utilized to define the dimensional range of discretization error. All these values are presented in Table 9.

Table 9. Calculations of discretization error.

Parameter	**Maximum temperature**	**Average outlet temperature**	**Total pressure at dilution inlet**
Value with fine mesh	1770.3 K	1104.4 K	1288 Pa
Value with main mesh	1763.2 K	1102.3 K	1274 Pa
Value with coarse mesh	1765.0 K	1103.4 K	1285 Pa
Apparent order	2.00	1.65	0.69
Approximate relative error	0.4%	0.2%	1.1%
Extrapolated relative error	0.4%	0.3%	3.8%
Fine-grid convergence index	0.5%	0.3%	5.0%
Discretization error	± 8.9 K	± 3.5 K	± 63.4 Pa

Note that the values of the last four rows refer to the difference between the fine and the main meshes, however they are also calculated between the main and coarse meshes, as it will be shown in next figures. According to ASME (2008), an agreement of the apparent order with the formal order of the schemes utilized – in this case second order, or 2 – is a good sign that the grids are asymptotic. However, the contrary does not necessarily mean unsatisfactory calculations, but it can indicate oscillating convergence, as it is the case here. This is clearly observed in Table 9, in which the values of the main mesh do not fall between the values of the fine and coarse meshes. This behavior persisted even after running the simulations for several thousands of iterations after a reasonable convergence, as exemplified in Figure 39 for the total pressure at the dilution air inlet with the finer grid.

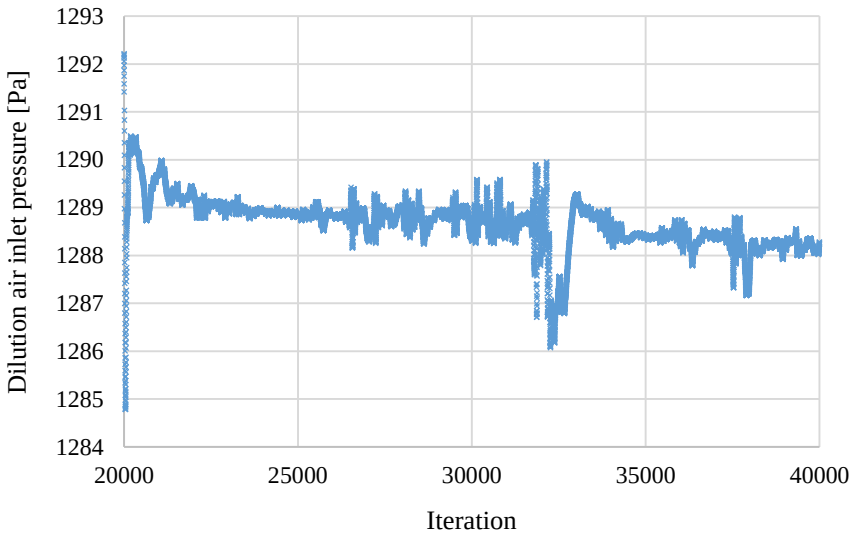

Figure 39. Behavior of the total pressure at the dilution air inlet between iterations 20,000 and 40,000 with the finer mesh.

Another necessary clarification is that the apparent order for the maximum temperature was limited to 2.00 because of the second order schemes utilized, although the result of the method was 3.66. Having all these been stated, the data of Table 9 and analog calculations for the error between the main and coarse mesh are graphically represented with error bars in Figure 40, Figure 41 and Figure 42.

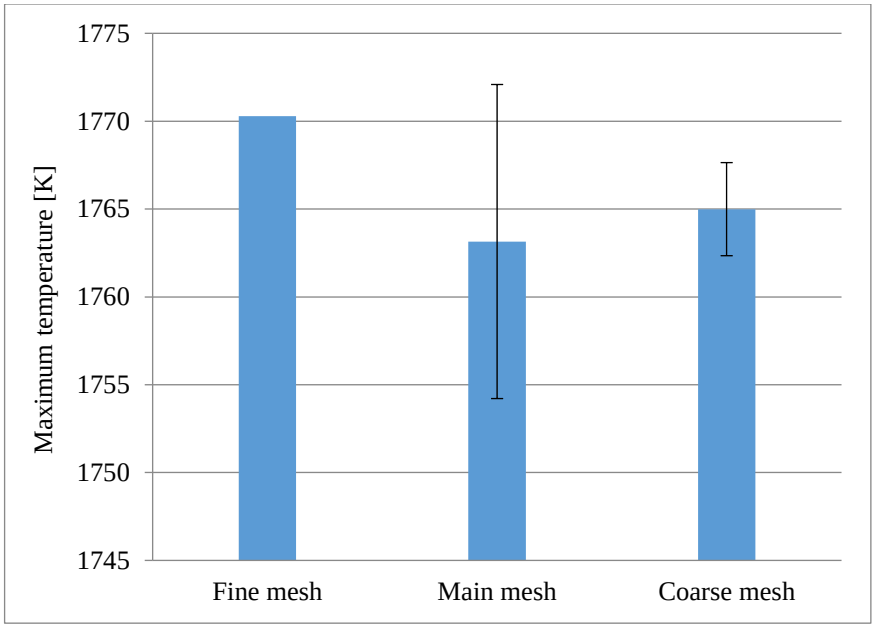

Figure 40. Discretization uncertainty of maximum temperature at the fluid domains.

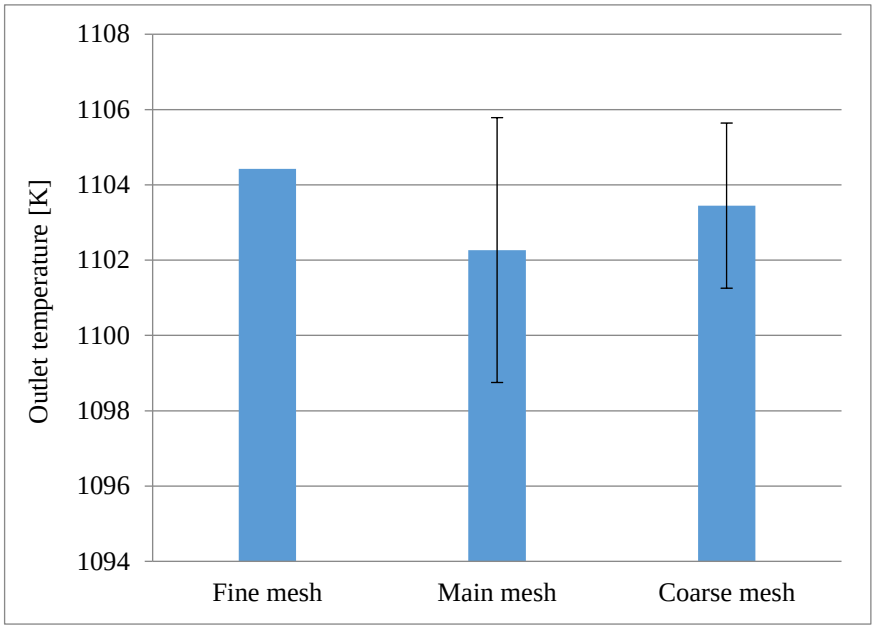

Figure 41. Discretization uncertainty of mass-weighted temperature at the outlet.

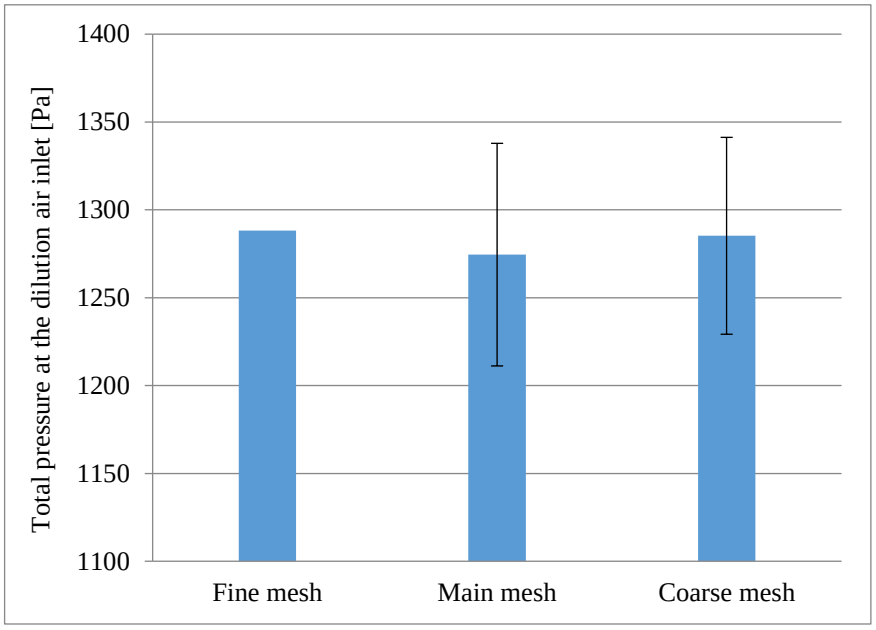

Figure 42. Discretization uncertainty of mass-weighted pressure at the dilution air inlet.

10 CONCLUSIONS AND DISCUSSION

This thesis investigated the phenomenon of flameless combustion applied to gas turbines, and a new combustor for 2-kW_{el} micro gas turbines was designed and analyzed through computational fluid dynamics (CFD). The flameless concept is already an established technology for industrial furnaces, however its application in gas turbines is still a research topic. Therefore, there are still several uncertainties, especially related to CFD in the sense of which models are the most suitable, how/if they have to be specially calibrated and how accurate they are. These reasons emphasize the necessity of studies as the present one, followed by experimental investigation to develop further this high-potential technology.

Flameless combustion requires high exhaust gases recirculation and high preheating temperatures to be established. It was demonstrated that external recirculation, commonly used in furnaces, is not practical for gas turbines application. The reason is the imminent penalty to the thermal efficiency of the engine, caused by the injection of hot gases at the compressor inlet. Therefore, internal recirculation is preferred, characterizing the combustor as adiabatic. In turn, the high preheating temperatures are necessary to maintain a continuous self-ignition of the fuel, characteristic of flameless combustion. This also means that the flameless regime cannot be established in ambient conditions, and a stable flame is necessary to realize the preheating task. The fact that a stable flame and the flameless combustion cannot exist under similar circumstances is one of the main challenges in the design of such a combustor.

The design proposed has straight-through configuration, favoring the cooling of the walls with the dilution air, that flows along the outside of the liner. It should be reminded that film cooling through small holes is not possible in flameless combustion due to the interference on the recirculation flow and the cooling of the primary zone, what could prevent the self-ignition reactions. The presented combustor deals with the challenge of handling both flame and flameless regimes by adopting different equivalence ratios for each operational mode. The equivalence ratio for flameless combustion is adjusted in order to reach optimum temperatures for combined low emissions of CO and NO_x, while for flame mode it is fixed in a higher value. In this way, more air is injected into the primary zone in flameless mode, providing higher velocities, more turbulence and recirculation, necessary to establish the regime. On the other hand, less primary air is used in flame mode, reducing the velocities to levels in which a flame can be stabilized.

The straight-through design with a central inlet jet is ideal to produce a stable flame. However, the utilization of the same inlet for flameless mode, even with higher velocities, brings the recognized drawback of weak recirculation. This design choice was done to keep the combustor simple, easy to manufacture and operate. Indeed, CFD simulations predicted a successful operation in flameless mode, but in case these results cannot be reproduced experimentally, it is suggested to create separated and dedicated air inlets for flameless combustion. These inlets could be a circular pattern of six or eight high-speed jets around the central jet already present in the design, that could provide higher turbulence and recirculation. In addition, the described transition procedure from stable-flame to flameless regime includes a switch of the fuel inlet from the axial small jet to upstream inlets that would premix the fuel with the air before entering the chamber. There is a possibility that this action is not necessary, and the flameless mode can be established just by increasing the primary air velocity, keeping the axial fuel inlet and eliminating the premixing. However, such case was not simulated, and one should note that the flame has to be extinguished for correct start of flameless combustion. Cutting the fuel inlet is a safer way to guarantee this, rather than just increasing the velocity.

The results obtained from CFD analysis are very encouraging for the application of flameless technology in gas turbines. Besides the attractive features of flameless combustion as uniform temperature distribution, low noise, low vibration and the capacity to handle low-quality fuels, the reduction in emissions demonstrated to be dramatic. In flameless mode, the combustor produced about 3 ppmv (dry and corrected for 15% O_2) of both NO_x and CO, compared to 99 ppmv of CO and 146 ppmv of NO_x in flame mode. Combustion applications that produce less than 10 ppmv of NO_x are considered very low emission. Besides, the combustor demonstrated to be operational with both natural gas and landfill gas, although particulates that may be present in low grade fuels as landfill gas were not modelled. Moreover, the feature of distributed temperature could be even better explored if the TIT can reach values such as 1800 K. In this case, the dilution zone could be completely eliminated, providing an extremely uniform temperature profile. Even with lower TIT it is possible to eliminate the dilution zone by adopting lower equivalence ratios. However, this can be done just up to certain limit and it would bring the temperatures out of the low emissions span, increasing the CO amount at the outlet.

Another part of the results that should be highlighted is not directly related to the flameless combustion, but to the scale of the planned gas turbine. Although the thermal efficiency of

a 2-kW_{el} gas turbine is penalized by some issues, especially related to the small-size turbomachinery, the pressure drop through the combustor can be greatly minimized, creating a counterpoint to these losses. This is possible because in such small scale it is easy to adopt a combustion chamber relatively large, if the application allows. Therefore, the velocities are lower, and consequently, also are the losses. The simulations showed a pressure drop of 0.27% in full-load flameless mode burning natural gas. Compared to a typical value of 5%, the gain in electrical efficiency is close to 2%.

Further studies on this topic would necessarily require prototyping and experimental investigation to validate the CFD results. This is especially important to clarify if the numerical models adopted are suitable and accurate for this application, and to evaluate the necessity for special refinement and calibration. It should be noted that CFD analysis of flameless combustion applied to gas turbines is not extensively documented yet and there are some divergences about the ideal models for it. In addition, further numerical investigations could include the necessity of air-fuel premixing for flameless condition, the pollutant analysis utilizing landfill gas and the flameless operation in partial load. Nevertheless, some auxiliary systems still have to be planned and implemented, such as the control of the primary air valve in partial load, the ignition and premixing systems – the latter just in case it is necessary.

To conclude, flameless combustion is a technology with high potential to be applied in gas turbines that will compose the future energy systems. In the preset thesis, a combustion chamber with this concept was designed for a 2-kW_{el} micro gas turbine, following the market trend for distributed generation and respecting the straightening emission requirements. Gas turbines burning renewable fuels, as landfill gas, might become an essential player to balance future energy systems, that have an each-day higher participation of intermittent renewables, as wind and solar power.

REFERENCES

Andreades, C., Scarlat, R. O., Dempsey, L. & Peterson, P., 2014. Reheat-Air Brayton Combined Cycle Power Conversion Design and Performance Under Nominal Ambient Conditions. *Journal of Engineering for Gas Turbines and Power,* 136(6).

ANSYS Inc., 2017. *Fluent theory guide,* Canonsburg: ANSYS.

Arghode, V. K. & Gupta, A. K., 2010. Effect of flow field for colorless distributed combustion (CDC) for gas turbine combustion. *Applied Energy,* Volume 87, pp. 1631-1640.

Arghode, V. K., Gupta, A. K. & Bryden, K. M., 2012. High intensity colorless distributed combustion for ultra low emissions and enhanced performance. *Applied Energy,* Volume 92, pp. 822-830.

ASME, 2008. Procedure for Estimation and Reporting of Uncertainty Due to Discretization in CFD Applications. *Journal of Fluids Engineering,* 130(7), pp. 078001(1)-078001(4).

Backman, J., Larjola, J. & Timonen, J., 2002. *Calculation of Gas Turbine Types (EN C-154),* Lappeenranta: Lappeenranta University of Technology.

Bakalis, D. P. & Stamatis, A. G., 2012. Full and part load exergetic analysis of a hybrid micro gas turbine fuel cell system based on existing components. *Energy Conversion and Management,* Volume 64, pp. 213-221.

Bao, H., 2017. *Development and validation of a new Eddy Dissipation Concept (EDC) model for mild combustion,* Delft: Delft University of Technology.

Bauer, C. & Forest, T., 2001. Effect of hydrogen addition on the performance of methane-fueled vehicles. Part I: effect on S.I. engine performance. *International Journal of Hydrogen Energy,* 26(1), pp. 55-70.

Benini, E. & Giacometti, S., 2007. Design, manufacturing and operation of a small turbojet-engine for research purposes. *Applied Energy,* Volume 84, pp. 1102-1116.

Borgnakke, C. & Sonntag, R. E., 2009. *Fundamentals of thermodynamics.* 7th ed. Hoboken: John Wiley & Sons.

Boyce, M. P., 1982. *Gas turbine engineering handbook.* Houston: Gulf Publishing Co.

Boyce, M. P., 2012. *Gas turbine engineering handbook.* 4th ed. Oxford: Elsevier Inc.

Bussar, C. et al., 2014. *Optimal allocation and capacity of energy storage systems in a future European power system with 100% renewable energy generation.* Berlin, Elsevier.

Cameretti, M. C., Tuccillo, R. & Piazzesi, R., 2013. Study of an exhaust gas recirculation equipped micro gas turbine supplied with bio-fuels. *Applied Thermal Engineering,* Volume 59, pp. 162-173.

Clay, A. & Tansley, G., 2011. Exploration of a simple, low cost, micro gas turbine recuperator solution for a domestic combined heat and power unit. *Applied Thermal Engineering,* Volume 31, pp. 2676-2684.

Danon, B., Cho, E.-S., de Jong, W. & Roekaerts, D., 2011. Numerical investigation of burner positioning effects in a multi-burner flameless combustion furnace. *Applied Thermal Engineering,* Volume 31, pp. 3885-3896.

Fortunato, V., Galletti, C., Tognotti, L. & Parente, A., 2015. Influence of modelling and scenario uncertainties on the numerical simulation of a semi-industrial flameless furnace. *Applied Thermal Engineering,* Volume 76, pp. 324-334.

Forzatti, P., 2001. Present status and perspectives in de-NOx SCR catalysis. *Applied Catalysis A: General,* 222(1-2), pp. 221-236.

Galletti, C., Parente, A. & Tognotti, L., 2007. Numerical and experimental investigation of a mild combustion burner. *Combustion and Flame,* Volume 151, pp. 649-664.

Han, S. et al., 2010. *Design and simulation of 500W ultra-micro gas turbine generator.* Leuven, International Conference on Micro- and Nano-Technology for Power Generation and Energy Conversion Applications.

Hewson, J. C. & Bollig, M., 1996. Reduced mechanisms for NOx emissions from hydrocarbon diffusion flames. *Twenty-Sixth Symposium (International) on Combustion,* pp. 2171-2179.

Hyung Do, K., Choi, B.-I., Han, Y.-S. & Kim, T., 2016. Experimental investigation on the pressure drop and heat transfer characteristics of a recuperator with offset strip fins for a micro gas turbine. *International Journal of Heat and Mass Transfer,* Volume 103, pp. 457-467.

Jaatinen-Värri, A. et al., 2016. *Design of a 400 kW gas turbine prototype.* Seoul, ASME Turbo Expo.

Khalil, A. E. & Gupta, A. K., 2017. Towards colorless distributed combustion regime. *Fuel,* Volume 195, pp. 113-122.

Khidr, K. I., Eldrainy, Y. A. & EL-Kassaby, M. M., 2017. Towards lower gas turbine emissions: Flameless distributed combustion. *Renewable and Sustainable Energy Reviews,* Issue 67, pp. 1237-1266.

Kim, J. P., Schnell, U. & Scheffknecht, G., 2008. Comparison of different global reaction mechanisms for MILD combustion of natural gas. *Combustion Science and Technology,* 180(4), pp. 565-592.

Kruse, S. et al., 2015. Experimental and numerical study of MILD combustion for gas turbine applications. *Applied Energy,* Volume 148, pp. 456-465.

Lagerström, G. & Xie, M., 2002. *High performance & cost effective recuperator for micro-gas turbines.* Amsterdam, ASME Turbo Expo.

Lammel, O. et al., 2010. FLOX® Combustion at high power density and high flame temperatures. *Journal of Engineering for Gas Turbines and Power,* Volume 132, pp. 12503 (1-10).

Launder, B. E. & Spalding, D. B., 1972. *Lectures in Mathematical Models of Turbulence,* London: Academic Press.

Lefebvre, A. H. & Ballal, D. R., 2010. *Gas turbine combustion - Alternative fuels and emissions.* 3rd ed. Boca Raton: CRC Press.

Levy, Y., Sherbaum, V. & Arfi, P., 2004. Basic thermodynamics of FLOXCOM, the low-NOx gas turbines adiabatic combustor. *Applied Thermal Engineering,* Volume 24, pp. 1593-1605.

Li, S. & Williams, F., 1999. NOx formation in two-stage methane–air flames. *Combustion and Flame,* 118(3), pp. 399-414.

Mackenzie, F. & Mackenzie, J., 1995. *Our changing planet.* 1st ed. Upper Saddle River: Prentice-Hall.

McBride, B. J., Gordon, S. & Reno, M. A., 1993. *NASA Technical Memorandum 4513 - Coefficients for Calculating Thermodynamic and Transport Properties of Individual Species,* Cleveland: National Aeronautics Space Administration (NASA).

MDEP, 2016. *Basics of landfill gas,* Boston: Massachusetts Department of Environmental Protection.

Micheli, D., Pediroda, V. & Pieri, S., 2007. *Multi-objective optimization of a microturbine compact recuperator.* Montreal, ASME Turbo Expo.

Miniati, G., Galletti, C., Parente, A. & Tognotti, L., 2015. Chemistry Reduction for Modelling Flameless Combustion of Ethylene. *Chemical Engineering Transactions,* Volume 43, pp. 2125-2130.

Nagasaki, T., Tokue, R., Kashima, S. & Ito, Y., 2003. *Conceptual Design of Recuperator for Ultramicro Gas Turbine.* Tokyo, Proceedings of the International Gas Turbine Congress.

Najjar, Y. S. H., 2011. Gaseous Pollutants Formation and Their Harmful Effects on Health and Environment. *Innovative Energy Policies,* Volume 1, pp. 1-9.

Noor, M. M., Wandel, A. P. & Yusaf, T., 2013. Analysis of recirculation zone and ignition position of non-premixed bluff-body for biogas MILD combustion. *International Journal of Automotive and Mechanical Engineering,* Volume 8, pp. 1176-1186.

Outokumpu, 2018. *High temperature grades –performance at 550°C and above.* [Online] Available at: http://www.outokumpu.com/en/products-properties/more-stainless/stainless-steel-types/heat-resistant/Pages/default.aspx
[Accessed 10 May 2018].

Panwar, N., Kaushik, S. & Kothari, S., 2011. Role of renewable energy sources in environmental protection: A review. *Renewable and Sustainable Energy Reviews,* 12 January, Volume 15, pp. 1514-1524.

Parente, A., Galletti, C. & Tognotti, L., 2008. Effect of the combustion model and kinetic mechanism on the MILD combustion in an industrial burner fed with hydrogen enriched fuels. *International Journal of Hydrogen Energy,* Volume 33, pp. 7553-7564.

Pavri, R. & Moore, G. D., 2001. *Gas turbine emissions and control,* Atlanta: General Electric Report No. GER-4211.

Pepermans, G. et al., 2005. Distributed generation: definition, benefits and issues. *Energy Policy,* Volume 33, pp. 787-798.

Plessing, T., Peters, N. & Wünning, J. G., 1998. Laseroptical investigation of highly preheated combustion with strong exhaust gas recirculation. *Twenty-Seventh Symposium (International) on Combustion,* pp. 3197-3204.

Rao, A. G. & Yeshayahou, L., 2010. *A new combustion methodology for low emission gas turbine engines,* Delft: s.n.

Rogiers, F., Stevens, T. & Baelmans, M., 2006. *Optimal recuperator design for use in a micro gas turbine.* Berkeley, The Sixth International Workshop on Micro and Nanotechnology for Power Generation and Energy Conversion Applications.

Samuelsen, S., 2006. *Rich Burn, Quick Mix, Lean Burn (RQL) combustor,* Washington DC: US Department of Energy.

Saravanamuttoo, H. I. H., Rogers, G. F. C. & Cohen, H., 2001. *Gas turbine theory.* 5th ed. Harlow: Pearson Education Ltd.

Schiffmann, J. & Favrat, D., 2010. Design, experimental investigation and multi-objective optimization of a small-scale radial compressor for heat pump applications. *Energy,* 35(1), pp. 436-450.

Shih, T. H. et al., 1995. A New k-ε Eddy-Viscosity Model for High Reynolds Number Turbulent Flows - Model Development and Validation. *Computers Fluids,* 24(3), pp. 227-238.

Sorrentino, G. et al., 2015. Development of a novel cyclonic flow combustion chamber for achieving MILD/Flameless Combustion. *Energy Procedia,* Volume 66, pp. 141-144.

Stazi, M., Battaglia, V., Malfa, E. & Fantuzzi, M., 2011. *Flameless combustion modelling using detailed chemistry mechanism.* Cardiff, European Combustion Meeting.

Stevens, T. & Baelmans, M., 2008. Optimal pressure drop ratio for micro recuperators in small sized gas turbines. *Applied Thermal Engineering,* Volume 28, pp. 2353-2359.

Tabacco, D., Innarella, C. & Bruno, C., 2002. Theoretical and numerical investigation on flameless combustion. *Combustion Science and Technology*, 174(7), pp. 1-35.

Tiainen, J., Grönman, A., Jaatinen-Värri, A. & Backman, J., 2017. Flow Control Methods and Their Applicability in Low-Reynolds-Number Centrifugal Compressors - A Review. *International Journal of Turbomachinery, Propulsion and Power,* 3(1), pp. 1-38.

Traverso, A. & Massardo, A. F., 2005. Optimal design of compact recuperators for microturbine application. *Applied Thermal Engineering,* Volume 25, pp. 2054-2071.

Tuttle, S., Hinnant, K. & Vick, M., 2017. *Preliminary design, ignition, and fuel injection for a high temperature recuperated microturbine combustor.* Charlotte, ASME.

U.S. Code of Federal Regulations, 2010. *Standards of performance for new stationary sources - Appendix B,* Washington: U.S. Government Publishing Office.

Union Gas Ltd., 2017. *Chemical Composition of Natural Gas.* [Online] Available at: https://www.uniongas.com/about-us/about-natural-gas/chemical-composition-of-natural-gas
[Accessed 19 March 2018].

Vascellari, M. & Cau, G., 2012. Influence of turbulence–chemical interaction on CFD pulverized coal MILD combustion modeling. *Fuel,* Volume 101, pp. 90-101.

Veríssimo, A., Rocha, A. & Costa, M., 2013. Importance of the inlet air velocity on the establishment of flameless combustion in a laboratory combustor. *Experimental Thermal and Fluid Science,* Volume 44, pp. 75-81.

Vick, M. et al., 2016. *A simple recuperated ceramic microturbine: design concept, cycle analysis, and recuperator component prototype tests.* Seoul, ASME Turbo Expo.

Wilcox, D. C., 2006. *Turbulence Modelling for CFD.* 3rd ed. La Canada: DCW Industries.

Wilson, D. G., 1984. *The design of high-efficiency turbomachinery and gas turbines.* Cambridge: MIT Press.

Wünning, J. A. & Wünning, J. G., 1997. Flameless oxidation to reduce thermal no-formation. *Progress in Energy and Combustion Science,* Volume 23, pp. 81-94.

Xiao, G. et al., 2017. Recuperators for micro gas turbines: A review. *Applied Energy,* Volume 197, pp. 83-99.

Xing, F. et al., 2017. Flameless combustion with liquid fuel: A review focusing on fundamentals and gas turbine application. *Applied Energy,* Issue 193, pp. 28-51.

APPENDIX I – VBA CODE FOR MIXTURE PROPERTIES

```
'Universal constant of gases, J/(mol K)'

Public Const R As Double = 8.31451

'Molar mass, kg/mol'

Public Const O2_molar_mass = 0.0319988, N2_molar_mass = 0.0280134, CO2_molar_mass = 0.0440095, H2O_molar_mass = 0.01801528, CH4_molar_mass = 0.0160425

Function cp_O2(ByVal T As Double) As Double

If T > 1000 Then

    a1 = 3.66096083
    a2 = 0.000656365523
    a3 = -0.000000141149485
    a4 = 2.05797658E-11
    a5 = -1.29913248E-15
    b1 = -1215.97725
    b2 = 3.41536184

Else

    a1 = 3.78245636
    a2 = -0.00299673415
    a3 = 0.000009847302
    a4 = -9.68129508E-09
    a5 = 3.24372836E-12
    b1 = -1063.94356
    b2 = 3.65767573

End If

    cp_O2 = (a1 + a2 * T + a3 * T ^ 2 + a4 * T ^ 3 + a5 * T ^ 4) * R / O2_molar_mass

End Function

Function cp_Ar(ByVal T As Double) As Double

    a1 = 2.5
    a2 = 0
    a3 = 0
    a4 = 0
    a5 = 0
    b1 = -745.375
    b2 = 4.37967491

    cp_Ar = (a1 + a2 * T + a3 * T ^ 2 + a4 * T ^ 3 + a5 * T ^ 4) * R / Ar_molar_mass
```

```
End Function

Function cp_N2(ByVal T As Double) As Double

If T > 1000 Then

    a1 = 2.95257626
    a2 = 0.00139690057
    a3 = -0.000000492631691
    a4 = 7.86010367E-11
    a5 = -4.60755321E-15
    b1 = -923.948645
    b2 = 5.87189252

Else

    a1 = 3.53100528
    a2 = -0.000123660987
    a3 = -0.000000502999437
    a4 = 2.43530612E-09
    a5 = -1.40881235E-12
    b1 = -1046.97628
    b2 = 2.96747468

End If

    cp_N2 = (a1 + a2 * T + a3 * T ^ 2 + a4 * T ^ 3 + a5 * T ^ 4) * R / N2_molar_mass

End Function

Function cp_CO2(ByVal T As Double) As Double

If T > 1000 Then

    a1 = 4.63659493
    a2 = 0.00274131991
    a3 = -0.000000995828531
    a4 = 1.60373011E-10
    a5 = -9.16103468E-15
    b1 = -49024.9341
    b2 = -1.93534855

Else

    a1 = 2.35677352
    a2 = 0.00898459677
    a3 = -0.00000712356269
    a4 = 2.45919022E-09
    a5 = -1.43699548E-13
    b1 = -48371.9697
    b2 = 9.90105222
```

```
End If

    cp_CO2 = (a1 + a2 * T + a3 * T ^ 2 + a4 * T ^ 3 + a5 * T ^ 4) * R / CO2_molar_mass

End Function

Function cp_H2O(ByVal T As Double) As Double

If T > 1000 Then

    a1 = 2.67703787
    a2 = 0.00297318329
    a3 = -0.00000077376969
    a4 = 9.44336689E-11
    a5 = -4.26900959E-15
    b1 = -29885.8938
    b2 = 6.88255571

Else

    a1 = 4.19864056
    a2 = -0.0020364341
    a3 = 0.00000652040211
    a4 = -5.48797062E-09
    a5 = 1.77197817E-12
    b1 = -30293.7267
    b2 = -0.849032208

End If

    cp_H2O = (a1 + a2 * T + a3 * T ^ 2 + a4 * T ^ 3 + a5 * T ^ 4) * R / H2O_molar_mass

End Function

Function h_O2(ByVal T As Double) As Double

If T > 1000 Then

    a1 = 3.66096083
    a2 = 0.000656365523
    a3 = -0.000000141149485
    a4 = 2.05797658E-11
    a5 = -1.29913248E-15
    b1 = -1215.97725
    b2 = 3.41536184

Else

    a1 = 3.78245636
    a2 = -0.00299673415
    a3 = 0.000009847302
    a4 = -9.68129508E-09
```

```
    a5 = 3.24372836E-12
    b1 = -1063.94356
    b2 = 3.65767573

End If

    'enthalpy, kJ/kg'

    h_O2 = (a1 + a2 * T / 2 + a3 * T ^ 2 / 3 + a4 * T ^ 3 / 4 + a5 * T ^ 4 / 5 + b1 / T) * R * T
/ O2_molar_mass / 1000

End Function

Function h_N2(ByVal T As Double) As Double

If T > 1000 Then

    a1 = 2.95257626
    a2 = 0.00139690057
    a3 = -0.000000492631691
    a4 = 7.86010367E-11
    a5 = -4.60755321E-15
    b1 = -923.948645
    b2 = 5.87189252

Else

    a1 = 3.53100528
    a2 = -0.000123660987
    a3 = -0.000000502999437
    a4 = 2.43530612E-09
    a5 = -1.40881235E-12
    b1 = -1046.97628
    b2 = 2.96747468

End If

    'enthalpy, kJ/kg'

    h_N2 = (a1 + a2 * T / 2 + a3 * T ^ 2 / 3 + a4 * T ^ 3 / 4 + a5 * T ^ 4 / 5 + b1 / T) * R * T
/ N2_molar_mass / 1000

End Function

Function h_Ar(ByVal T As Double) As Double

    a1 = 2.5
    a2 = 0
    a3 = 0
    a4 = 0
    a5 = 0
    b1 = -745.375
```

```
    b2 = 4.37967491

    'enthalpy, kJ/kg'

    h_Ar = (a1 + a2 * T / 2 + a3 * T ^ 2 / 3 + a4 * T ^ 3 / 4 + a5 * T ^ 4 / 5 + b1 / T) * R * T
/ Ar_molar_mass / 1000

End Function

Function h_CO2(ByVal T As Double) As Double

If T > 1000 Then

    a1 = 4.63659493
    a2 = 0.00274131991
    a3 = -0.000000995828531
    a4 = 1.60373011E-10
    a5 = -9.16103468E-15
    b1 = -49024.9341
    b2 = -1.93534855

Else

    a1 = 2.35677352
    a2 = 0.00898459677
    a3 = -0.00000712356269
    a4 = 2.45919022E-09
    a5 = -1.43699548E-13
    b1 = -48371.9697
    b2 = 9.90105222

End If

    'enthalpy, kJ/kg'

    h_CO2 = (a1 + a2 * T / 2 + a3 * T ^ 2 / 3 + a4 * T ^ 3 / 4 + a5 * T ^ 4 / 5 + b1 / T) * R *
T / CO2_molar_mass / 1000

End Function

Function h_H2O(ByVal T As Double) As Double

If T > 1000 Then

    a1 = 2.67703787
    a2 = 0.00297318329
    a3 = -0.00000077376969
    a4 = 9.44336689E-11
    a5 = -4.26900959E-15
    b1 = -29885.8938
    b2 = 6.88255571
```

```
Else

    a1 = 4.19864056
    a2 = -0.0020364341
    a3 = 0.00000652040211
    a4 = -5.48797062E-09
    a5 = 1.77197817E-12
    b1 = -30293.7267
    b2 = -0.849032208

End If

    'enthalpy, kJ/kg'

    h_H2O = (a1 + a2 * T / 2 + a3 * T ^ 2 / 3 + a4 * T ^ 3 / 4 + a5 * T ^ 4 / 5 + b1 / T) * R *
T / H2O_molar_mass / 1000

End Function

Function h_CH4(ByVal T As Double) As Double

If T > 1000 Then

    a1 = 1.63552643
    a2 = 0.0100842795
    a3 = -0.00000336916254
    a4 = 5.34958667E-10
    a5 = -3.15518833E-14
    b1 = -10005.6455
    b2 = 9.99313326

Else

    a1 = 5.14987613
    a2 = -0.0136709788
    a3 = 0.0000491800599
    a4 = -4.84743026E-08
    a5 = 1.66693956E-11
    b1 = -10246.6476
    b2 = -4.64130376

End If

    'enthalpy, kJ/kg'

    h_CH4 = (a1 + a2 * T / 2 + a3 * T ^ 2 / 3 + a4 * T ^ 3 / 4 + a5 * T ^ 4 / 5 + b1 / T) * R *
T / CH4_molar_mass / 1000

End Function

Function cp_CH4(ByVal T As Double) As Double
```

```
If T > 1000 Then

    a1 = 1.63552643
    a2 = 0.0100842795
    a3 = -0.00000336916254
    a4 = 5.34958667E-10
    a5 = -3.15518833E-14
    b1 = -10005.6455
    b2 = 9.99313326

Else

    a1 = 5.14987613
    a2 = -0.0136709788
    a3 = 0.0000491800599
    a4 = -4.84743026E-08
    a5 = 1.66693956E-11
    b1 = -10246.6476
    b2 = -4.64130376

End If

    'enthalpy, kJ/kg'

    cp_CH4 = (a1 + a2 * T + a3 * T ^ 2 + a4 * T ^ 3 + a5 * T ^ 4) * R / CH4_molar_mass

End Function

Function R_NGas() As Double

    'mass of element / total mass'

    CH4_mf = Range("CH4_NGas_mf").Value

    CO2_mf = Range("CO2_NGas_mf").Value

    N2_mf = Range("N2_NGas_mf").Value

    R_NGas = R / (CH4_mf * CH4_molar_mass + CO2_mf * CO2_molar_mass + N2_mf *
N2_molar_mass)

End Functio

Function cp_NGas(ByVal T As Double) As Double

    'mass of element / total mass'

    CH4_mf = Range("CH4_NGas_mf").Value

    CO2_mf = Range("CO2_NGas_mf").Value

    N2_mf = Range("N2_NGas_mf").Value
```

```
    cp_NGas = CH4_mf * cp_CH4(T) + CO2_mf * cp_CO2(T) + N2_mf * cp_N2(T)

End Function

Function h_NGas(ByVal T As Double) As Double

    'mass of element / total mass'

    CH4_mf = Range("CH4_NGas_mf").Value

    CO2_mf = Range("CO2_NGas_mf").Value

    N2_mf = Range("N2_NGas_mf").Value

    h_NGas = CH4_mf * (h_CH4(T) - h_CH4(273.15)) + CO2_mf * (h_CO2(T) - h_CO2(273.15)) + N2_mf * (h_N2(T) - h_N2(273.15))

End Function

Function R_air() As Double

    O2_mt = 0.2095 * O2_molar_mass

    N2_mt = 0.7808 * N2_molar_mass

    Ar_mt = 0.0093 * Ar_molar_mass

    CO2_mt = 0.0004 * CO2_molar_mass

    'mass of element / total mass'

    O2_mf = O2_mt / (O2_mt + N2_mt + Ar_mt + CO2_mt)

    N2_mf = N2_mt / (O2_mt + N2_mt + Ar_mt + CO2_mt)

    Ar_mf = Ar_mt / (O2_mt + N2_mt + Ar_mt + CO2_mt)

    CO2_mf = CO2_mt / (O2_mt + N2_mt + Ar_mt + CO2_mt)

    R_air = R / O2_molar_mass * O2_mf + R / N2_molar_mass * N2_mf + R / Ar_molar_mass * Ar_mf + R / CO2_molar_mass * CO2_mf

End Function

Function cp_Air(ByVal T As Double) As Double

    O2_mt = 0.2095 * O2_molar_mass

    N2_mt = 0.7808 * N2_molar_mass

    Ar_mt = 0.0093 * Ar_molar_mass

    CO2_mt = 0.0004 * CO2_molar_mass
```

```
    'mass of element / total mass'

    O2_mf = O2_mt / (O2_mt + N2_mt + Ar_mt + CO2_mt)

    N2_mf = N2_mt / (O2_mt + N2_mt + Ar_mt + CO2_mt)

    Ar_mf = Ar_mt / (O2_mt + N2_mt + Ar_mt + CO2_mt)

    CO2_mf = CO2_mt / (O2_mt + N2_mt + Ar_mt + CO2_mt)

    cp_Air = N2_mf * cp_N2(T) + O2_mf * cp_O2(T) + Ar_mf * cp_Ar(T) + CO2_mf *
cp_CO2(T)

End Function

Function h_Air(ByVal T As Double) As Double

    O2_mt = 0.2095 * O2_molar_mass

    N2_mt = 0.7808 * N2_molar_mass

    Ar_mt = 0.0093 * Ar_molar_mass

    CO2_mt = 0.0004 * CO2_molar_mass

    'mass of element / total mass'

    O2_mf = O2_mt / (O2_mt + N2_mt + Ar_mt + CO2_mt)

    N2_mf = N2_mt / (O2_mt + N2_mt + Ar_mt + CO2_mt)

    Ar_mf = Ar_mt / (O2_mt + N2_mt + Ar_mt + CO2_mt)

    CO2_mf = CO2_mt / (O2_mt + N2_mt + Ar_mt + CO2_mt)

    h_Air = N2_mf * (h_N2(T) - h_N2(273.13)) + O2_mf * (h_O2(T) - h_O2(273.15)) +
Ar_mf * (h_Ar(T) - h_Ar(273.13)) + CO2_mf * (h_CO2(T) - h_CO2(273.13))

End Function

Function R_SG_NGas() As Double

    'mass of element / total mass'

    CO2_mf = Range("CO2_SG_NGas_mf").Value

    H2O_mf = Range("H2O_SG_NGas_mf").Value

    N2_mf = Range("N2_SG_NGas_mf").Value

    R_SG_NGas = R / (CO2_mf * CO2_molar_mass + H2O_mf * H2O_molar_mass +
N2_mf * N2_molar_mass)
```

```
End Function

Function cp_SG_NGas(ByVal T As Double) As Double

    'mass of element / total mass'

    CO2_mf = Range("CO2_SG_NGas_mf").Value

    H2O_mf = Range("H2O_SG_NGas_mf").Value

    N2_mf = Range("N2_SG_NGas_mf").Value

    cp_SG_NGas = CO2_mf * cp_CO2(T) + H2O_mf * cp_H2O(T) + N2_mf * cp_N2(T)

End Function

Function h_SG_NGas(ByVal T As Double) As Double

    'mass of element / total mass'

    CO2_mf = Range("CO2_SG_NGas_mf").Value

    H2O_mf = Range("H2O_SG_NGas_mf").Value

    N2_mf = Range("N2_SG_NGas_mf").Value

    h_SG_NGas = CO2_mf * (h_CO2(T) - h_CO2(273.15)) + H2O_mf * (h_H2O(T) -
h_H2O(273.15)) + N2_mf * (h_N2(T) - h_N2(273.15))

End Function

Function R_LGas() As Double

    'mass of element / total mass'

    CH4_mf = Range("CH4_LGas_mf").Value

    CO2_mf = Range("CO2_LGas_mf").Value

    N2_mf = Range("N2_LGas_mf").Value

    R_LGas = R / (CH4_mf * CH4_molar_mass + CO2_mf * CO2_molar_mass + N2_mf *
N2_molar_mass)

End Function

Function cp_LGas(ByVal T As Double) As Double

    'mass of element / total mass'

    CH4_mf = Range("CH4_LGas_mf").Value

    CO2_mf = Range("CO2_LGas_mf").Value
```

```
    N2_mf = Range("N2_LGas_mf").Value

    cp_LGas = CH4_mf * cp_CH4(T) + CO2_mf * cp_CO2(T) + N2_mf * cp_N2(T)

End Function

Function h_LGas(ByVal T As Double) As Double

    'mass of element / total mass'

    CH4_mf = Range("CH4_LGas_mf").Value

    CO2_mf = Range("CO2_LGas_mf").Value

    N2_mf = Range("N2_LGas_mf").Value

    h_LGas = CH4_mf * (h_CH4(T) - h_CH4(273.15)) + CO2_mf * (h_CO2(T) - h_CO2(273.15)) + N2_mf * (h_N2(T) - h_N2(273.15))

End Function

Function R_SG_LGas() As Double

    'mass of element / total mass'

    CO2_mf = Range("CO2_SG_LGas_mf").Value

    H2O_mf = Range("H2O_SG_LGas_mf").Value

    N2_mf = Range("N2_SG_LGas_mf").Value

    R_SG_LGas = R / (CO2_mf * CO2_molar_mass + H2O_mf * H2O_molar_mass + N2_mf * N2_molar_mass)

End Function

Function cp_SG_LGas(ByVal T As Double) As Double

    'mass of element / total mass'

    CO2_mf = Range("CO2_SG_LGas_mf").Value

    H2O_mf = Range("H2O_SG_LGas_mf").Value

    N2_mf = Range("N2_SG_LGas_mf").Value

    cp_SG_LGas = CO2_mf * cp_CO2(T) + H2O_mf * cp_H2O(T) + N2_mf * cp_N2(T)

End Function

Function h_SG_LGas(ByVal T As Double) As Double

    'mass of element / total mass'
```

```
    CO2_mf = Range("CO2_SG_LGas_mf").Value

    H2O_mf = Range("H2O_SG_LGas_mf").Value

    N2_mf = Range("N2_SG_LGas_mf").Value

    h_SG_LGas = CO2_mf * (h_CO2(T) - h_CO2(273.15)) + H2O_mf * (h_H2O(T) - h_H2O(273.15)) + N2_mf * (h_N2(T) - h_N2(273.15))

End Function
```